A Study on the Hot Events in the Western Equatorial Pacific - Their Characteristics, Mechanisms and Interactions with the Pacific Warm Pool

博士論文

A Study on the Hot Events in the Western Equatorial Pacific – Their Characteristics, Mechanisms and Interactions with the Pacific Warm Pool

西部太平洋赤道域におけるホット・イベントに関する研究
－ それらの特性、メカニズム、そして太平洋暖水プールとの相互作用

Anindya Wirasatriya

平成 27 年

Doctoral Thesis

A Study on the Hot Events in the Western Equatorial Pacific – Their Characteristics, Mechanisms and Interactions with the Pacific Warm Pool

（西部太平洋赤道域におけるホット・イベントに関する研究 － それらの特性、メカニズム、そして太平洋暖水プールとの相互作用）

Anindya Wirasatriya
（アニンディア ウィラサトォリア）

Department of Geophysics
Graduate School of Science, Tohoku University

Thesis Committee Members
Professor Hiroshi Kawamura (Chair, Supervisor)
Professor Shuji Aoki
Professor Toshio Suga
Professor Tadahiro Hayasaka
Associate Professor Shoichi Kizu
Associate Professor Futoki Sakaida

2015

Abstract

The western equatorial Pacific is potential for the Hot Event (HE) study since the previous study showed that among the equatorial regions, most of HEs occurred in this area. Moreover, it is also known as an important area for oceanography and climatology since the warmest equatorial pool, which is responsible to transport heat and water vapor to the higher latitude is located in this area. Therefore, the investigation of HE in the western equatorial Pacific can give a better understanding of their characteristics and mechanisms as well as their interactions with the Pacific warm pool.

Chapter 1 introduces the research backgrounds of the high SST in the western equatorial Pacific and the summary of the previous HE study. The previous studies on the high SST in the western equatorial Pacific were mainly focused on the seasonal, intraseasonal, and interannual variations. HE phenomena correspond to the occurrence of very high SST (>30°C) with a short time scale (< a month). These phenomena are sensitive to the measurements bias/errors and sparsely occur because of their requirement on the particular mechanisms for their formation. Therefore, the appropriate dataset and method are needed to capture their occurrence. The previous studies of HE used the optimally interpolated daily SST data with a spatial resolution of 0.1° × 0.1° merging the infrared and microwave satellite SSTs to detect HEs. They also developed a method called the time-dependent threshold, a SST threshold which follows the interanual variation of SST in the equatorial oceans. They found 31 HE cases during 10 years observation in the equatorial region which were generated by the condition of high solar radiation and low wind speed. In some cases the high solar radiation generated during the HE occurrence is associated with a sub-surface high SST anomaly during El Niño event controlled by the "remote convection" mechanism. However, their studies cannot reveal the relation between HEs and the long-term SST pattern in the warm pool due to the limited HE case numbers. This relation becomes the important issues for the present HE study. This short period variability of SST may have the climatic consequences if accumulated and then affected the long-term statistic pattern in the warm pool.

I examined the performance of three global SST datasets and evaluated the previous HE detection method in Chapter 2. Three global SST datasets which have the same temporal and spatial resolution i.e., daily and 0.25° grid interval were examined against the SSTs obtained from

the TAO/TRITON buoys in detecting HE. After the analysis of Power Spectral Density, probability test and comparison with the original AMSR-E snapshots, NGSST-O-Global-V2.0a was chosen for investigating HE in the western equatorial Pacific. The two microwave sensors composing NGSST-O-Global-V2.0a, significantly improve the observation coverage and the diurnal correction on the processing of NGSST-O-Global-V2.0a reduces the errors arising from merging observations at different times. The method used by the previous study has a limitation for detecting HE in the cold season. Improving new detection method which is free from seasonal effect, I defined an HE as a connected region with a SST higher than the space-time dependent threshold of about 30°C, with a minimum areal size of 2×10^6 km, and a duration period longer than 6 days.

Chapter 3 conducts the climatological study of HE in the western equatorial Pacific. During 9 years observation from 2003 to 2011, I found 71 HE cases which have characteristics as follows : a mean areal size of 6.30×10^6 km^2, a mean period of 18.14 days, a mean amplitude of 0.33 °C, and a mean speed of development (decay) of 0.28 (0.31) $\times 10^6$ km^2/day. They were distributed within the equatorial band to subtropical Pacific (20°S to 30°N) and extended eastward to 150°W. They frequently occurred along the northern coasts of New Guinea and the Solomon Islands, with an eastward extension to 180°E. Their distribution also exhibited seasonal variation. The observed distribution of the HE occurrences indicates that the HE formation is statistically related to the formation of the Pacific warm pool via the long-term SST. Higher occurrence rates of HE correspond to higher climatological SSTs. For the HE mechanisms, I found that although high solar radiation of more than ~200 W/m^2 was required, wind speeds lower than ~4 m/s become the key for the HE occurrence in the western equatorial Pacific. In areas where wind speeds are low, latent heat loss are reduced and high SSTs occur, leading to the occurrence of HEs.

The atmospheric variability during the development and decay stage of HE is described in Chapter 4. The HE development in the western equatorial Pacific is indicated by positive anomaly of solar radiation from its climatology while its decay is denoted by the anomaly of surface wind direction. During the development stage, the solar radiation (wind speed) in the HE area is much more enhanced (reduced) than during the decay stage. The theory of ‘remote convection’ is proven for the formation mechanisms of HE occurred in the late May 2003 (i.e., HE030528). Moreover, the high solar radiation during the development stage of HE is partly contributed by

the suppressed phase of the MJO in the western equatorial Pacific. I also found the indication of the air-sea-land interaction process which generates the strong westerly wind during the decay of HE030528. Surface wind plays important role to influence the variability of solar radiation during the HE occurrence by controlling the water vapor supply in the upper troposphere through surface evaporation and surface convergence variation. Thus, surface wind becomes the key factor for the HE occurrence in the western equatorial Pacific.

Chapter 5 focuses on the oceanic variability during the development and decay stage of HE. The west side of the Pacific warm pool is characterized by the warm and relatively stable thermal structure. These characteristics may become the anvil for the HE occurrence so that the highest occurrence rate of HE is found in this area. The occurrence of HE in the western equatorial Pacific can be identified by the trapezoidal shape of the thermal structure change in the mixed layer which is described as follows: during the development stage, the higher temperature is accumulated at the surface layer while during the decay stage, the temperature at the surface (deeper layer) decrease (increase). This trapezoidal shape is formed by the heat accumulation at the surface layer under the condition of high solar radiation and low wind speed during the development stage. During the decay stage, high latent heat loss and the transport of sensible heat to the deeper water column occur under the condition of low solar radiation and strong wind speed. These mechanisms may contribute to maintain the warm mixed layer in the Pacific warm pool. Since surface winds control heat accumulation at the surface layer and heat distribution in the mixed layer by influencing current speed, current divergence and latent heat flux, surface winds become the key factor for the HE occurrence and the formation of the thermal structure in the Pacific warm pool.

The general conclusions and remarks are mentioned in chapter 6. Future studies of HE are directed to investigate : 1) the mechanisms governing the characteristics of HE detected in the western equatorial Pacific (duration, amplitude, areal size, and speed of development and decay), 2) further analysis of the HE-MJO-tropical cyclone relationship, 3) the role of HE in governing the mixed layer temperature variations involving all possible factors such as subduction, entrainment lateral mixing and also interannual background, 4) the possible mechanisms of rainfall on influencing the HE occurrence and 5) the possible effect of HEs on influencing the global climate.

Contents

Chapter 1

General Introduction

1.1. Characteristic of the Pacific warm pool

The western equatorial Pacific is an important area for oceanography and climatology because of the existence of the warmest warm pool i.e., the Pacific warm pool. The Pacific warm pool is an important influence on global climate variations via the deep overturning meridional (Hadley) and zonal (Walker) cells. These largescale circulations transport heat and water vapor from the warm pool to higher latitudes. On the interannual scale, it was found that water vapor transport is suppressed during El Niño years, as shown by the sparse northward plumes of moist air in the mid troposphere (Pierrehumbert 2000). The horizontal boundary of the Pacific warm pool is defined by the 28°C isotherm of long term mean sea surface temperature (SST) in the western equatorial Pacific (Wyrtki 1989; Yan et al. 1992; Thoron et al. 2005; Clement et al. 2005) as shown in Fig. 1.1.

To date, most studies on the Pacific warm pool have focused solely on the seasonal, intraseasonal, and interannual variations in SST. For example, Waliser (1996) investigated SSTs >29.75 °C in the equatorial Pacific and Indian Oceans using a 2° × 2° grid and monthly SST data with a blended analysis of satellite-derived and in situ measurements. His analysis indicated that the occurrence of high SSTs varies strongly on interannual, annual, and 30–60-day timescales. Shinoda et al. (1998) described the relation between SST and intraseasonal variation in surface heat flux in the tropical western Pacific and Indian oceans using weekly and 1° × 1°

grid SST analysis. Employing the same dataset, Lin et al. (2011) found that interannual variability in the heat flux influences the variability of the western Pacific warm pool. Moreover, the seasonal and interannual variations in properties of the warm pool such as areal size, zonal shift, and SST have been described by Kim et al. (2012) using monthly and 2° × 2° grid extended reconstructions of historical SSTs. Thus, all of the studies mentioned above used relatively low spatiotemporal resolution of the data (>1° × 1° and weekly to monthly). Higher spatiotemporal resolution of the SST dataset is needed to detect the shortterm occurrences of high SSTs in the warm pool (i.e., over periods of less than a month for SSTs >30 °C). In fact, only a few studies have focused on the short-period variability of the SSTs in the Pacific warm pool.

1.2. Previous Hot Event studies

Hot Event (HE) phenomena correspond to the occurrence of very high SST (>30°C) in a short time scale (<a month). These phenomena are sensitive from the measurements bias/errors (e.g., Kawamura et al. 2008, Hosoda et al. 2013) and sparsely occur because they require particular mechanisms for their formation as shown in Waliser and Graham (1993). Despite using low temporal and spatial resolution of SST dataset (i.e., monthly and 2° grid interval), Fig. 1.2 shows the relation between SSTs and deep convection which is indicated by highly reflective cloud (HRC) data. From 26°C to 29.5°C the increase of SST is parallel with the HRC. Conversely, from 29.5°C to 32°C, the HRC decreases with the increase of SST which denotes the different mechanisms of increasing SSTs below and above 29.5°C. Moreover, the SSTs distribution is also negatively skewed with the peak at 29.5°C which shows the sparse occurrence of SSTs larger than 29.5°C. Therefore, appropriate SST dataset and method are needed for capturing the occurrence of very high SST phenomena.

The study of HE over the tropical oceans has been initiated by the Tohoku University as summarized in Table 1.1 (Qin et al. 2007; Kawamura et al. 2008; Qin et al. 2008 and Qin and Kawamura 2009, 2010). Qin et al. (2007) used the optimally interpolated daily SST data with a spatial resolution of 0.1° × 0.1° merging the infrared and microwave satellite SSTs (Kawai et al. 2006) to detect HEs. They also developed a method called time-dependent threshold, a SST threshold which follows the interanual variation of SST in the equatorial oceans. Then, they defined HE as a connected region with SST larger than the time dependent threshold (of about

30°C), having a minimum areal size of 3 x 10^6 km^2 and lasting period longer than 10 days. Their analysis showed that the HEs were generated by the condition of high solar radiation and low wind speed which correspond to the condition of high amplitude of diurnal SST (DSST) as shown in Fig. 1.3 (Qin et al. 2007; Kawamura et al. 2008). Over the course of 10 years (1993-2003), they identified 31 HEs, distributing in the Indian Ocean, the western and equatorial Pacific, the South China Sea and the north of Australia (Fig. 1.4). The western equatorial Pacific is the important area for the HE study since most of the 31 HEs (68%) were identified there.

Furthermore, the fact that HEs frequently occur in the western equatorial Pacific raises a question about the relation between the western Pacific warm pool and the HEs. Previous studies have focused solely on limited factors associated with increased SST in the western Pacific warm pool, which has a mode SST of 28 °C. For example, Ramanathan and Collins (1991) and Waliser and Graham (1993) proposed local cooling mechanisms, whereas Wallace (1992) and Arking and Ziskin (1994) focused on the role of large-scale atmospheric circulation in regulating tropical SSTs. Clement et al. (2005) explored the mechanisms by considering both atmospheric and oceanic processes through several modeling schemes. Thus, no studies have examined the relation between HEs and the western Pacific warm pool.

On the other hand, a series case study of HE in the Pacific warm pool have been conducted by Qin et al. (2008); Qin and Kawamura (2009b, 2010). They investigated the air-sea interaction processes underlying the occurrence of HE in November 2006 (named HE0611). They indicated that the high solar radiation during the HE occurrence is controlled by the "remote convection" mechanism associated with a sub-surface high SST anomaly during an El Niño event. However, neither the analysis of HE0611 nor the previous HE study can reveal the relation between the HEs and the long-term SST pattern in the warm pool due to the limited number of the analyzed HE cases. This relation become the important issues for the present HE study. This short period variability of SST might have the climatic consequences if accumulated and then affected the long-term statistic pattern in the warm pool.

1.3. Scope of the present study

Purposes of the present study are to investigate the characteristics and mechanisms of HEs in the western equatorial Pacific and to analyze their interaction with the Pacific warm pool through case studies and climatological analyses. First, I examine SST datasets to select the most

appropriate one for capturing the HE occurrence. We also evaluate the HE detection method of the previous HE studies. Then, we redefine HE by proposing the new detection method. The SST dataset selection and new HE detection method are presented in Chapter 2. Chapter 3 elucidates the distribution and the occurrence mechanisms of HE in the western equatorial Pacific. Moreover, its relation with the climatological SST of the Pacific warm pool is also discussed statistically in Chapter 3. Chapter 4 emphasizes the mechanisms of the HE generation in term of the air-sea interaction processes, while Chapter 5 focuses on the oceanic factors regulating HEs by analyzing the vertical structure of oceanic parameters in the Pacific warm pool. In this chapter, the relation between the Pacific warm pool and HE occurrence is investigated in terms of its physical process. Finally, I give the conclusions and remarks in Chapter 6.

Table 1.1 Summary of the previous HE studies.

No	Article	Result
1	Qin et al. (2007)	• HE is defined as a connected region with SST > the time dependent threshold of about 30°C, having a minimum areal size greater than $3\times10^6 km^2$ and lasting for a period longer than 10 days. • 31 HEs were identified in the equatorial Indo-Pacific warm pool. • The HE area shifts with season inside the SST contour of 28°C in the Indo-Pacific oceans. • HE occurrence corresponds to the large amplitude of diurnal SST as a result of high solar radiation and low wind speed.
2	Kawamura et al. (2008)	• This study provides observational evidence of the high diurnal amplitude of SST during HE which results in the enhanced systematic positive bias of satellite SST against in-situ SST
3	Qin et al. (2008)	• Two distinct mechanisms govern the generation of HE in November 2006 (HE0611) in the western equatorial Pacific. • At the western side, the air-sea interaction process governs the HE generation denoted by large diurnal SST amplitude. The large solar radiation, suppressed latent heat loss and stratified subsurface temperature at the mixed layer were observed in the HE generation process. • The high SST of HE0611-east was supported by a subsurface high SST anomaly associated with the El Niño.
4	Qin and Kawamura (2009a)	• Atmospheric response of HE0611 was examined by using Atmospheric Infrared Sounder product. • The lagged atmospheric response (temperature and geopotential height) in the western part of HE0611 associated with deep convection in the eastern part and subsidence in the western part. • The very high SST phenomenon of HE needs to be considered as a coupled system of the ocean and atmosphere in the Indo-Pacific warm pool.
5	Qin and Kawamura (2009b)	• Surface heat fluxes analysis during hot events shows that large daily heat gain in the HE formation phase can be expected to increase SSTs and produce large amplitudes of diurnal SST variations during HEs.
6	Qin and Kawamura (2010)	• This study provides the satellites evidence of the convergent (divergent) flow over the HE0611-west (east) indicating the true appearance of “remote convection” which has been suggested as a mechanism of very high SST generation in the tropical oceans.

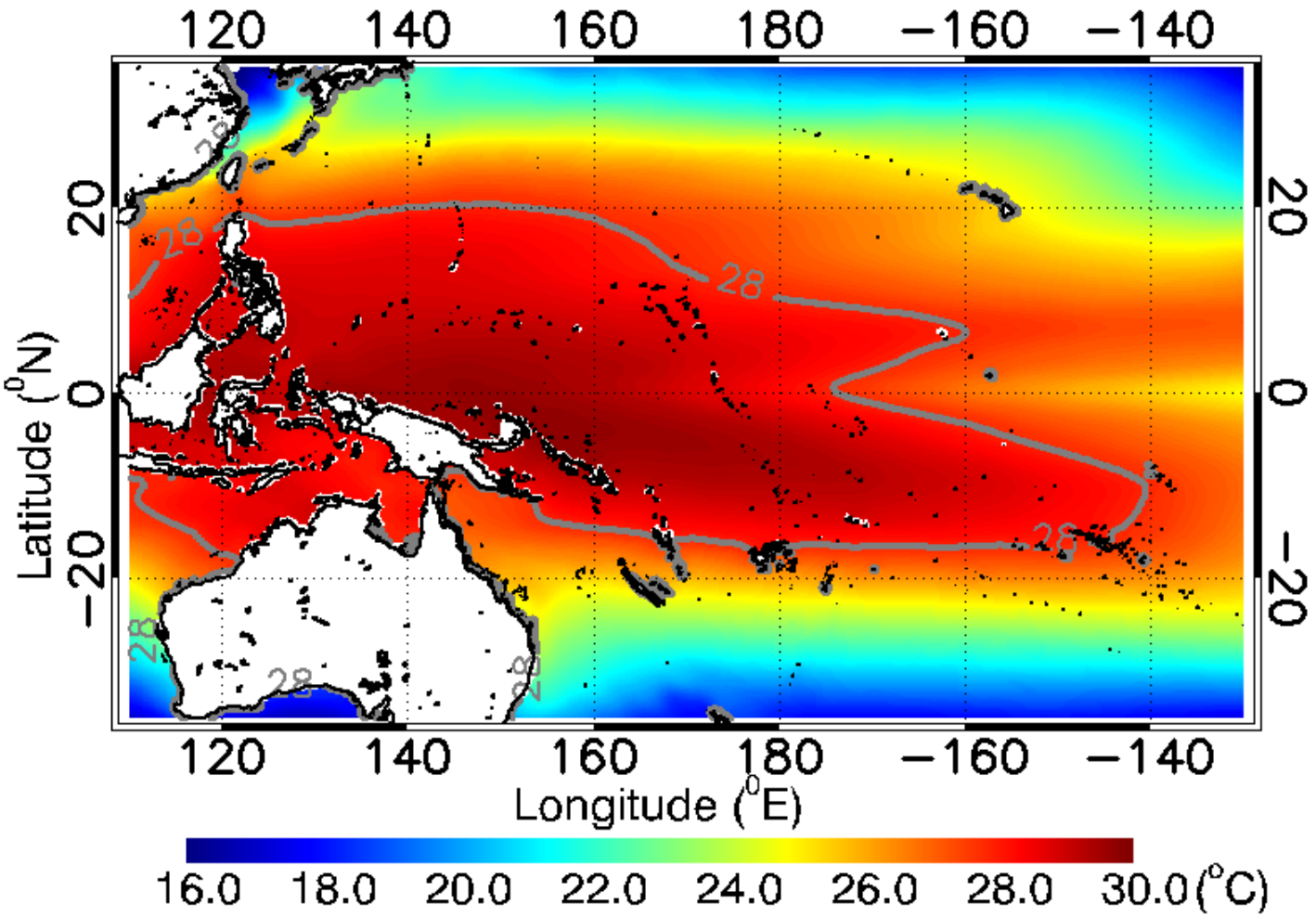

Fig. 1.1 SST climatology for 2003-2011 in the western equatorial Pacific. The *gray contour* indicates 28C isotherm, which defines the western Pacific warm pool.

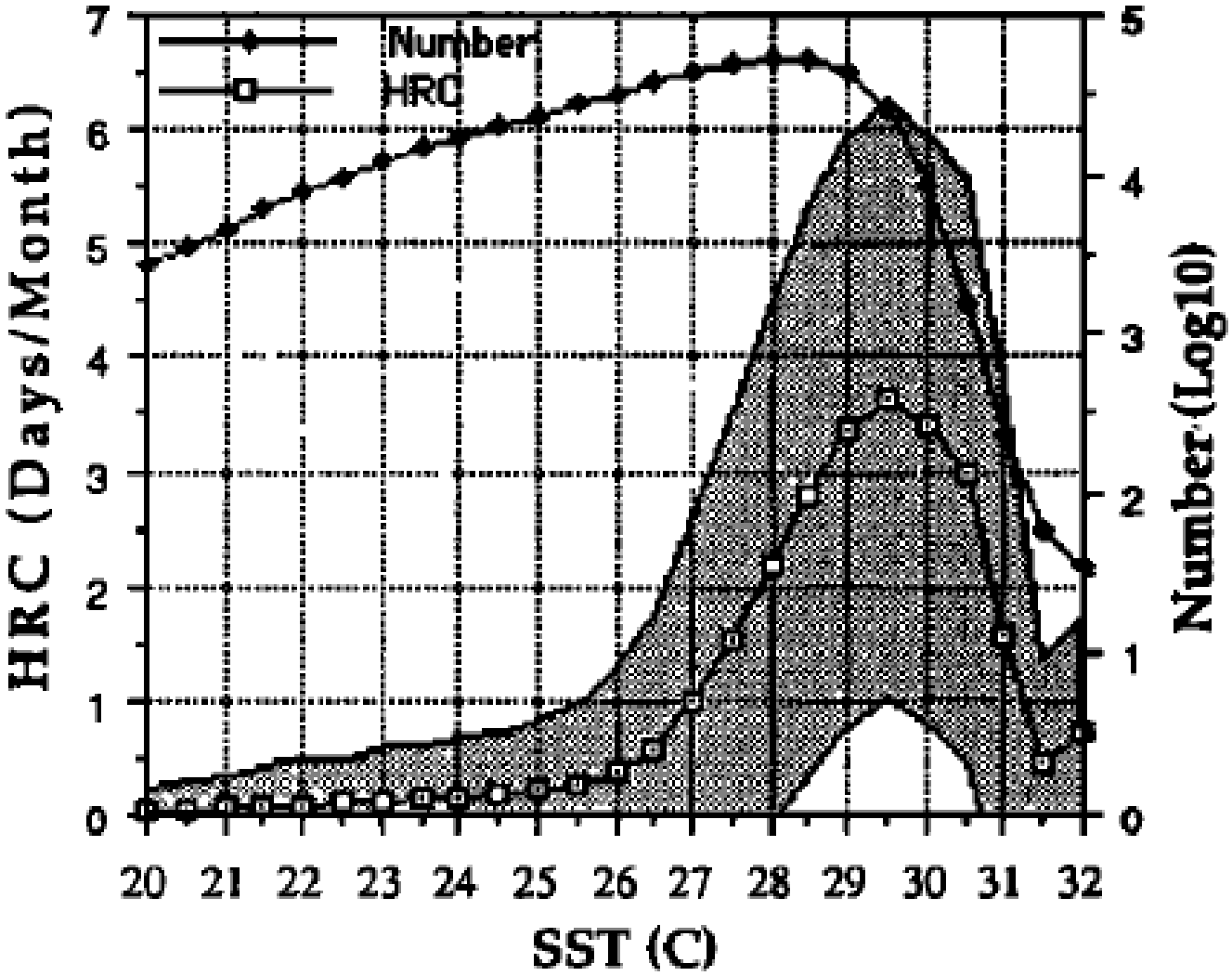

Fig. 1.2 Relation between SSTs and highly reflective cloud (HRC) between 1975-1987 for the global tropical oceans between 25°N and 25°S. Cited from Waliser and Graham (1993).

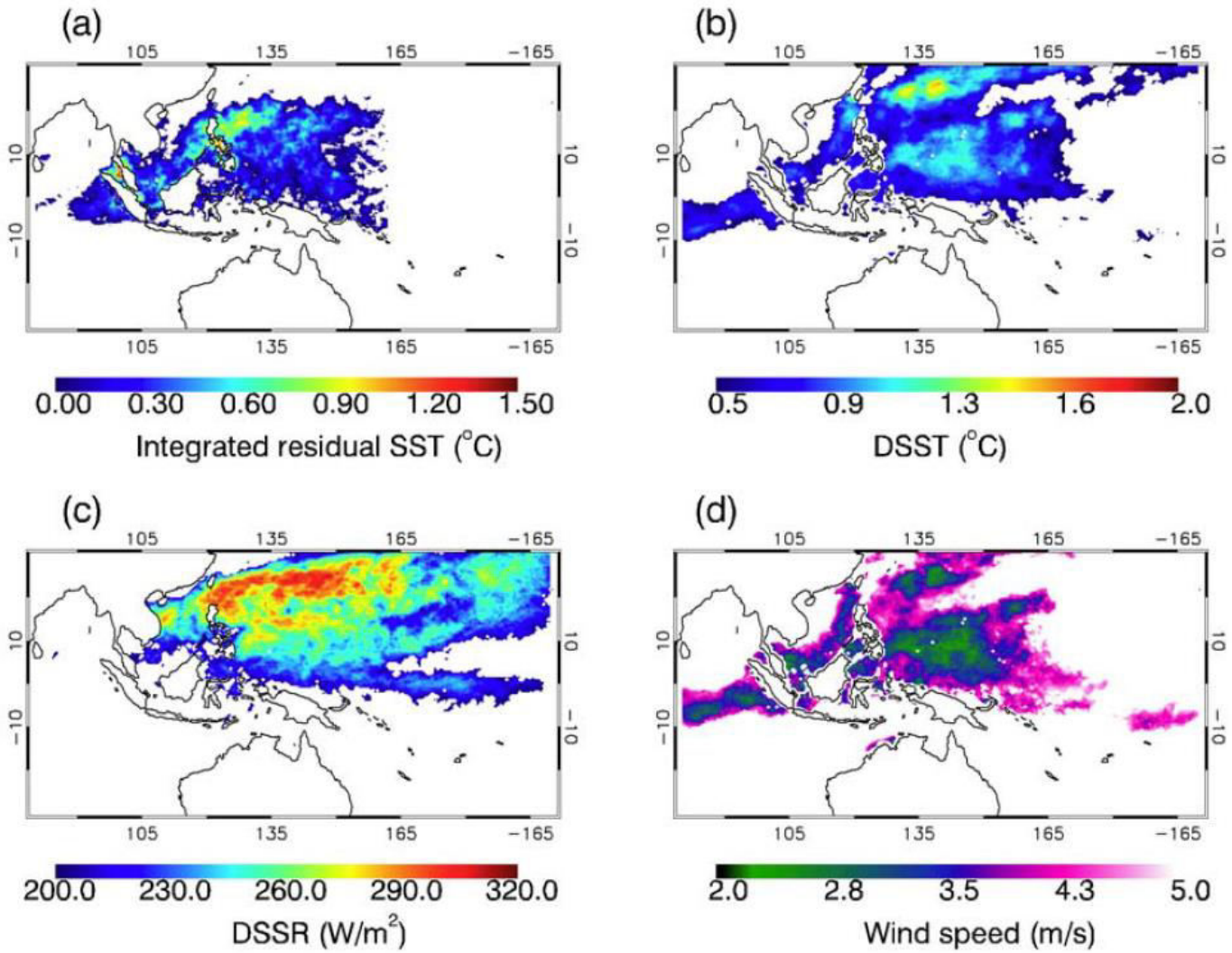

Fig. 1.3 Statistical features of the HE lasting from 3 to 15 June 2001 (a) The hot event intensity, with SST residual of SST higher than threshold. (b) Mean DSST, (c) mean DSSR, and (d) mean wind speed. Cited from Qin et al. (2007).

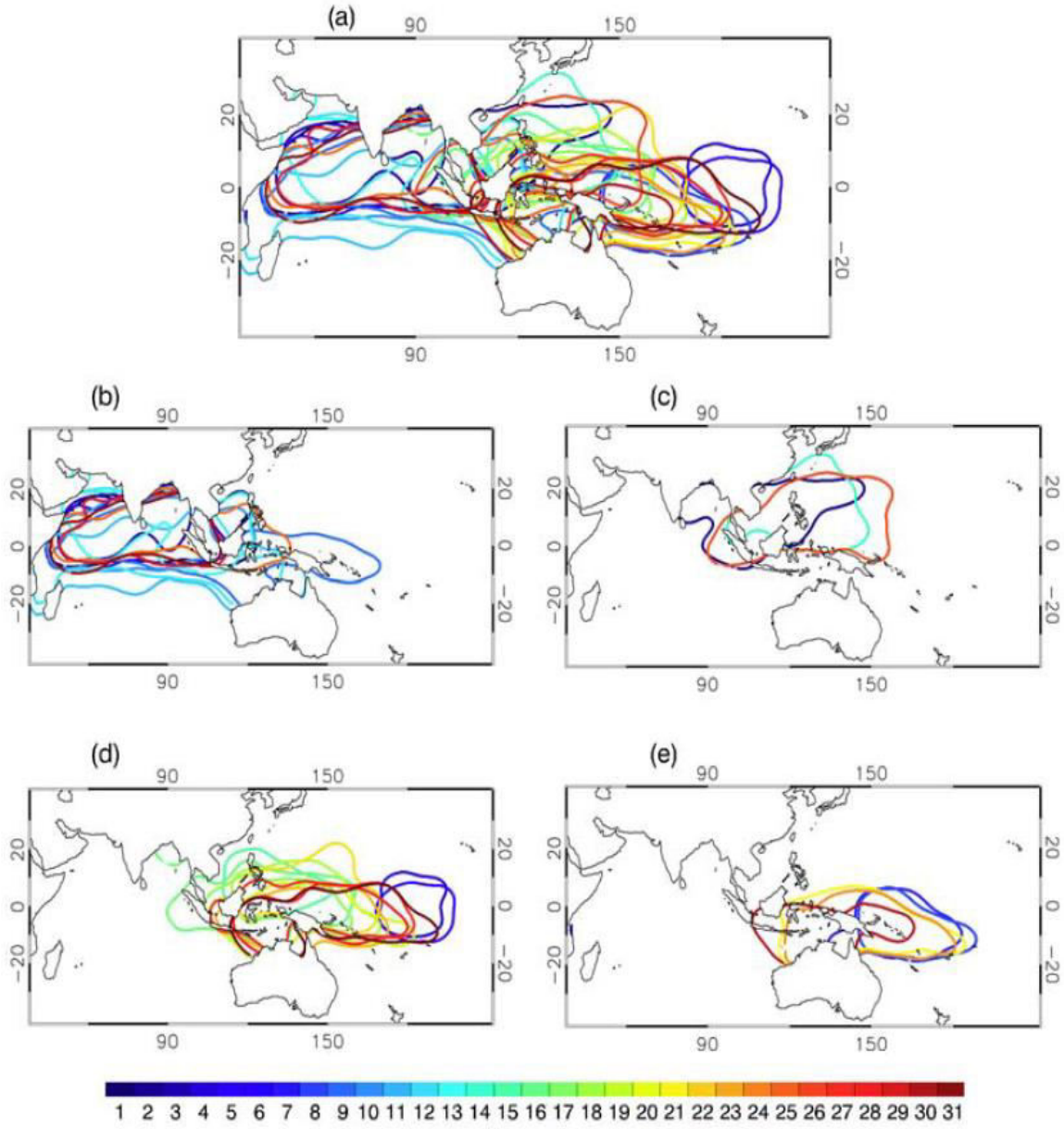

Fig. 1.4 All HEs schematic diagram. Color index shows the HE numbers. (a) All HEs in 1993–2003, (b) all HEs in spring (March, April, and May) of 1993–2003, (c) the same as Fig.1.4b but in summer (June, July, and August), (d) the same as Fig.1.4b but in autumn (September, October, and November), and (e) the same as Fig.1.4b but in winter (December, January, and February). Cited from Qin et al. (2007).

Chapter 2

Datasets and methods

2.1. SST dataset selection

2.1.1. Introduction

Satellite remote sensing has been widely used for measuring SST since 1980s and revolutionary increased our ability to observe the spatial and temporal variations of the global SST field. It started with infrared measurements which can provide high spatial resolution of SST data (1 km or more) but only under the clear sky condition. Then, microwave measurements were developed in the late 1990s to overcome the blocky SST observation under the cloudy condition. However, their spatial resolution (i.e.,~25 km) is much lower than those of the infrared measurements. Nowadays, the benefit of satellite measurements is used to produce various gridded SST datasets by using the optimum interpolation method.

I investigated HEs over nine years (2003–2011) in the western equatorial Pacific (20°S–20°N, 128°E–140°W) except the Indonesian inner seas and the seas north of Australia (Fig. 2.1) by using the satellite-based gridded SST product. Since HE is the high SST phenomenon with a short period, high spatial and temporal resolution of SST data obtained from the satellite measurements is required for detecting HEs. However, since the occurrence of HE is associated with high amplitude of diurnal SST, the accuracy of the SST dataset is to be regarded. The blended SST product based on the microwave and infrared radiometers can be contaminated by the diurnal warming (Hosoda 2013). Moreover, Kawamura et al. (2008) have shown that the satellite SSTs have a systematic positive bias against the corresponding buoy SSTs in the HE region. The bias is enhanced in conditions of large in-situ DSST. In addition, the western

equatorial Pacific is the area with high convection activity. In the convection area, the SST data obtained from infrared radiometer are contaminated by cloud, which lead to anomalously cold SST signals (Hosoda 2013). Therefore, before starting the investigation, I examined the performance of three global SST product obtained from various satellite measurements and observations to select the most reliable SST dataset for the HE analysis by comparing with the in situ SST observations of the TAO/TRITON buoys. They were Merged satellite and in-situ data Global Daily Sea Surface Temperature (MGDSST) (Kurihara et al. 2006), Optimum Interpolation Sea Surface Temperature ver. 2.0 (OISST V2) (Reynold et al. 2007) and New Generation Sea Surface Temperature version 2.0a (NGSST-O-Global-V2.0a) (Hosoda, in preparation).

2.1.2. Merged satellite and in-situ data Global Daily Sea Surface Temperature

Merged satellite and in-situ data Global Daily Sea Surface Temperature (MGDSST) is analyzed at the Office of Marine Prediction of the JMA with daily and 1/4-degree grid resolution on the near-real-time basis with global coverage. MGDSSTs are available from January 4th, 1985 to the latest. The SSTs derived from satellite's infrared sensors (Advanced Very High Resolution Radiometer (AVHRR)) and microwave sensor (Advanced Microwave Scanning Radiometer on the Earth Observing System (AMSR-E)), and in-situ SST (buoy and ship) are used in the analysis. In-situ data are used for bias correction of satellites' SSTs. In particular, its bias (root mean square error) against the TAO/TRITON buoy SST in the study area is 0.007°C (0.262°C) (Fig. 2.2a).

2.1.3. Optimum Interpolation Sea Surface Temperature ver. 2.0

The NOAA 1/4° daily Optimum Interpolation Sea Surface Temperature ver. 2.0 (OISST V2) is an analysis constructed by combining observations from different platforms (satellites, ships, buoys) on a regular global grid. The satellite SST sensors are the AVHRR and AMSR-E. A spatially complete SST map is produced by interpolating to fill in gaps. Besides for bias correction, in-situ data was also averaged onto the 1/4° grid and involved in the calculation of optimum interpolation. This dataset has bias (root mean square error) of -0.054°C (0.278°C) against the TAO/TRITON buoy SST in the study area (Fig. 2.2b).

2.1.4. New Generation Sea Surface Temperature for Open Ocean version 2.0a

The New Generation Sea Surface Temperature for Open Ocean is a gridded SST products released by the Tohoku University. The first version (NGSST-O-V1.0) is produced in 2003 by blending infrared (MODIS, AVHRR) and microwave (AMSR-E) SST. Their detailed description and validation is provided by Sakaida et al. (2009). Declining the disadvantage of infrared SST, they released NGSST-O-V1.5 and NGSST-O-V1.6 by using 2 satellite microwave sensors, i.e., AMSR-E and Windsat. The difference between these versions is their sub-sampling methods (Hosoda et al. 2015).

NGSST-O-Global-V2.0a is produced by merging SST observations acquired by two satellite microwave sensors (AMSR-E onboard Aqua and WindSat onboard Coriolis) after applying diurnal correction to estimate 1 m depth SST at the time of local dawn (06:00LT) at each longitude (Hosoda 2013). It is daily and has grid interval of 0.25°. Its bias (root mean square error) against the TAO/TRITON buoy SST in the study area is -0.107°C (0.428°C) (Fig. 2.2c). The summary of the NGSST-O development is listed in Table 2.1.

2.1.5. Examination of SST datasets

Since investigating HEs involves studying the high-frequency variations in SSTs with periods of less than a month, power spectral density (PSD) analysis was performed. Figure 2.3 shows that MGDSST has the weakest power to capture short-term signals (<20 days), while NGSST and OISST are able to capture the high-frequency signals sensed by buoys. Thus, the MGDSST dataset was ignored in this analysis.

Next, to test the HE-detection performance of each dataset against the buoy dataset, statistical evaluations were performed using a 2 × 2 matrix called a contingency table. Four components (A, B, C, D) held a number of combinations between the examined datasets and the observation by buoys in detecting HEs in a given statistical population (Wilks 2006). Firstly, the space–time-dependent threshold was determined for each dataset (explained in Section 2.3). When the SST of the observation (buoy) exceeded the threshold, it meant that the buoy had sensed an HE. Component A corresponded to the proportion of observations in which the examined SST dataset and the corresponding buoy SST dataset both passed the SST threshold. Component B corresponded to the proportion of observations in which only the examined SST dataset passed the SST threshold. Component C corresponded to the proportion of observations

in which only the buoy SST dataset passed the SST threshold. Component D corresponded to the proportion of observations in which neither the examined SST dataset nor the buoy SST dataset passed the SST threshold. The performance of each merged SST product was defined based on five attributes: accuracy, bias, false alarm ratio, misses alarm ratio, and probability of detection. The formulae used in this analysis and results of it are shown in Table 2.2.

The results showed that OISST and NGSST were the most accurate. However, based on the bias, FAR, MAR, and POD, NGSST was deemed better than OISST since it gave scores that were closer to the best value for each parameter. Diurnal correction applied in NGSST may reduce the measurement bias in the high SSTs. This analysis also revealed another fact: that the high-frequency signals captured by OISST in PSD analysis do not always correspond to HEs.

I also made comparisons between SST AMSR-E snapshots and the examined SST datasets. Figure 2.4 shows that OISST is very sensitive to the observation area of AMSR-E. Once the AMSR-E missed the observation, OISST included anomalously cold SST pattern. On the other hand, because of using the two microwave sensors i.e. AMSR-E and Windsat, the anomalously cold SST signals less appear in the NGSST product. Moreover, the high SST signals detected on the daytime AMSR-E image at around 155°E and 5°S was also not emerged on the NGSST image due to the diurnal correction.

Considering the results of PSD, probability test and AMSR-E snapshot comparison analysis, NGSST becomes the chosen dataset for detecting HE in the western equatorial Pacific. It also has been confirmed that for high SST (≥29°C), NGSST has small bias (-0.06°C) and root mean square error (0.47°C). The two microwave sensors significantly improve the observation coverage, and the diurnal correction reduces the errors arising from merging observations at different times. Moreover, because the HEs are characterized by enhanced diurnal variation of SST, the dataset with the diurnal correction has an advantage for detecting organized HEs.

2.2. HE detection method

2.2.1. Introduction

Besides selecting the reliable SST dataset, the HE detection method also becomes the important factor for investigating HE. The Pacific warm pool has strong seasonal variation. It shifts to the north (south) during boreal summer (winter) and only about half of the average area size of the pool is covered permanently in both seasons (Wyrtki, 1989). Qin et al. (2007) used a

time-dependent SST threshold of approximately 30°C to detect HEs, and Qin et al. (2008) used a fixed SST threshold of 30°C. Both of these methods are affected by seasonal variation and may underestimate SST variations associated with HE during the cold season. I proposed a new HE detection method independent from the seasonal variation described in Section 2.2.3.

2.2.2. Limitations of the previous HE detection method

For detecting HE in the Indo-Pacific warm pool, Qin et al. (2007) applied the following three thresholds:

(1) SST threshold of around 30°C,

(2) Areal threshold of 3×10^6 km^2,

(3) Time threshold of 10 days.

These thresholds emphasize the interannual variation in the tropical warm pool and then set that interannual variation as the background SST for determining the SST threshold. Qin et al. (2007) stated that a constant threshold is not robust due to the fluctuating background SST. Thus, their SST threshold is called the "time-dependent threshold" since it changes over time, following the interannual variation of the tropical warm pool (Fig. 2.5a). Therefore, the seasonal variation in the warm pool is not considered in this method, and HEs are rarely detected in the cold season. To overcome this problem, I improved the SST threshold method. I still used an SST of around 30 °C as my SST threshold, but, since the area monitored in this study is much smaller than that monitored by Qin et al. (2007), I modified the areal and time thresholds. Thus, this study proposes the new thresholds as describe in the following section.

2.2.3. New HE detection method

I developed the new HE detection method by improving the same threshold criteria as used by Qin et al (2007). They are SST threshold, area threshold and time threshold.

(1) SST threshold

To reduce the influence of season on HE detection, I used the daily mean SST averaged over the region where the daily temperature exceeded 27 °C (area within the 27 °C isotherm) to produce the background SST. Compared with the method of Qin et al.

(2007), our method significantly reduces seasonal variation in the background SST and is able to detect short-term variations (Fig. 2.5a). To identify the threshold while accounting for interannual and seasonal variations, the daily mean SST was low-pass filtered with a 101-day cutoff. The threshold was defined as the filtered background SST plus 1.4 °C, so the mean HE threshold was 30 °C. Because my threshold was defined by considering the variability in the SST over time as well as daily changes in the area of the 27 °C isotherm, I termed this threshold the "space–time-dependent threshold" (Fig. 2.5a).

(2) Area threshold

The area threshold was determined by the mean area with SST ≥ 30 °C in the study area during 2003–2011. This value was about 2×10^6 km^2.

(3) Time threshold

Webster et al. (1996) reported that, due to changes in ocean surface evaporation caused by SST variations, a timescale of 3–6 days was required for changes in cloud properties to feed back to the SST through their effects on the surface heat flux in the unstable tropical atmosphere. The time threshold was therefore determined by considering this timescale. Because HEs occurring under clear sky conditions may maintain their high SSTs for longer than 6 days, I set our time threshold to 6 days.

Thus, I defined an HE as a connected region with SSTs that are larger or equal to the space–time-dependent threshold (~30 °C), a minimum areal size of 2×10^6 km^2, and a duration of longer than 6 days. Figure 2.5b is an example of the temporal changes in areal size of regions with SSTs higher than the space–time-dependent threshold in 2004. For comparison, the results derived using the time-dependent threshold defined by Qin et al. (2007) are also shown in Fig. 2.5b. That time-dependent threshold did not detect high SSTs at the end of April and at the end of July. Therefore, my method is better suited to exploring the seasonal variation in HEs in the western equatorial Pacific.

2.2.4. Parameters for the HE characteristic

To examine the characteristics of the HEs, I used the following five parameters: duration, mean amplitude, mean areal size, speed of development, and speed of decay. The former three parameters were proposed in Qin et al. (2007) and the last two in this study. The duration of an HE in days is the period during which the HE is defined. The mean amplitude is the deviation of the areal-mean SST from the threshold (Qin et al. 2007):

$$Amplitude(x, y) = \frac{1}{T}\sum_{t=0}^{(t+T)}(SST(x, y, t) - threshold(t)) \quad (1)$$

where t is the time sequence (in days) from the HE start date to the HE end date. $T(x, y)$ denotes an HE duration for a given location (x, y). If SST(x, y, t) is lower than the threshold SST, summation in Eq. (1) is not computed. The area in which the HE amplitude is higher than 0°C is defined as the HE areal size.

The speeds of development and decay measure how fast the HE develops and decays. The temporal evolution of the area of the HE can be estimated using a linear function during the development and decay of the HE (Fig. 2.6), as follows:

$$a = vT + c \quad (2)$$

where a is the areal size (km^2), v is the developing or decaying speed (km^2/day), T is the number of days since the start of the developmental or decay stage, and c is a constant. The developmental stage is defined as the period of time from the day when the areal size starts to increase to the day when the areal size reaches its maximum (peak). The decay stage is defined as the period of time from the day when the areal size starts to decrease from the maximum to the day when the areal size reaches its minimum. To determine the speeds of development and decay, a correlation coefficient R^2 of ≥0.8 is required. In some cases, the HE had multiple peaks. In such cases, the development speed was calculated between the start point and the first peak and the decay speed was calculated between the last peak and the minimum.

2.3. Supporting datasets

Supporting datasets are needed to investigate the physical processes underlying the HE occurrence. In Chapter 3, I emphasize the effects of surface wind and solar radiation. For surface wind speed, I used 6-hourly reanalysis data from the Japanese 25-year Reanalysis (JRA-

25)/Japan Meteorological Agency (JMA) Climate Data Assimilation System (JCDAS) on a 1.25° horizontal grid (Onogi et al. 2007) for 2003–2011. I used daily net surface solar radiation on a 1°×1° grid for 2003–2009 from the International Satellite Cloud Climatology Project (ISCCP) dataset (Zhang et al. 2004). Daily latent heat and sensible heat fluxes on a 1° grid for 2003–2011 are obtained from the Objectively Analyzed Air-Sea Fluxes project (Yu and Weller 2007). These datasets are interpolated into 0.25° grid to synchronize with the SST dataset.

In Chapter 4, I emphasize the atmospheric effect and response during the development and decay of HEs. I used the parameters from 6-hourly reanalyses data by the Japanese 55-year Reanalysis (JRA55) on a 1.25° horizontal grid which consists of surface and 3-dimensional (3D) data (Kobayashi et al. 2015) for 2003-2011. The 3D dataset contains 37 isobaric surfaces. They are 1000, 975, 950, 925, 900, 875, 850, 825, 800, 775, 750, 700, 650, 600, 550, 500, 450, 400, 350, 300, 250, 225, 200, 175, 150, 125, 100, 70, 50, 30, 20, 10, 7, 5, 3, 2, and 1 hPa. The parameters are cloud cover (3D), convective heating rate (3D), vertical velocity (3D), divergence (3D), relative humidity (3D), surface wind, Sea Level Pressure (SLP), surface evaporation and precipitation. Additionally, I calculated surface divergence from surface wind data. I still used the ISCCP data for solar radiation (Zhang et al. 2004). These datasets are interpolated into 0.25° grid to synchronize with SST dataset. I also used the Global 30 Arc-second elevation (GTOPO30) for land elevation data.

For investigating the oceanic structure under the HE occurrence in Chapter 5, I used observational measurements from the TAO/TRITON buoys (McPhaden et al. 2009) located at the western equatorial Pacific (Fig.2.1). The parameters are temperature (surface and subsurface), surface wind, solar radiation, subsurface density (σ_τ) and surface current (10 m depth). The surface current divergence was calculated from the surface current data. Since the data consist of 6 quality grades, only the highest and default quality are used in the analysis. The position and depth interval of TAO/TRITON buoys for the measurement of temperature, density and current are shown in Fig. 2.7. Subsurface temperature and density are linearly interpolated into 1m, 10m, 20m, 30m, 40m, 50m, 60m, 70m, 80m, 90m, and 100m. Then, all parameters are interpolated into 1°grid interval (Akima, 1996). I used a critical temperature gradient of 0.02°C/m to determine mixed layer depth following the criteria of Wyrtki (1964) and Bathen (1972). I also calculated ocean heat content for each layer from subsurface temperature and density following this equation :

$$H = \rho_\tau C_p \int_{h2}^{h1} T(z)dz \quad (3)$$

where H is heat content (J/m^2), ρ_τ is density (kg/m^3), C_p is heat capacity of the ocean ≈ 4184 J/KgK, T is temperature (K), h2 and h1 are the deeper and shallower depth respectively. Again, the latent heat flux from ISCCP is also used in the analysis (Zhang et al. 2004).

2.4. Conclusions

In Chapter 2, I have described the datasets and method used in this study. The conclusions are as follows.

1) NGSST-O-Global-V2.0a was chosen for investigating HEs in the western equatorial Pacific. The two microwave sensors composing NGSST-O-Global-V2.0a, significantly improve the observation coverage, and the diurnal correction on the processing of NGSST-O-Global-V2.0a reduces the errors arising from merging observations at different times.
2) Improving new detection method which is free from seasonal effect, I defined an HE as a connected region with a SST higher than the space-time dependent threshold of about 30°C, with a minimum areal size of 2×10^6 km, and a duration period longer than 6 days.

Table 2.1 The specification of NGSST-O series developed by the Tohoku University (Modified from Table 1 of Hosoda et al. 2015)

Parameter	V. 1.0	V. 1.5	V. 1.6	V.2.0a
Infrared sensor	MODIS, AVHRR			
Microwave sensor	AMSR-E	AMSR-E, Windsat	AMSR-E, Windsat	AMSR-E, Windsat
Sub-sampling method	Nearest-neighbor	Nearest-neighbor	Bi-cubic or bi-linear	Bi-cubic or bi-linear
Diurnal correction	no	no	no	yes
Buoy validation (RMSE)[a]	0.79°C	0.74°C	0.61°C	0.48°C

[a]Version 1.0, 1.5 and 1.6 are validated against the buoy SST in the global ocean while V.2.0a is validated against the TAO/TRITON buoy SSTs within the study area.

Table 2.2 Contingency table component and attributes to examine the HE-detection performance of SST dataset.

Component / Parameter	Formula	Best Score	Examined SST datasets	
			OISST	NGSST
A[b]	-	-	6.65%	11.65%
B[b]	-	-	3.17%	5.12%
C[b]	-	-	6.05%	3.75%
D[b]	-	-	84.13%	79.49%
Accuracy (ACC)	ACC = (A+D)/(A+B+C+D)	1	0.91	0.91
Bias (Bi)	Bi = (A+B)/(A+C)	1	0.77	1.09[c]
False alarm ratio (FAR)	FAR = B/(A+B)	0	0.32	0.31[c]
Misses alarm ratio (MAR)	MAR = C/(A+C)	0	0.48	0.24[c]
Probability of detection (POD)	POD = A/(A+C)	1	0.52	0.76[c]

[b]See the text for the explanation of each component.

[c]The best value

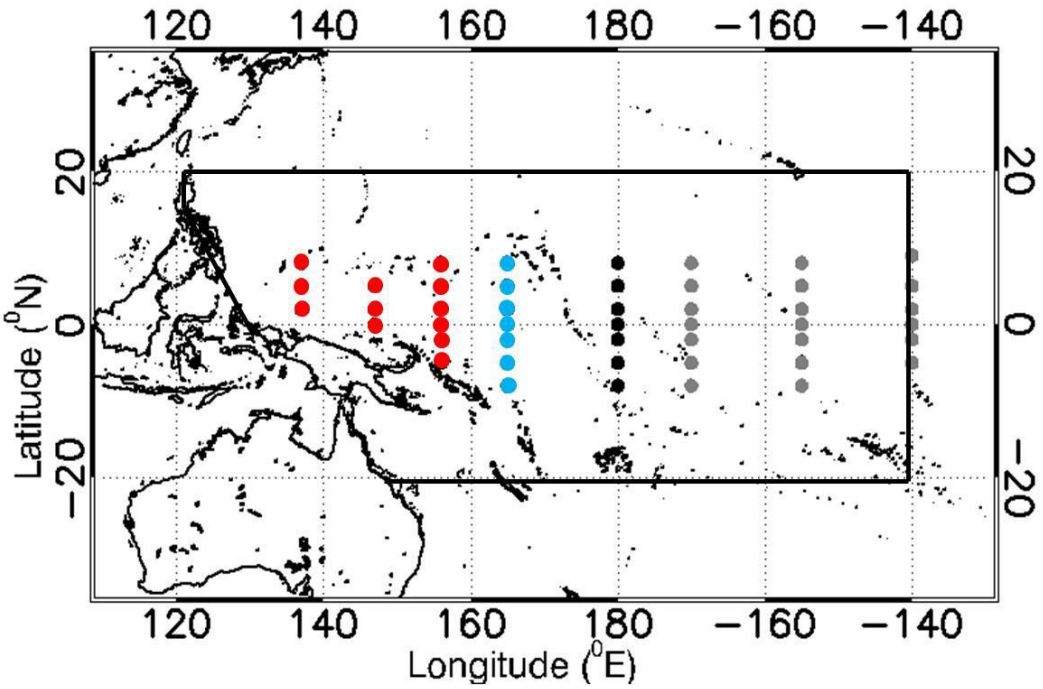

Fig. 2.1 The study area and the position of the TAO/TRITON buoys. The study area is rimmed by the black line. All dots are the positions of the TAO/TRITON buoys for SST, subsurface temperature and surface wind measurements used in the analysis. The *black/blue/red dots* are the TAO/TRITON buoys used for examining the SST dataset. The *blue/red dots* are the TAO/TRITON buoys for solar radiation measurements. The *red dots* are the position of 10m depth current and subsurface density (σ_τ) measurements used in the analysis.

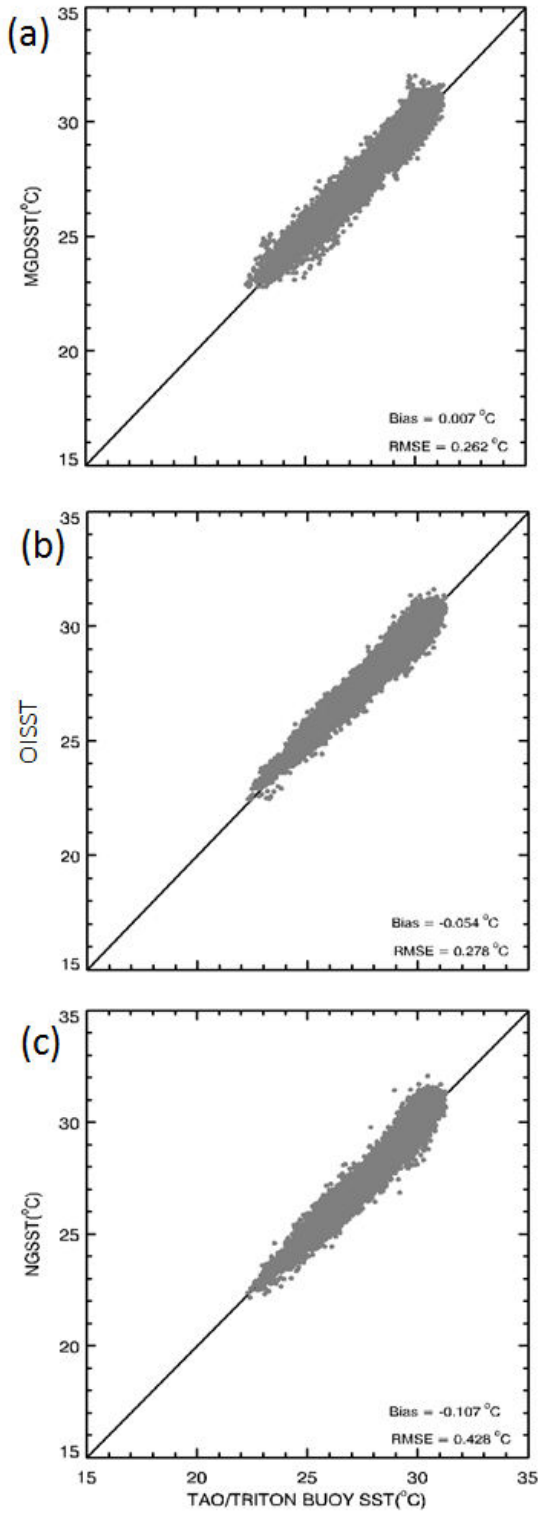

Fig. 2.2 Validation of (a) MGDSST, (b) OISST and (c) NGSST datasets against the TAO/TRITON buoy SSTs.

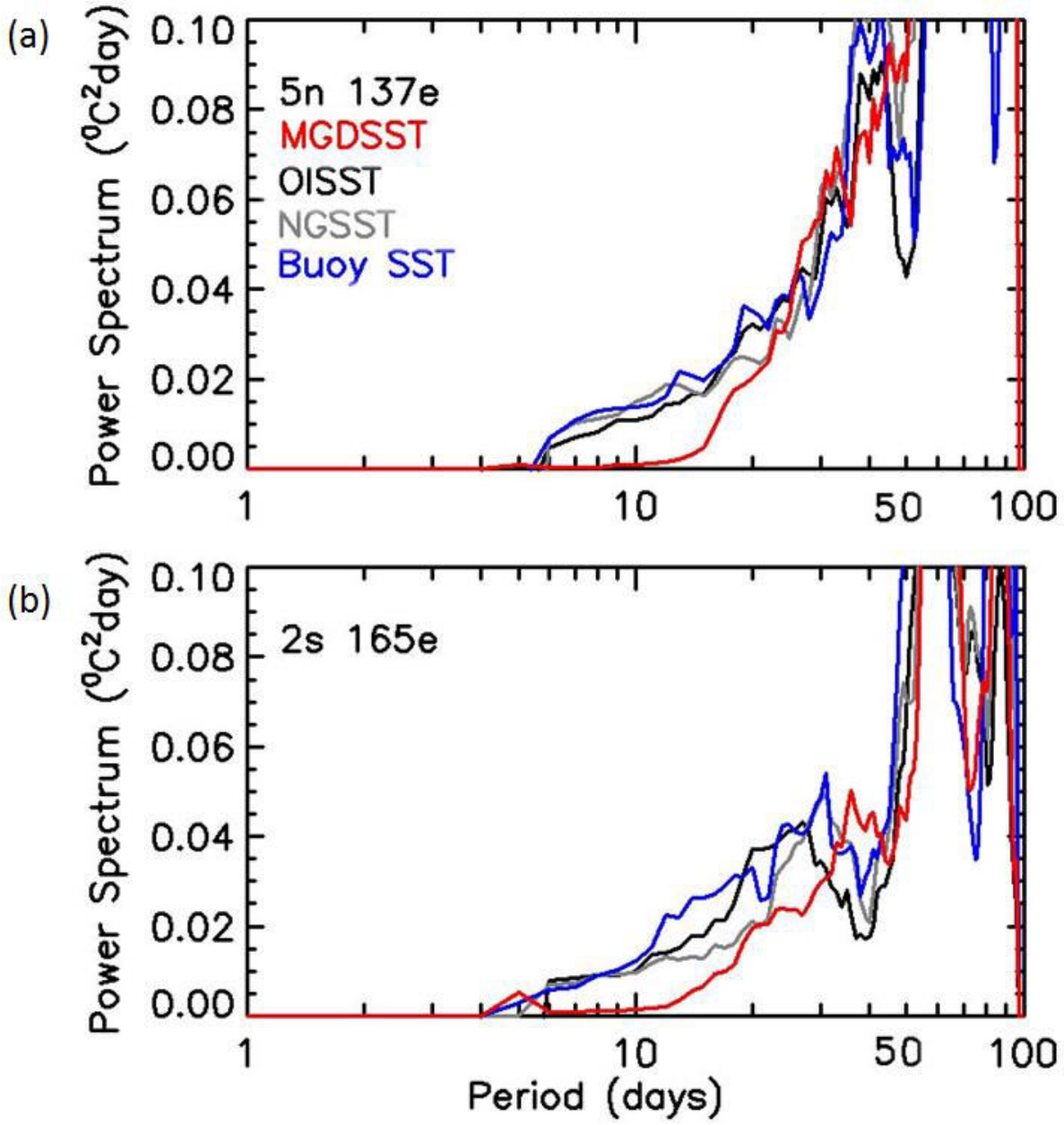

Fig. 2.3 Power Spectral Density analysis of SST datasets and SST obtained from the TAO/TRITON buoy at (a) 5°N, 137°E and (b) 2°S, 165°E.

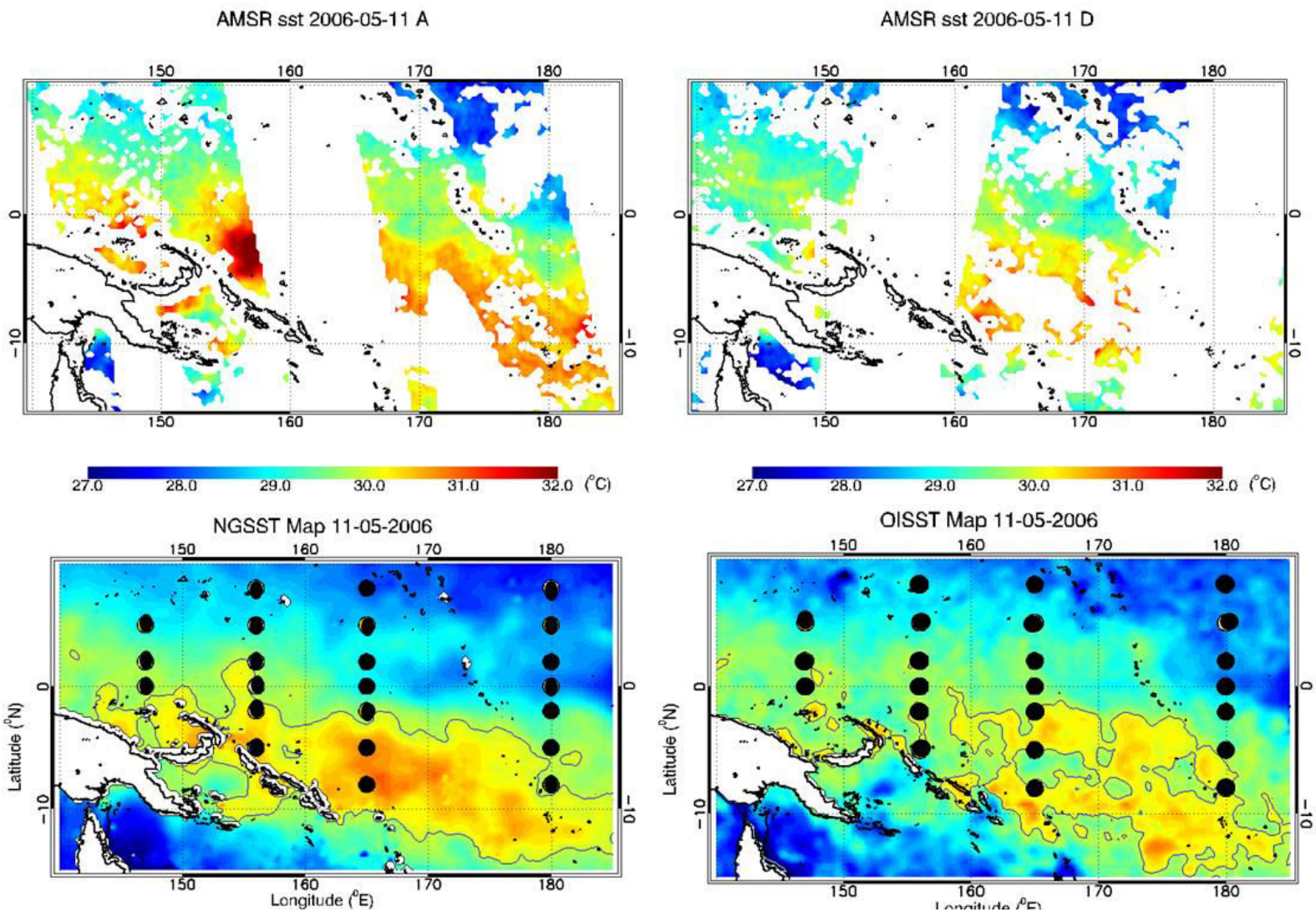

Fig. 2.4 Comparison of NGSST and OISST with AMSR-E Snapshot at 2006-05-11 A (Ascending/daytime) and D (Descending/nighttime). The *gray contour* in the lower panels denotes the SST threshold.

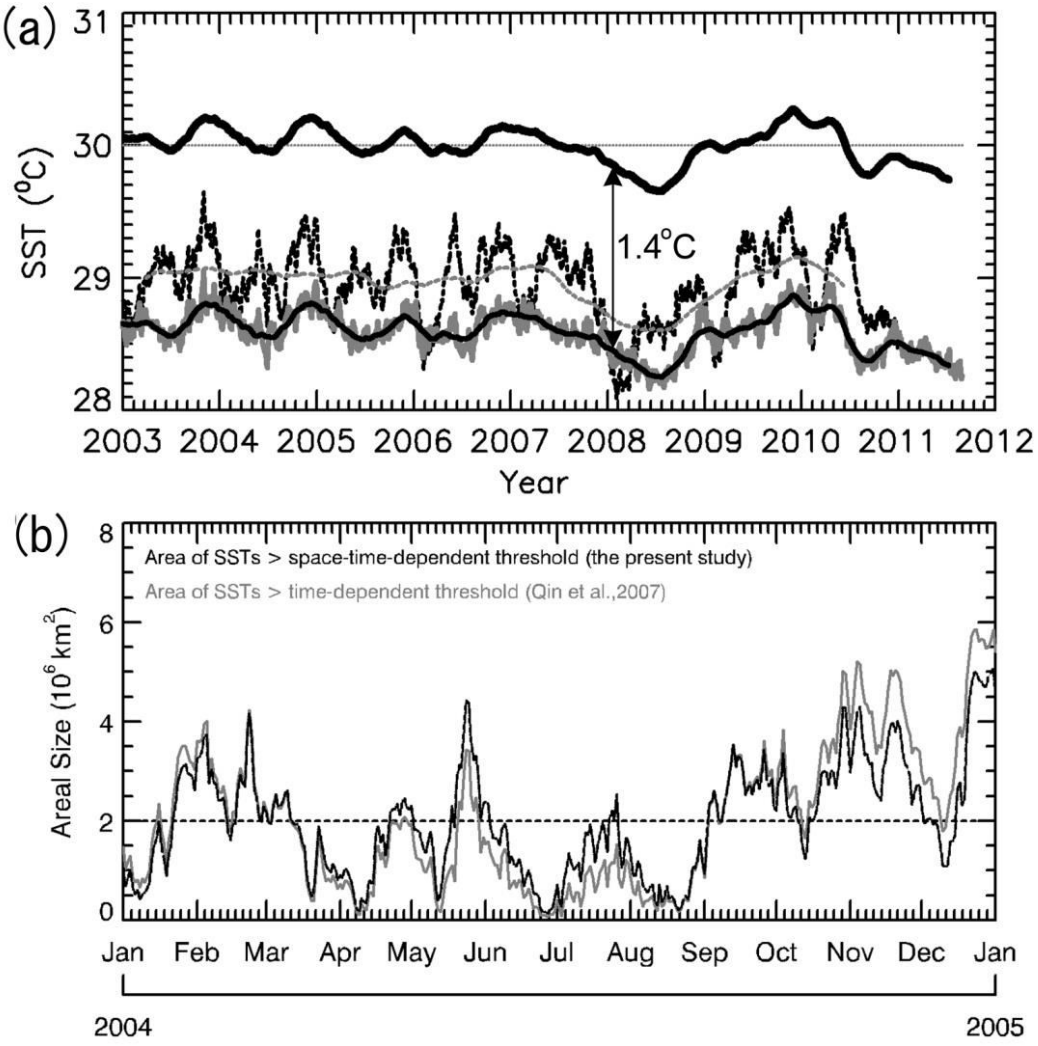

Fig. 2.5 (a) Description of the SST threshold. The *dotted gray line* denotes the reference SST threshold (i.e., 30 °C) that was used in previous HE studies. The *broken gray line* represents the time-dependent threshold assigned by Qin et al. (2007) and produced by the 400-day low-pass filter of the daily mean SST in the warm pool (*black broken line*). The *solid gray line* (the background SST) represents the daily mean SST inside the daily 27 °C isotherm. The *thin black line* (the filtered background SST) is produced by the 101-day low-pass filter of the *solid gray line*. The *thick black line* denotes the space–time dependent threshold calculated from the filtered background SST plus 1.4 °C. (b) Temporal changes in the size of the area where SSTs were higher than the thresholds in 2004. The *black line* represents the change in the areal size, based on the space–time-dependent threshold of the present study; the *gray line* denotes the change based on the time-dependent threshold of Qin et al. (2007). The *dashed line* represents the areal size threshold (i.e., 2×10^6 km^2).

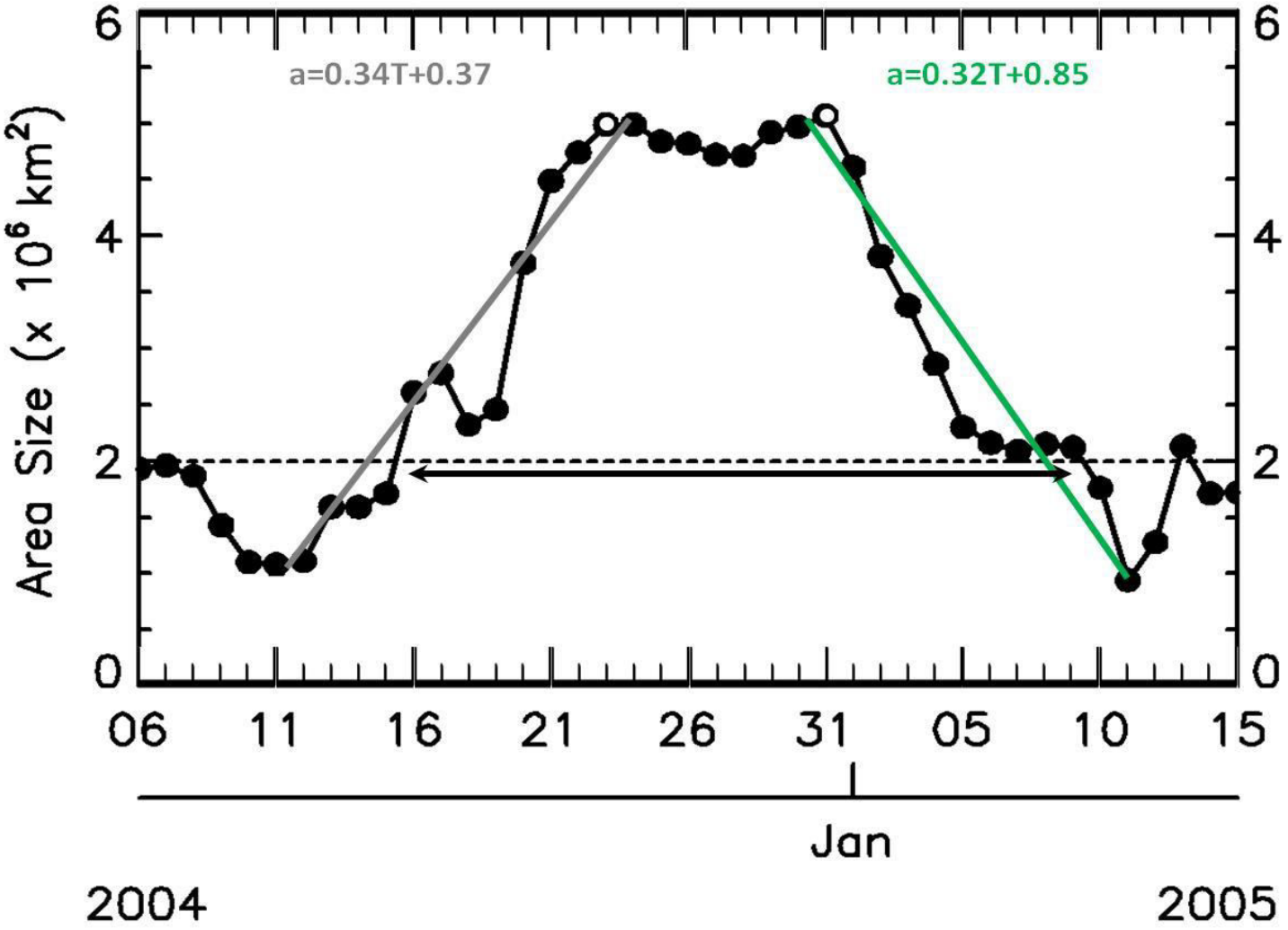

Fig. 2.6 Temporal changes of the areal size with SSTs higher than the threshold for HE041216 (*black circles* with a *black line*). *Hollow points* represent HE peaks. The *black dashed line* denotes the area threshold. The *black arrow* denotes the HE period. The *gray* and *green lines* represent the linear fits for developing and decaying speeds, respectively.

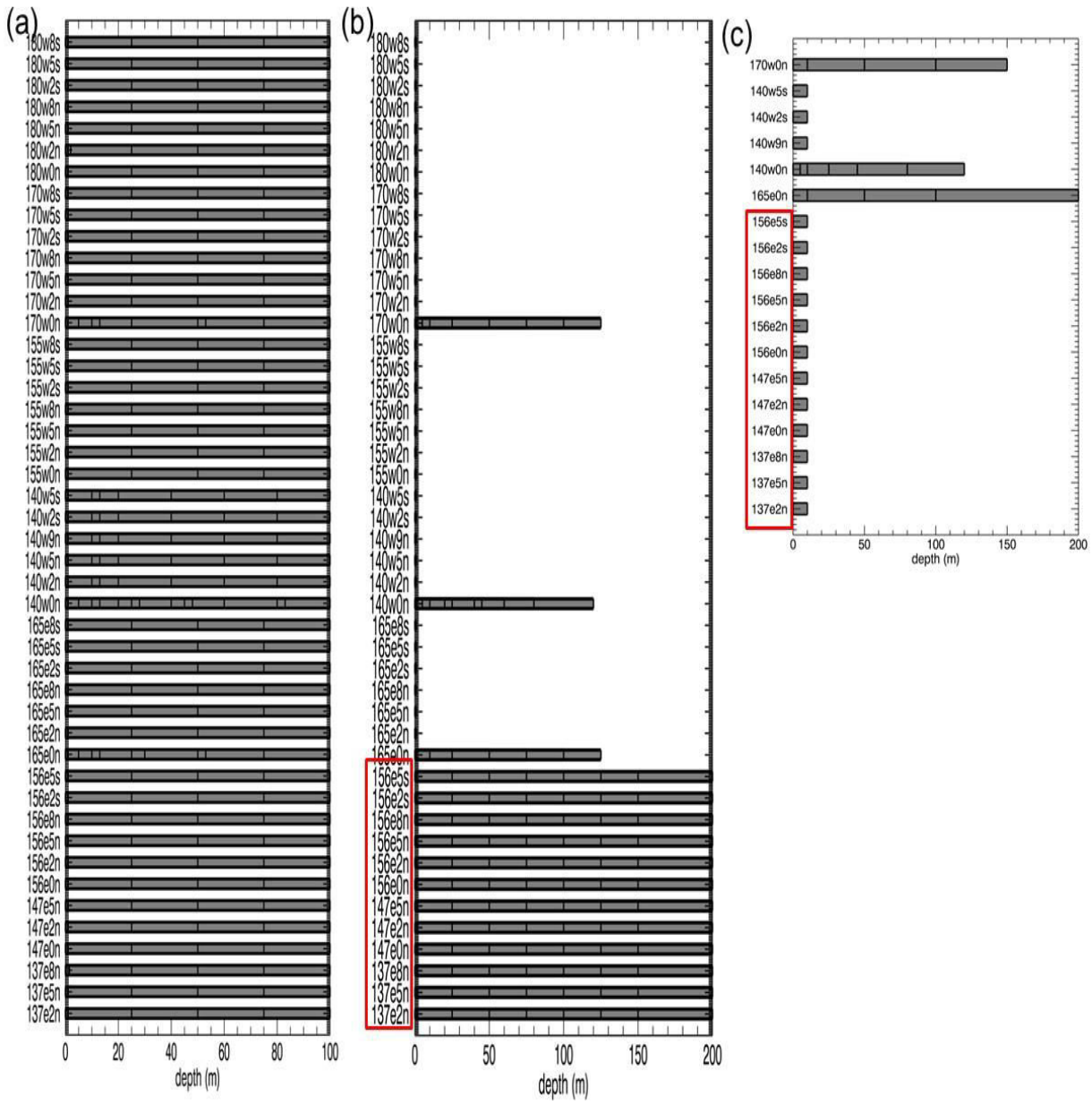

Fig. 2.7 The histogram of the position and depth interval of the TAO/TRITON buoys for the measurement of (a) temperature , (b) density and (c) current. The *red boxes* denote the chosen buoy for density and current measurements.

Chapter 3

Climatology of hot events in the western equatorial Pacific

3.1. Introduction

Qin et al. (2007) has investigated the climatology of HE in the equatorial region. Since their SST threshold is still influenced by the seasonal variation and also their area (period) threshold are larger (longer) than my threshold they only detected 31 HE cases during 10 years observation. Thus, the seasonal variation of HE and the relation between the HE occurrence and the climatological SST in the Indo-Pacific warm pool were less pronounced in their analysis.

Proposing the new threshold independent from seasonal variation, I focused the climatological study of the HEs in the western equatorial Pacific. The distribution and seasonal variation of the HEs is described in Section 3.2 along with its relation with climatological SST in the Pacific warm pool. Section 3.3 clarifies their occurrence mechanism. Since the present HE study cannot be separated with the previous one, I made comparison of them in Section 3.4. The summary is given in Section 3.5.

3.2. Distribution, seasonal variation and relation with the Pacific warm pool

3.2.1. Distribution

I identified 71 cases of HEs in the western equatorial Pacific for 2003–2011. Table 3.1 lists the properties of HEs, and Fig. 3.1 presents their histograms with their seasonal distribution. Their durations ranged from 7–44 days with a mean of 18.14 days. Areal sizes ranged from 2.17 $\times 10^6$ km^2 – 11.48 $\times 10^6$ km^2 with a mean of 6.30 $\times 10^6$ km^2. The mean amplitude was 0.33°C. The speed of development (decay) ranged from 0.08 $\times 10^6$ km^2/day – 0.81 $\times 10^6$ km^2/day (0.08 $\times 10^6$ km^2/day – 1.34 $\times 10^6$ km^2/day), with a mean of 0.28 $\times 10^6$ km^2/day (0.31 $\times 10^6$ km^2/day). The

mean period during the boreal summer (April–September) was 16.7 ± 8.84 days which was shorter than that during the boreal winter (October–March) i.e., 19.4 ± 9.48 days. The amplitude during the boreal summer (0.31 ± 0.06°C) was a bit lower than in the boreal winter (0.35 ± 0.05°C). During the boreal summer, HEs developed and decayed faster (i.e., 0.31 ± 0.12 × 10^6 km^2/day and 0.36 ± 0.28 × 10^6 km^2/day) than during the boreal winter (i.e., 0.25 ± 0.15 × 10^6 km^2/day and 0.27 ± 0.17 × 10^6 km^2/day). The areal size was almost the same in both season i.e., 6.3 × 10^6 km^2. The location of all detected HE is shown by the amplitude map depicted in the Appendix.

3.2.2. Seasonal variation

I show in Fig. 3.2 the HE occurrence rates in each grid of the study area for the whole season, for the boreal summer, and for the boreal winter. The HEs are distributed in the equatorial band to the subtropical Pacific (20°S to 30°N), with an eastward extension to 150°W. Moreover, a high occurrence rate of HEs (>10 %) is observed along the northern coasts of New Guinea and the Solomon Islands to 180°E. The HE occurrence distribution exhibits seasonal shifts: a northward shift during boreal summer and a southward shift during boreal winter (Fig. 3.2b and c). These seasonal shifts are consistent with the seasonal shifts in SST climatology, which have been analyzed by many researchers (e.g., Wyrtki 1989; Kim et al. 2012). The north–south shift of the region of HE occurrence is confined to the west of 170°E. By applying the new detection method, which can detect HEs regardless of the seasonal variation in SST, I have been able to demonstrate a seasonal variation in HEs for the first time.

3.2.3. Relation with the Pacific warm pool

From Fig. 3.2, we can see that most HEs occurred in the western Pacific warm pool. The area where the SSTs exceed 28 °C usually corresponds to the warm pool area. Figure 3.2a shows that the pattern of long-term SSTs agrees well with the HE occurrence distribution. Furthermore, the climatological isotherm of 29.5 °C coincides with an HE occurrence rate of >15 % during both boreal summer and boreal winter (Fig. 3.2b and c). Thus, higher rates of the HE occurrence correspond to higher climatological SSTs. I also produced histograms of mean relative frequency of SSTs for the whole study period and for periods during which HEs were present in the study

area (Fig. 3.3). HEs contributed 51.5 % of the SSTs >30 °C in the warm pool; the high SST tail of the histogram consists of an accumulation of well-organized high SSTs associated with HEs. These results suggest that the HE occurrence distribution corresponds to the climatological SST of the Pacific warm pool.

I understand that I cannot analyze the relation between HE occurrence and the warm pool using the SST alone. For instance, the water column below the warm pool may or may not influence the occurrence of HEs. The relation between HE and the water column below the warm pool is shown by buoy analysis for the HE started on 16 December 2004 (hereafter HE041216; Fig. 3.4a). Before 17 December 2004, the SST was similar to the temperatures at depths of 25 m and 50 m, indicating the existence of a well-mixed ocean layer. This occurred under conditions of strong wind speeds. From 17 to 31 December 2004, the wind speed was weaker, the water column was more stratified, and an HE occurred during this period. This indicates that a low wind speed is important for suppressing oceanic mixing and entrainment during the period of the HE. However, a general conclusion can only be drawn following the analysis of more HEs and buoy data. The physical processes between the HEs and the water column of the Pacific warm pool is discussed in Chapter 5.

3.3. Mechanisms of the HE occurrence

3.3.1. Case study of HE041216

Qin et al. (2007) suggested that HE occurs with large amplitude of diurnal SST under the condition of high solar radiation and low wind speed. The same conclusion was also drawn based on the results of my investigation into HEs. For example, I show a time evolution of a HE041216 (Fig. 3.4a). HE041216 was chosen for this case study since this HE has the closest characteristic (period, areal size, amplitude and speed of development and decay) to the mean value. Thus, this can be a representative for HEs occurred in the western equatorial Pacific. The temporal change in HE041216 area is correlated with the variation of solar radiation, but inversely correlated with the variation of wind speed. I found the evidence of large amplitude of diurnal SSTs, as estimated from hourly SST of the TAO/TRITON buoys and an example is provided for buoy at 0°N, 156°E (Fig. 3.4b). From 17 to 31 December 2004, the increases of daily SST are coincident with the large amplitude of diurnal SSTs caused by high levels of solar radiation and low wind

speeds. Thus, the result of this case study is consistent with those of Qin et al (2007).

3.3.2. Climatological analysis

I performed an analysis of all HEs in order to obtain a general consensus about the mechanisms that generate HEs in the western equatorial Pacific. Figure 3.5a, b present the relative frequency of each value of solar radiation and wind speed inside and outside HEs during periods when HEs were present. For comparison, the corresponding climatological relative frequencies in our study area throughout the study period are also plotted. The frequency distributions for solar radiation and wind speed outside HEs are similar to the corresponding climatological frequencies (Fig. 3.5a, b). The solar radiation outside HEs ranges from 50 to 350 W/m^2, with the mode being 280 W/m^2. The negatively skewed distribution indicates that the solar radiation outside HEs is mainly high in the western equatorial Pacific. Inside HEs, the peak is slightly lower (260 W/m^2), but the relative frequency of this peak is higher (10 % rather than 8 %). The relative frequencies of solar radiation levels from ~200 to 290 W/m^2 increase in HEs. Nevertheless, this is compensated for by the change in the top end of the distribution, from ~340 to 320 W/m^2. Thus, the mean solar radiation levels observed inside and outside the HEs were almost equal (i.e., ~225 W/m^2) when HEs were present.

Contrasting results are seen for the wind speed distribution. The peak in the relative frequency distribution of wind speed is 7 m/s outside HEs but only 2 m/s inside HEs. The normal distribution observed for the wind speed outside HEs becomes a positively skewed distribution inside HEs. This result explains the large difference between the mean wind speeds inside and outside HEs (i.e., 2.56 and 5.99 m/s, respectively). Moreover, Fig. 3.6 clarifies that, during HEs, high solar radiation levels of ~200 to 300 W/m^2 often occur both inside and outside HEs, whereas low wind speeds of 0–5 m/s often occur only in the HEs, as indicated by relative frequencies of >1 %. The high relative frequencies of high levels of solar radiation and low wind speeds inside HEs (when they are present) also represent positive anomalies compared to the climatology of the study area. Thus, climatologically, high solar radiation levels often occur throughout the study area during HEs, while low wind speeds only often occur within HEs during the HE periods. Therefore, low wind speeds are key to the persistence of high SSTs inside HEs during the HE periods.

The composite map of solar radiation and wind speed during the HE periods demonstrated the same tendencies, and these tendencies also explained the mechanisms for the seasonal shifts in the HE. Although the area receiving solar radiation levels of more than 200 W/m^2 shifts northward during boreal summer (Fig. 3.7a) and southward during boreal winter (Fig. 3.7c), almost the whole of the study area receives high levels of solar radiation during both seasons, which indicates that the sea surface receives high levels of solar radiation both inside and outside HEs during HE periods. During boreal summer, the area that receives solar radiation levels of more than 200 W/m^2 extends from 0°N to 40°N. The area in which the HE occurrence rate >5 % expands to the north. Solar radiation levels of less than 200 W/m^2 that occur south of the Solomon Islands extend south-eastwardly. The low levels of solar radiation (<200 W/ m^2) observed south of the Solomon Islands coincide with HE occurrence rates of <5 %. During boreal winter, the area with high levels of solar radiation shifts to the south, suppressing the occurrence of HEs to the north. In both seasons, the area with solar radiation levels of more than 230 W/m^2 shows a lower rate of HE occurrence. This result indicates that, although the HE occurrence requires solar radiation levels of more than 200 W/m^2, higher levels of solar radiation do not always lead to higher rates of HE occurrence. Moreover, the seasonal shifts in the pattern of solar radiation influence the seasonal shifting in the HE distribution.

Wind speed shows the most prominent correlation with the HE occurrence rate. Low wind speeds of less than 4 m/s are localized along the northern coast of New Guinea and the Solomon Islands to 180°E during both seasons. This low wind speed area coincides with the high HE occurrence rate area (Fig. 3.7b, d). In both seasons, few HEs are detected on the east side of the study area (which receives solar radiation levels of more than ~230 W/m^2), since the wind speeds in those areas are also high (>4 m/s). During boreal summer, the low wind speed area expands to the north from 120°E to 140°E. Since the solar radiation levels are also high, HEs often occur in this area. On the other hand, the high wind speeds (>4 m/s) together with low solar radiation levels (<200 W/m^2) to the south of the Solomon Islands restrict the number of HEs. During boreal winter, the appearance of a high wind speed area (>6 m/s) along the band from 10°N to 20°N suppresses the occurrence of HEs, even though the solar radiation levels remain >200 W/m^2 in this area. This result suggests that the wind speed pattern is highly correlated to the HE occurrence rate, and the seasonal shifts in the HE distribution are influenced by the seasonal shifts in solar radiation levels and wind speeds.

I analyzed latent and sensible heat data in order to confirm the link between the low wind speeds and the persistence of high SST inside the HE area. As shown in Fig. 3.5c, the latent heat losses inside and outside the HE areas when HEs are present range from ~30 to 240 W/ m^2. The latent heat losses inside HEs are clearly lower than those seen outside HEs. Sensible heat losses are higher inside than outside HEs (Fig. 3.5d). However, this factor does not significantly affect the total heat loss because the maximum sensible heat loss is only ~20 W/m2. I can therefore conclude that, although the mean solar radiation levels inside and outside HEs are almost equal, the presence of low wind speeds inside HEs reduces latent heat loss, so high SSTs are maintained during HEs.

3.4. Discussion

I summarize the comparison of the present HE study with Qin et al. (2007) (Table 3.2). I emphasize 2 points for discussion as described below.

1) To investigate the mechanisms for the formation of HEs, both studies analyzed the atmospheric and heat flux parameters during HE periods. Comparison between Fig. 3.6a,b and Fig. 3.8a, b shows the difference between the mechanism for the occurrence of HEs across the whole equatorial region and the mechanism for the occurrence of HEs in the western equatorial Pacific. Across the whole equatorial region, high levels of solar radiation and low wind speeds are equally important for the HE occurrence; in the western equatorial Pacific, low wind speeds are the key factor. Nevertheless, since high levels of solar radiation and low wind speeds are much more (less) common during the development (decay) stage (Fig. 3.4b), analyzing stages of HEs may yield a better understanding of the mechanism leading to HEs. This work is described in Chapter 4.

2) Qin et al. (2007) found that HEs occur within the 28 °C isotherm of the long-term SST pattern. However, they did not mention anything about the long-term SST distribution. On the other hand, most studies of long-term SST patterns have ignored high-frequency phenomena. For example, Clement et al. (2005) only analyzed their dataset on an annual mean scale. Our results link the gap between short-term and long-term SST phenomena. I found that the HEs, which occur under conditions of low wind speeds and high levels of solar radiation, are related to the western Pacific warm pool via the statistical long-term mean SST.

3.5. Conclusions

The conclusions of the climatological study of HE in the western equatorial Pacific are described below.

1) I detected 71 HEs during 2003–2011 in the western equatorial Pacific. These HEs had a mean areal size of 6.30×10^6 km^2, a mean period of 18.14 days, a mean amplitude of 0.33 °C, and a mean speed of development (decay) of 0.28 (0.31) $\times 10^6$ km^2/day.

2) The HEs were distributed within the equatorial band to subtropical Pacific (20°S to 30°N) and extended eastward to 150°W. They frequently occurred along the northern coasts of New Guinea and the Solomon Islands, with an eastward extension to 180°E. The HE distribution also exhibited seasonal variation, shifting northward and southward during boreal summer and boreal winter, respectively. These seasonal shifts were similar to the seasonal shifts seen in the long-term SST patterns.

3) The observed distribution of HE occurrences indicates that HE formation is related to the formation of the Pacific warm pool via the long-term SST. Higher occurrence rates of HE correspond to higher climatological SSTs. In the warm pool area enclosed by the 29.5 °C isotherm of the climatological SST, HEs contributed 51.5 % of the SSTs >30 °C.

4) The presence of low wind speeds is a key factor in the mechanism for the occurrence of HEs in the western equatorial Pacific. During the HE periods, high solar radiation levels occur across much of the equatorial region. In areas where wind speeds are low, latent heat loss is reduced and high SSTs occur, leading to the occurrence of HEs.

5) The seasonal shifts in the HE distribution are influenced by the seasonal shifts in wind speed and solar radiation.

Table 3.1 Properties of HEs in the western equatorial Pacific[a].

No.	Start Date	Period (days)	Areal Size ($\times 10^6$ km^2)	Dev. Speed ($\times 10^6$ km^2/day)	Dec. Speed ($\times 10^6$ km^2/day)	Mean Amp. ($^\circ$C)	Number of Peaks	Location (See Appendix I)
1	16-Jan-03	8	4.21	0.22	0.13	0.32	1	HE030116
2	19-Feb-03	16	7.15	0.13	0.59	0.29	1	HE030219
3	20-Mar-03	20	6.6	0.37	0.19	0.27	>2	HE030320
4	13-Apr-03	18	6.15	0.14	0.20	0.22	1	HE030413
5	30-Apr-03	27	7.35	0.33	0.46	0.24	>2	HE030430
6	28-May-03	9	5.74	0.30	0.24	0.30	1	HE030528
7	27-Jun-03	14	5.32	0.37	0.23	0.27	2	HE030627
8	25-Jul-03	11	3.44	0.20	0.29	0.54	2	HE030725
9	25-Aug-03	12	5.94	0.48	1.34	0.28	>2	HE030825
10	18-Sep-03	10	6.01	0.47	0.21	0.28	1	HE030918
11	21-Oct-03	25	11.48	0.48	0.24	0.29	2	HE031021
12	14-Nov-03	21	6.12	0.21	0.08	0.29	>2	HE031114
13	4-Dec-03	19	5.95	0.23	0.18	0.42	1	HE031204
14	22-Dec-03	9	4.97	0.34	0.47	0.30	1	HE031222
15	22-Jan-04	23	6.76	0.30	0.17	0.35	2	HE040122
16	18-Feb-04	10	5.87	0.28	0.45	0.26	1	HE040218
17	4-Mar-04	8	4.99	0.30	0.19	0.26	2	HE040304
18	22-Apr-04	10	3.64	0.21	0.13	0.37	2	HE040422
19	20-May-04	14	6.15	0.32	0.21	0.28	1	HE040520
20	9-Sep-04	32	6.26	0.26	0.27	0.32	>2	HE040909
21	15-Oct-04	31	8	0.13	0.19	0.35	2	HE041015
22	14-Nov-04	18	7.12	0.21	0.16	0.32	1	HE041114
23	16-Dec-04	25	7.51	0.34	0.32	0.32	2	HE041216
24	20-Jan-05	16	6.36	0.49	0.19	0.30	1	HE050120
25	20-Mar-05	7	3.79	0.10	0.15	0.32	1	HE050320
26	1-Apr-05	15	5.23	0.23	0.24	0.35	>2	HE050401
27	13-May-05	22	8.12	0.39	0.13	0.30	>2	HE050513
28	6-Jul-05	10	6.94	0.37	0.93	0.28	1	HE050706
29	14-Oct-05	20	7.06	0.25	0.47	0.33	2	HE051014
30	18-Nov-05	23	6.21	0.14	0.13	0.38	1	HE051118
31	10-Dec-05	42	6.49	0.33	0.17	0.47	>2	HE051210
32	20-Apr-06	9	4.46	0.26	0.46	0.31	1	HE060420
33	8-May-06	9	5.68	0.16	0.11	0.31	1	HE060508
34	16-May-06	12	6.03	0.53	0.28	0.40	>2	HE060516
35	27-May-06	33	7.99	0.27	0.14	0.41	1	HE060527
36	28-Aug-06	33	11.18	0.30	0.90	0.31	>2	HE060828

Table 3.1 (Continued). Properties of HEs in the western equatorial Pacific[a].

No.	Start Date	Period (day)	Areal Size ($\times 10^6$ km^2)	Dev. Speed ($\times 10^6$ km^2/day)	Dec. Speed ($\times 10^6$ km^2/day)	Mean Amp. ($^\circ$C)	Number of Peaks	Location (See Appendix I)
37	10-Oct-06	23	5.43	0.26	0.42	0.36	>2	HE061010
38	5-Nov-06	16	7.31	0.17	0.77	0.33	1	HE061105
39	19-Dec-06	15	6.99	0.38	0.28	0.31	2	HE061219
40	2-Jan-07	16	5.99	0.21	0.23	0.41	2	HE070102
41	7-Mar-07	16	5.54	0.81	0.33	0.31	>2	HE070307
42	9-Apr-07	33	7.84	0.40	0.39	0.25	>2	HE070409
43	21-Jun-07	20	8.8	0.25	0.32	0.36	1	HE070621
44	16-Jul-07	18	6.93	0.72	0.29	0.37	2	HE070716
45	28-Aug-07	30	7.95	0.29	0.13	0.31	1	HE070828
46	3-Oct-07	42	8.5	0.20	0.47	0.39	>2	HE071003
47	13-Dec-07	8	4.16	0.59	0.19	0.37	1	HE071213
48	23-Dec-07	9	3.7	0.11	0.33	0.38	1	HE071223
49	19-Jul-08	11	5.87	0.33	0.89	0.26	2	HE080719
50	8-Aug-08	7	5.11	0.38	0.43	0.24	1	HE080808
51	18-Aug-08	8	5.97	0.39	0.15	0.25	1	HE080818
52	5-Sep-08	19	8.41	0.21	0.56	0.37	1	HE080905
53	26-Nov-08	44	7.38	0.13	0.59	0.45	>2	HE081126
54	10-Mar-09	10	5.69	0.42	0.26	0.31	1	HE090310
55	3-May-09	29	6.19	0.34	0.18	0.35	>2	HE090503
56	31-May-09	13	6.12	0.24	0.21	0.28	1	HE090531
57	7-Sep-09	9	6	0.23	0.64	0.32	1	HE090907
58	8-Oct-09	18	8.2	0.26	0.13	0.38	1	HE091008
59	25-Oct-09	15	8.04	0.13	0.37	0.40	1	HE091025
60	8-Nov-09	27	7.85	0.18	0.27	0.33	>2	HE091108
61	17-Dec-09	19	5.79	0.10	0.16	0.30	1	HE091217
62	4-Jan-10	25	7.7	0.21	0.21	0.41	1	HE100104
63	9-Apr-10	28	7.59	0.34	0.26	0.30	>2	HE100409
64	11-Dec-10	14	4.96	0.2	0.44	0.39	2	HE101211
65	9-Jan-11	9	3.86	0.15	0.08	0.41	1	HE110109
66	31-Jan-11	30	5.26	0.1	0.08	0.44	2	HE110131
67	1-Mar-11	13	3.56	0.08	0.09	0.45	1	HE110301
68	30-Mar-11	26	6.08	0.09	0.11	0.4	1	HE110330
69	28-Apr-11	9	3.63	0.12	0.09	0.36	1	HE110428
70	13-May-11	10	5.07	0.14	0.32	0.26	1	HE110513
71	29-May-11	8	5.27	0.25	0.34	0.32	1	HE110529
Mean		**18.14**	**6.30**	**0.28**	**0.31**	**0.33**		

[a]See the text for an explanation of each property.

Table 3.2 Comparison of Hot Events detected by Qin et al. (2007) and in the present study.

Item	Qin et al. (2007)	The present study
Dataset used	Global OI SST with a spatial resolution of 0.1°×0.1° (Kawai et al. 2006)	NGSST-O-Global-V2.0a with a grid interval of 0.25° (Hosoda manuscript in preparation)
Time frequency	Daily (Kawai et al. 2006)	Daily (Hosoda manuscript in preparation)
Study area	Equatorial region	Western equatorial Pacific
Period of observation	1993–2003	2003–2011
Definition	A connected region with SST > the time-dependent threshold (of about 30°C), having a minimum areal size > 3×10^6 km^2, and lasting for a period longer than 10 days	A connected region with SST > the space-time-dependent threshold (of about 30°C), having a minimum areal size > 2×10^6 km^2, and lasting for a period longer than 6 days
Total detected number (number/year)	31 (2.8/year)	71 (8.9/year)
Mean duration period	24.2 days (Qin et al, 2007, Table 2)	18.14 days (Table 1)
Mean areal size	15.7×10^6 km^2 (Qin et al. 2007, Table 2]	6.3×10^6 km^2 (Table 1)
Mean amplitude	0.25°C (Qin et al. 2007, Table 2)	0.33°C (Table 1)
Relationship with long-term SST pattern	HEs occur within the 28°C contour of the long-term SST pattern (Qin et al. 2007, Fig.6)	HEs make an important contribution to the formation of the long-term SST pattern (Fig. 5)
HE generating factor	HEs occur under conditions of low wind speeds and high solar radiation (Qin et al. 2007, Fig. 9)	Low wind speed is the key factor for HE occurrence mechanism(Fig. 8,9,10)

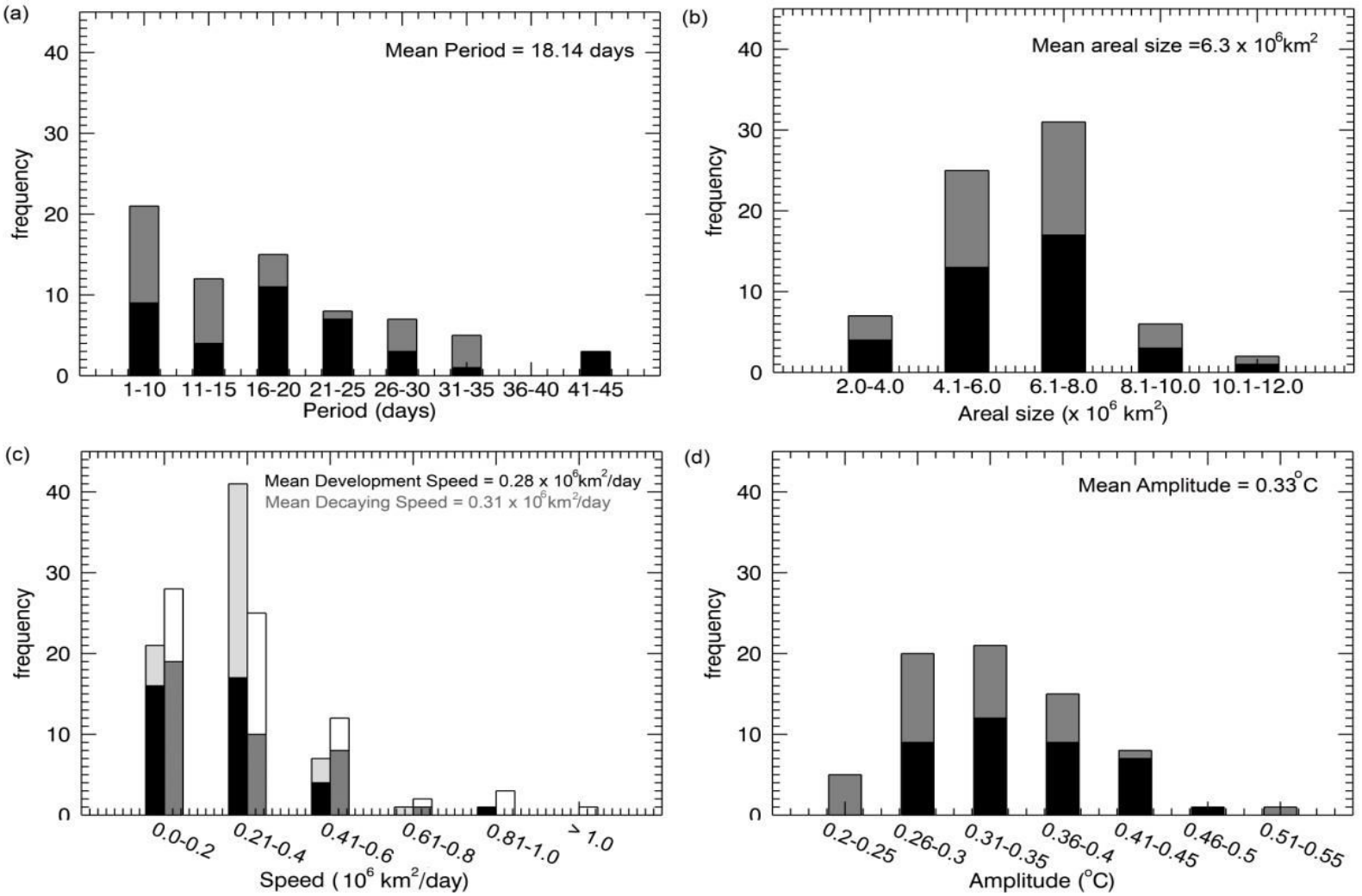

Fig. 3.1 Histograms of the properties of the 71 HE cases found in the western equatorial Pacific: (a) period, (b) areal size, (c) developing and decaying speeds, and (d) amplitude. *Upper (lower) bar* denotes boreal summer i.e., April-September (winter i.e., October–March).

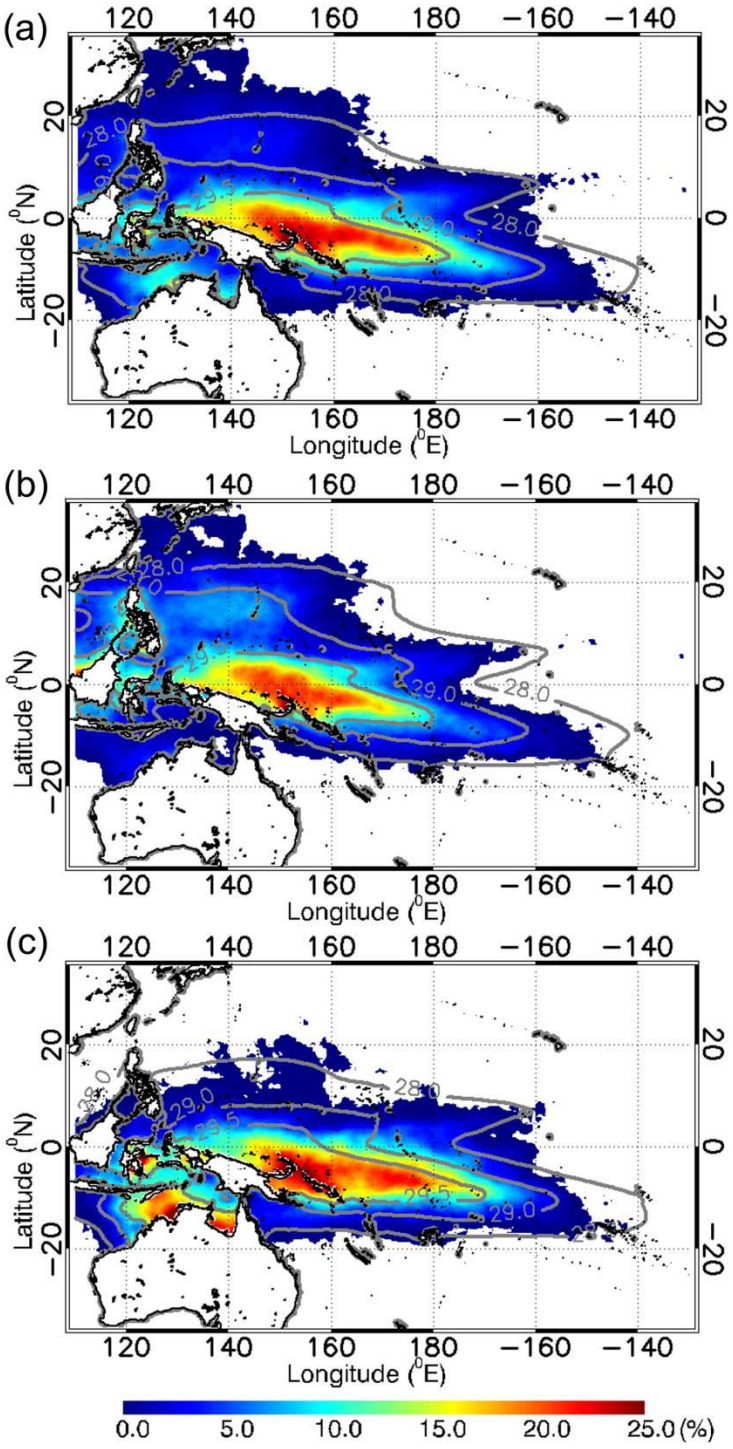

Fig. 3.2 Occurrence rates of HEs shown in frequency per bin (%) during 2003–2011, for (a) the whole period (100% is 3163 days; ≈ 9-year period), (b) boreal summer (April–September; 100% is 1615 days), and (c) boreal winter (October–March; 100% is 1548 days). The *gray contour* represents the mean SST climatology (2003–2011).

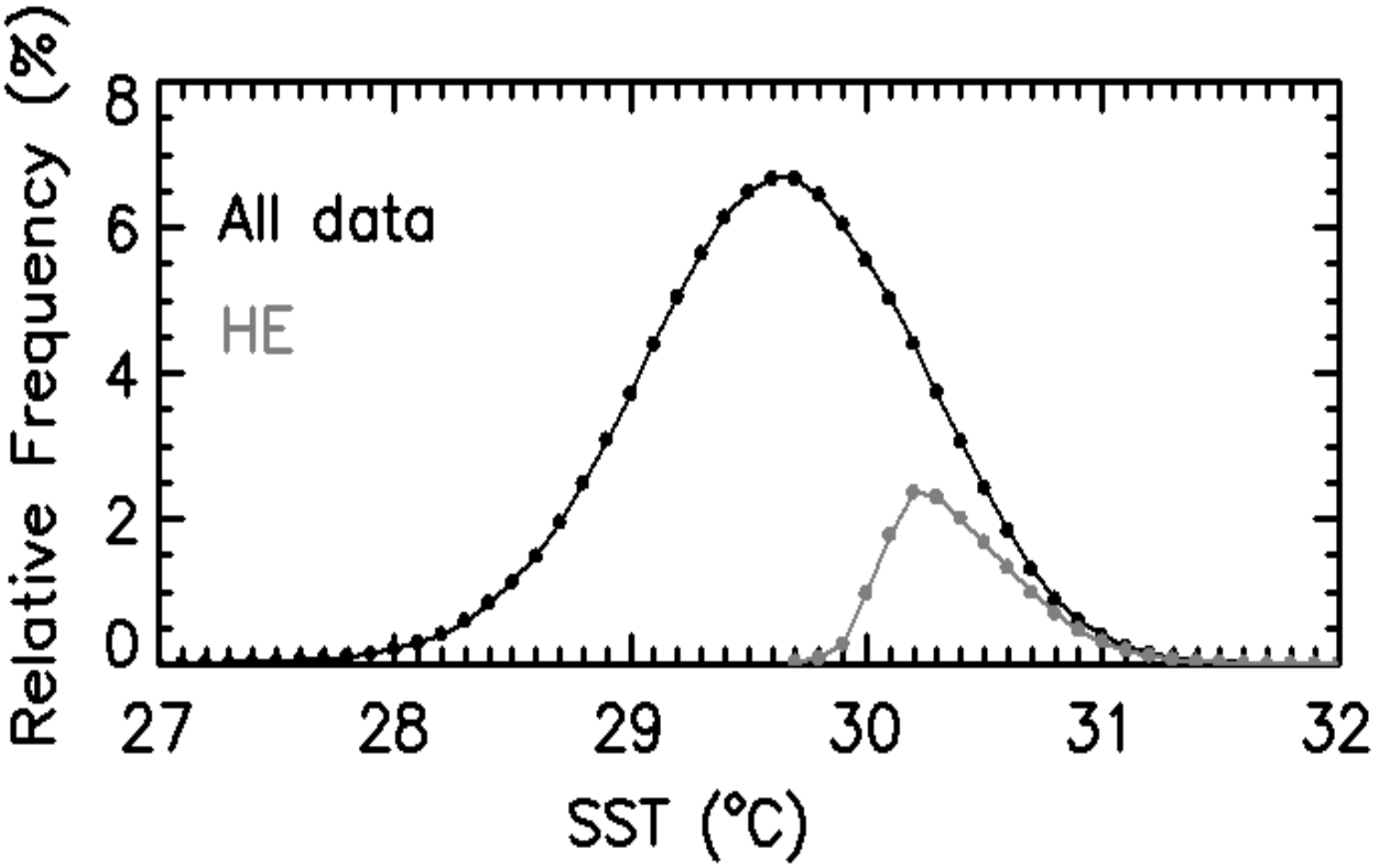

Fig. 3.3 Histogram (interval between points:0.1°C) of the mean relative frequency of SSTs for the whole study period (*black*) and periods during which HEs were presents (*gray*) during 2003−2011 in the area enclosed by 29.5°C isotherm of the climatological SST.

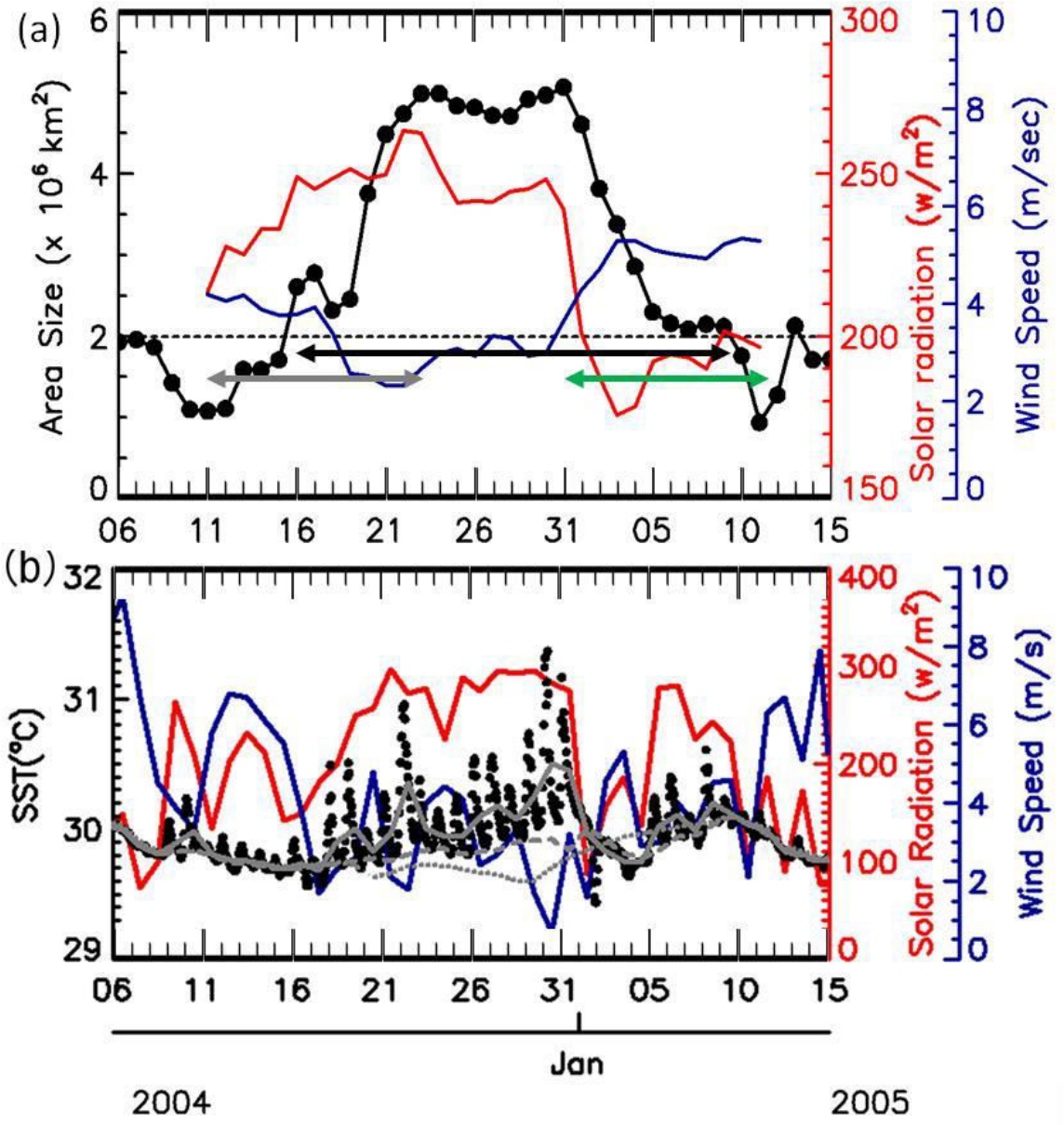

Fig. 3.4 (a) Temporal changes of the areal size with SSTs higher than the threshold for HE041216 (*black circles* with a *black line*). Time series of wind speed (*blue line*) and solar radiation (*red line*) averaged in the HE area are shown. The *black dashed line* denotes the area threshold. The *black arrow* denotes the HE period. The *gray* and *green arrows* represent the development and decay stage, respectively. (b) The time series of SST, wind speed and solar radiation measured by the TAO/TRITON buoy at 0°N, 156°E in 2004/2005. The *black dot, solid gray line, broken gray line* and *dotted gray line* denote hourly SST (1 m depth), daily SST (1 m depth), 25 m depth temperature and 50 m depth temperature respectively.

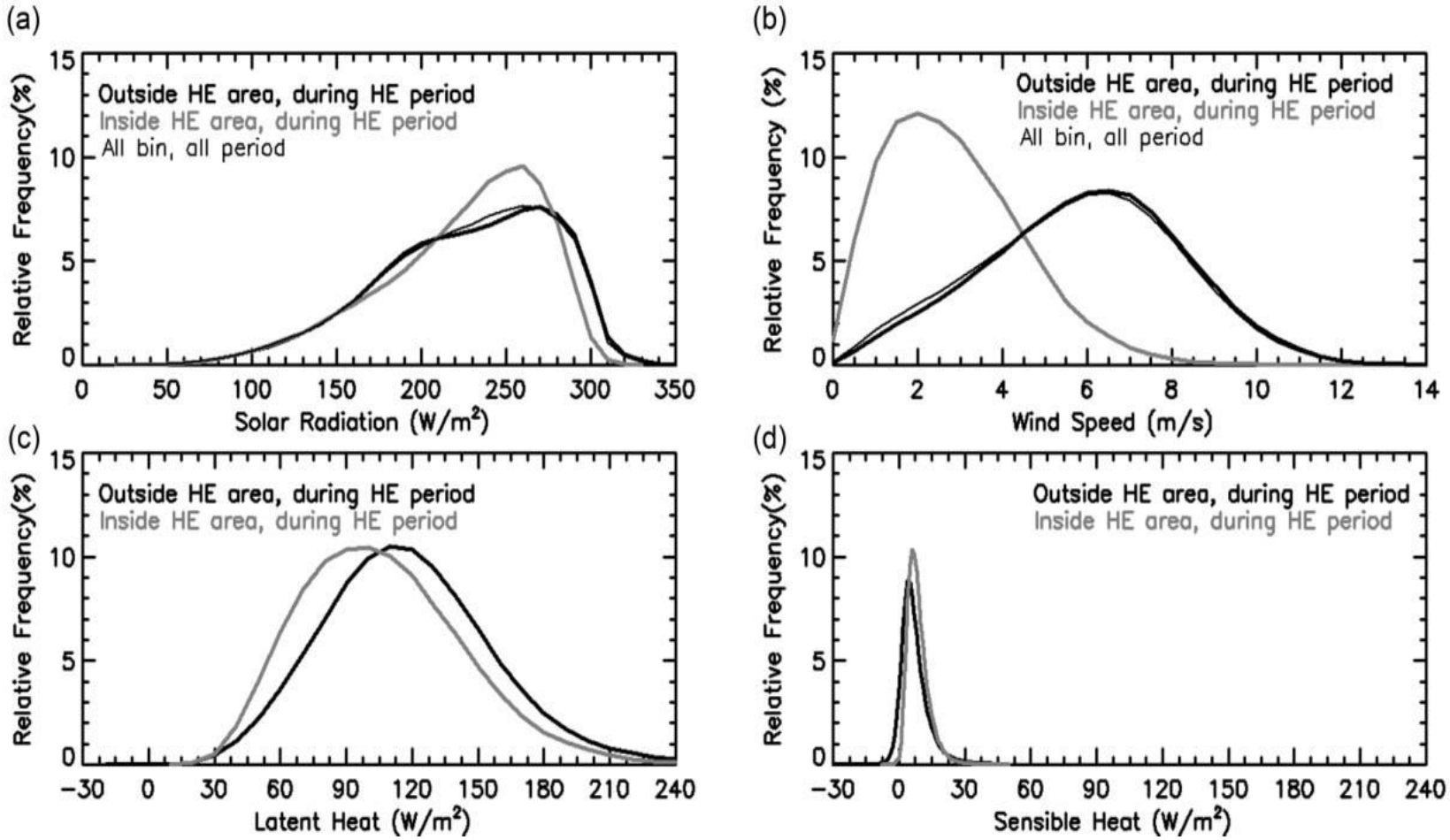

Fig. 3.5 The histogram of the mean relative frequencies of: (a) solar radiation values, with a discrete interval of 10 W/m^2; (b) wind speed values, with a discrete interval of 0.5 m/s; (c) latent heat values (positive upward), with a discrete interval of 10 W/m^2; and (d) sensible heat values (positive upward), with a discrete interval of 1 W/m^2, inside (*gray line*) and outside (*thick black line*) the HE areas within the study area during the HE periods. For (a) and (b), the climatological frequencies in the study area for 2003–2011 are also presented (*black thin line*).

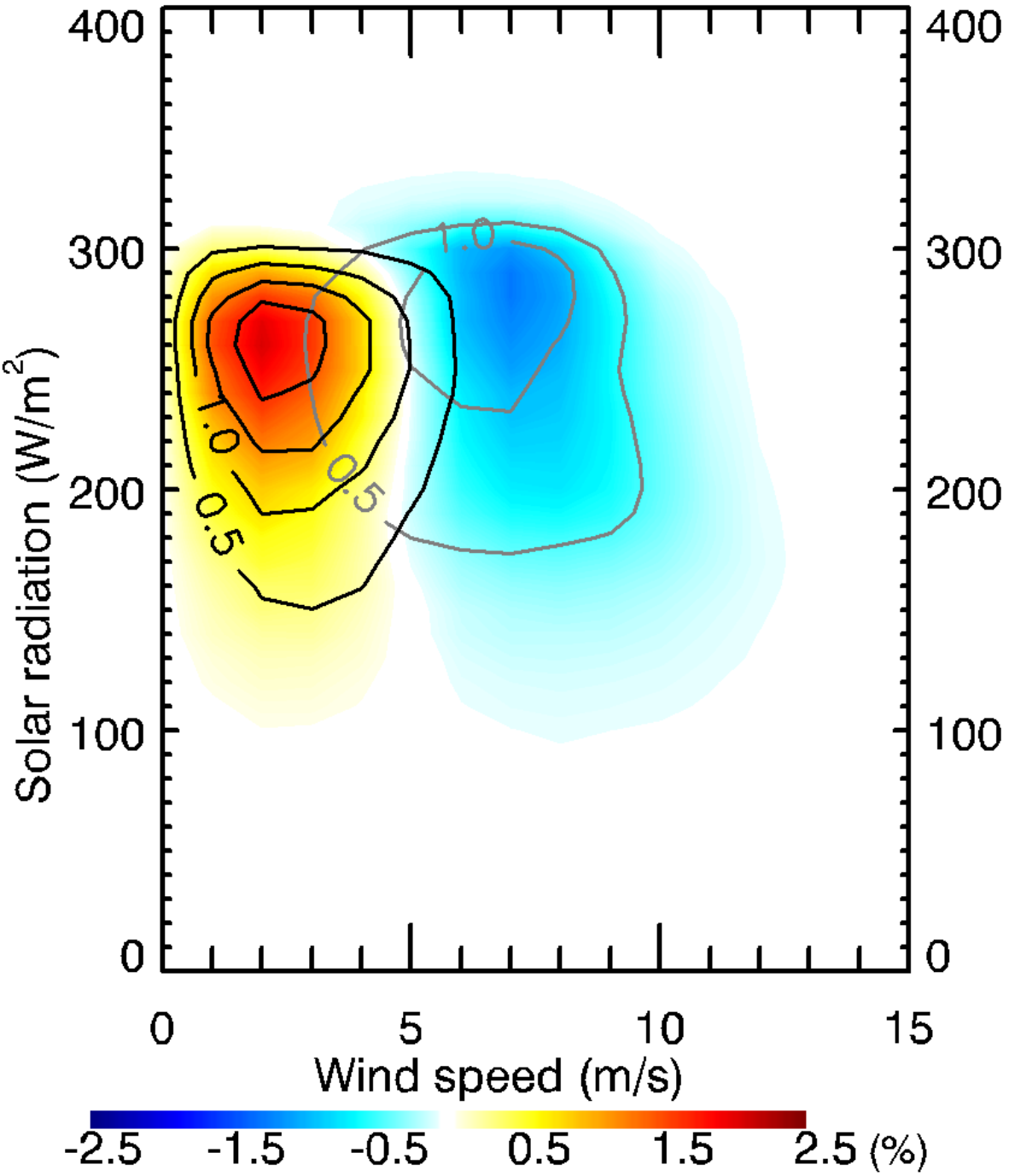

Fig. 3.6 Differences in the relative frequencies of solar radiation and wind speed values from their corresponding climatological values inside HEs during the HE periods (*color bar*). The *black contours* denote the original relative frequencies while the *gray contours* are the relative frequencies for the non-HE areas during the HE periods. Discrete intervals of 10 W/m^2 and 1 m/s were used for the solar radiation and wind speed, respectively, in the plot.

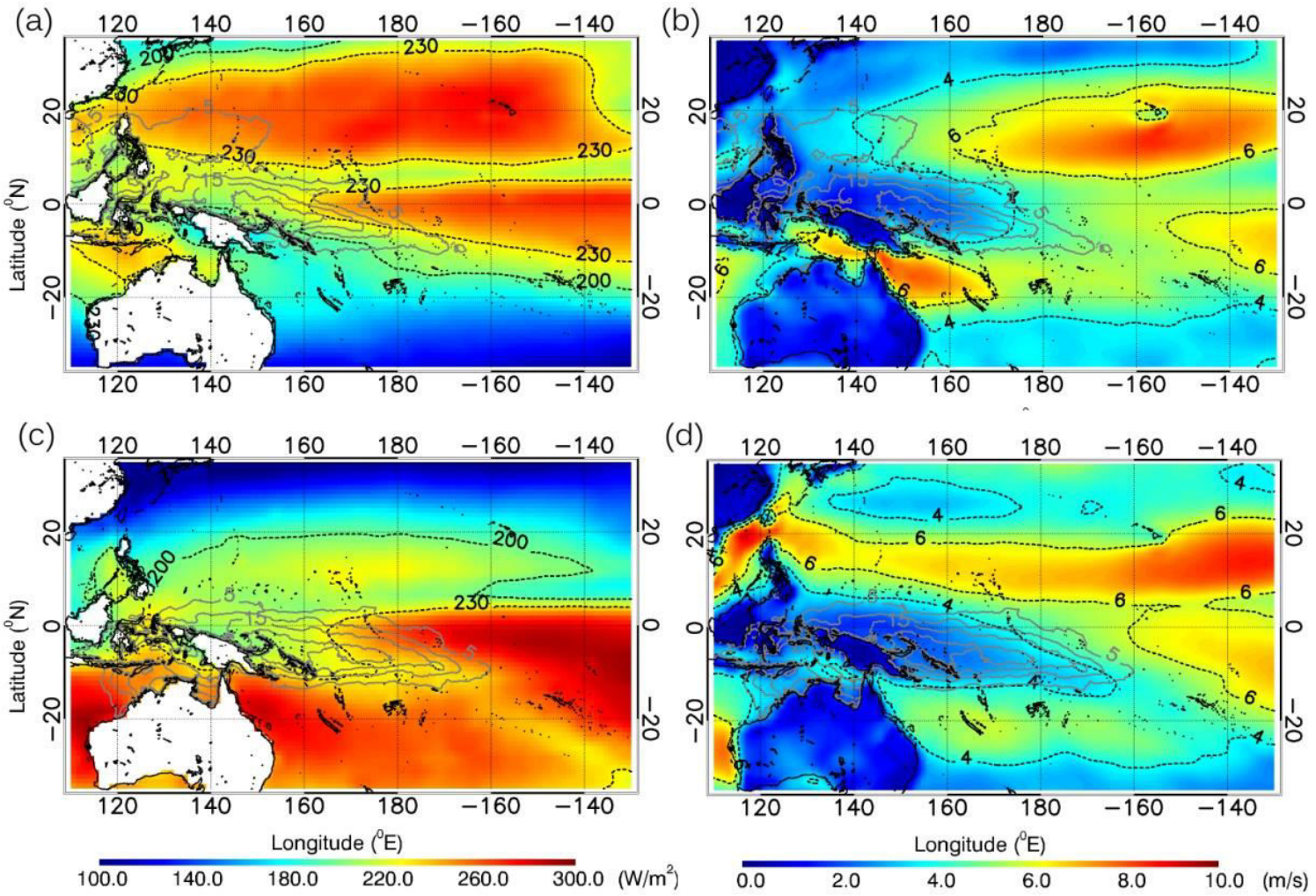

Fig. 3.7 **a**, **c** Solar radiation levels and **b**, **d** wind speeds of the HEs in **a**, **b** boreal summer and **c**, **d** boreal winter overlaid with the HE occurrence rate (%) contours, as shown in Fig. 3.2 (*solid gray lines*), as well as contours of **a**, **c** solar radiation and **b**, **d** wind speed (*broken black lines*).

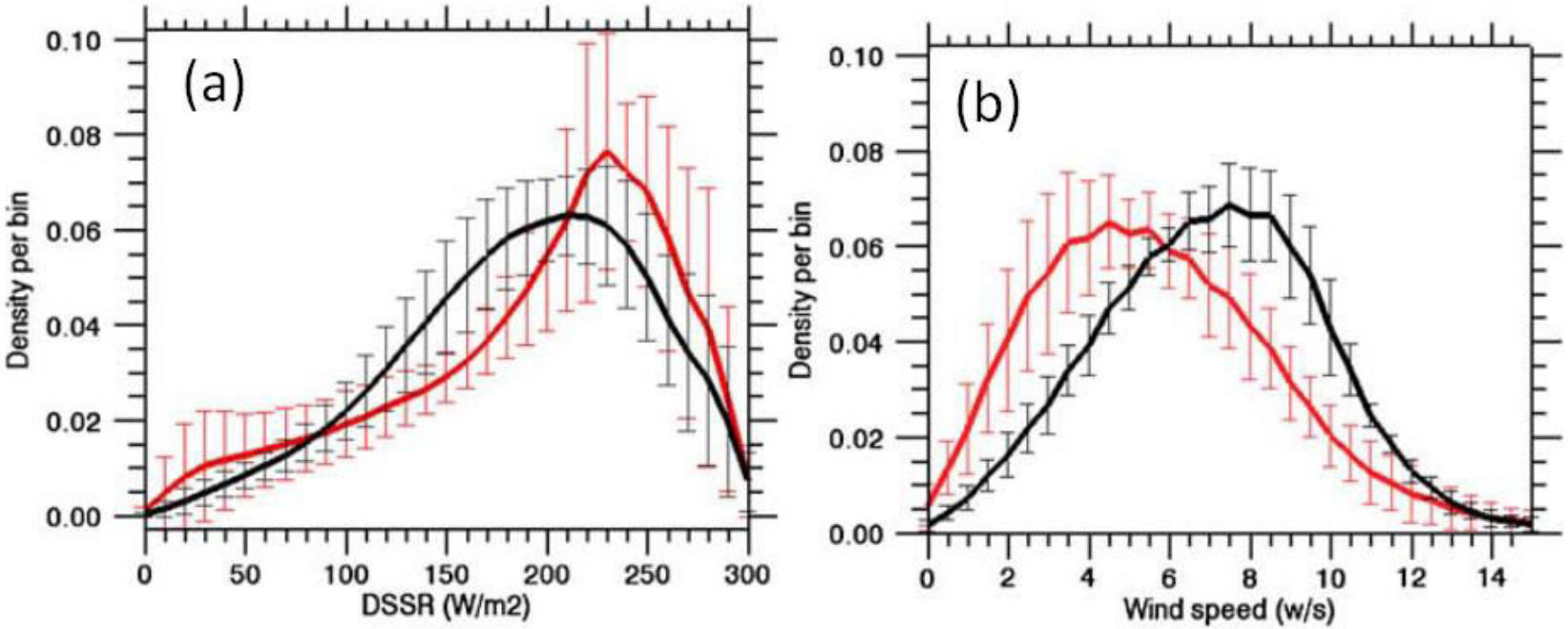

Fig. 3.8 Mean histogram densities for HE area (*red line*) and outside HE area (*black line*) (within 80°E–160°W, 30°S–30°N). (a) DSSR of all HEs during 1996–2001.06, and (b) wind speed of all HEs during 1996–2001.06. Error bars show the standard deviation of each bin. Cited from Qin et al. (2007).

Chapter 4

Atmospheric variability during the development and decay of HE

4.1. Introduction

The climatological study of HE in the western equatorial Pacific as elaborated in Chapter 3 invokes the importance of the area along the northern coast of the New Guinea Island and the Solomon Island as the frequent HE occurrence area (Fig. 4.1a). This area is collocated with the solar radiation > 200 W/m^2 and wind speed < 4 m/s. However, our further analysis shows that the relative frequency of simultaneously low wind speed (< 4 m/s) and high solar radiation (>200 W/m^2) inside the frequent HE area is 31.48% which is much more than the mean occurrence rate of HE in this area i.e., only 12.7% (Fig. 4.1b). Hence, simultaneous event of low wind speed and high solar radiation do not always result the occurrence of HE.

It has been mentioned in chapter 3.4 that the high solar radiation and low wind speed are much more enhanced (reduced) in the developing (decaying) stage (Fig.3.4b). In other words, the enhancing and reducing process of solar radiation and wind speed was neglected in the previous analysis since it only considered the mean value of solar radiation and wind speed during HE occurrence. Thus, the HE analysis by stages may give the better understanding of the HE mechanism.

To examine the detail process of HE, I used HE030528 for a case study instead of HE041216 which is introduced in Chapter 2 and 3. Since HE030528 is a single peak HE, the atmospheric variation between the development and decay stage of HE can be compared directly. The general feature of HE030528 is described in Figure 4.2. HE030528 was located along the northern coast of New Guinea Island extended until 190°E. The highest amplitude was observed at around 0°N, 135°E. HE030528 developed from 27 to 31 May 2003 and decays from 31 May to 11 Jun 2003. The maximum areal size was 3.32×10^6km^2 and that area was split into two parts during the decay stage. The mean solar radiation (wind speed) in the HE area during HE occurrence was about 220 W/m^2 (2 m/s). Furthermore, the solar radiation and surface wind variability during the development and decay of HE030528 is examined in Section 4.2 and 4.3 respectively. I proposed the role of surface wind on controlling the solar radiation variability in Section 4.4. The three dimensional JRA55 data is used in the analysis.

4.2. Solar radiation variability

4.2.1. Case study of HE030528

First, I compared the solar radiation maps between the development and decay stage and related them with total cloud cover maps (Fig.4.3). During development stage, the high solar radiation of more than 250 W/m^2 almost coincided with the HE area. This solar radiation intensity was much higher than during the occurrence of HE (Fig.4.2c). The high solar radiation corresponded to the low cloud cover of less than 40% in the HE area. During the decay stage, the total cloud cover increased and followed by the decrease of solar radiation. Thus, the variability of solar radiation is determined by the variability of cloud cover percentage. Moreover, the minimum solar radiation in the HE area was detected at 5°S-5°N, 150°E-160°E which caused the HE split into 2 parts.

The vertical section of atmospheric parameters shows the distinctive atmospheric features between development and decay stages (Fig.4.4 and 4.5). High (300-100hPa) and low (950-800 hPa) level cloud were dominated in the study area. During development stage, the clear sky condition at the HE area (5°S-5°N) was denoted by the vanishing cloud at the high level cloud and the reducing cloud at the low level. The clear sky area corresponded to the zero convection column. The zero convection column was filled by the air subsidence which brought the dry air from the top of the troposphere. The air subsidence was the result from divergence (convergence) at 950-800 hPa (300-100 hPa). During decay stage, the subsidence area turned back into the convection area, increasing the percentage of cloud cover at the low and high level atmosphere. The summary of these processes is listed in table 4.1.

Focusing on the low level atmosphere (1000-700 hPa), it is found that the convection process during the development stage of HE030528 did not entirely stop. Despite suppressed by the subsidence at the higher level, the convection still occurred and could produce the thin clouds at around 850 hPa (Fig. 4.6 and 4.7; table 4.2). Furthermore, figure 4.8 shows that this low cloud formation was located below the temperature inversion layer at around 800 hPa in the development stage. The suppressed convection above the HE area was the feedback result of the deep convection from remote area outside the HE. In this case, the convection area is clearly seen located at 17°S-5°S and 5°N-20°N. An inversion acts like a lid, keeping convective overturning of the atmosphere from penetrating through the inversion. In the decay stage the inversion layer reduced as the convection increased. Thus, the theory of ‘remote convection’

which was proposed by Zhang et al. (1995) and Tompkins (2001) as the mechanisms for the formation of very high SST is proven for HE030528.

4.2.2. Climatological analysis

The solar radiation variability of all HE cases during the development and decay stage of HE is statistically summarized in Figure 4.9. Figure 4.9a shows that HE frequently occurs at the area of solar radiation ~200W/m^2. However, solar radiation in that area is not stable since the standard deviation is high (>30 W/m^2). Figure 4.9b indicates that the HE develop when the relative frequency of solar radiation of more (less) than 230 W/m^2 increases (decreases) . Thus, the solar radiation of more than 230 W/m^2 is needed to generate HE. Next, the solar radiation of more than 200 W/m^2 is needed to maintain the occurrence of HE as explained in Chapter 3. Moreover, the relative frequency of solar radiation during decay stage is similar with its climatology. Therefore, the development of HE in the western equatorial Pacific can be indicated by positive anomaly of solar radiation.

4.3. Surface wind variability

4.3.1. Case study HE030528

I used SLP and land elevation parameters to investigate the surface wind variability during the development and decay stage of HE. Figure 4.10 shows that low surface wind speed area coincided with the HE area during the development stage. The SLP was relatively uniform (≈1010 hPa), causing the low SLP gradient magnitude in the HE area. Lower SLP was detected at eastern side at around 10°S, 180°E. During decay stage, low SLP area was moving to the northern coast of Solomon Islands, increasing the SLP difference with the southern part. The geographical location of the Solomon Islands, Bougainville Island, New Britain Island and New Ireland Island creates a gap, located between the western tip of Bougainville Island and the eastern tip of New Ireland Island. The large SLP difference between the area at the south side of the gap and the area at the northern coast of Solomon Islands during the decay stage of HE flew the strong wind through the gap to the low SLP area. Surface wind variability during the development and decay stage of HE030528 is summarized in table 4.3. Therefore, air-sea-land interaction process becomes the important factor for the mechanisms of HE030528. Furthermore,

the occurrence of strong winds at this area may also cause the splitting HE030528 as shown in Section 4.1.

The extraction of surface wind components shows that the variation of zonal wind component gives more influence to the HE process. In HE030528 the meredional wind component was relatively stable during development and decay stages of HE. Weak and negative zonal wind component was observed during the development stage and then turned into positive and strong component (westerly wind) during the decay stage (Fig. 4.10; table 4.2). Thus, the occurrence of westerly wind indicates the decay of HE030528.

It has been reported by many researchers (e.g., Keen 1982, Nitta 1989, Ogura and Chin 1987, Lander 1990) that the westerly bursts accompany the less frequent formation of "cyclone pairs," or two tropical depressions straddling the equator which appear to have dynamically associated origins. In this case study, the westerly bursts occurred because of the interaction between the low pressure system moving westward and the terrain topography of the Solomon Islands, Bougainville Island, New Britain Island and New Ireland Island.

4.3.2. Climatological analysis

The climatology of surface wind in the western equatorial Pacific is dominated by the easterly wind (Fig.4.11a). The frequent HE area corresponds to the easterly wind speed of lower than 3 m/s. However, it also corresponds to the area of intermittent wind denoted by the high standard deviation. Statistical summary of all cases is shown in Figure 4.11b. During the development stage, easterly wind is weaker than its climatology with the peak frequency at -2 m/s. In contrast, strong westerly winds come during the decay stage, denoted by the increase of relative frequency of positive zonal wind component. However, the easterly winds still become the highest relative frequency (i.e. -3 m/s) since the turning of wind direction in the decay stage is not needed for all HE area as shown in HE030528. Hence, the decay of HE can be characterized by the anomaly of surface wind direction.

4.4. The role of surface wind on controlling the solar radiation variability

Atmospheric boundary layer has an important role to control the convection process. Sherwood (1999) stated that low to mid tropospheric moisture is identified as dominant factor regulating convective outbreak. Additionally, dry boundary layers are associated with low

potential energy that are less likely to form deep convective events (Tompkins, 2001). Surface wind speed determines the surface evaporation process which becomes the moisture supply for the upper atmosphere and surface divergence determines the vertical air motion. Fig. 4.12 and table 4.4 shows that as the wind speed decreased during the development stage of HE030528, the surface evaporation also decreased and the weakening surface convergence reduced the upward motion strength. The existence of thermal inversion layer during the development stage also may contribute to the reduction of upward motion. At the upper atmosphere level, the variation of relative humidity was parallel with the surface evaporation and the variation of vertical velocity was parallel with surface convergence. On 25 May 2003, when the surface convergence and surface evaporation started to decrease, the convection process and relative humidity at the upper atmosphere level also started to decrease. Because of the decreasing convection, dry air from the top of troposphere sank and gave positive feedback to suppress the convection. Then, solar radiation increased as a result of the suppressed convection. During the decay stage, surface wind speed increased, surface convergence became stronger and convection process began to reduce solar radiation. Therefore, surface wind plays an important role on solar radiation variability during HE process. Thus, this result supports surface wind as the key factor for the HE occurrence as mentioned in Chapter 3.

4.5. Relation with the Madden-Julian Oscillation

Madden-Julian oscillation (MJO) is a remarkable feature of the atmospheric circulation and moist convection in the tropics which tend to be organized at planetary scales (spatial scale greater than 10^4 km in the zonal direction) and to propagate eastward at an averaged speed of 5 m/s across the equatorial Indian and western/central Pacific oceans, with a local intraseasonal period of 30-90 days. It features the eastward moving center of strong deep convection and precipitation (known as the active phase), flanked to both east and west by regions of weak deep convection and precipitation (known as inactive or suppressed phases) (Zhang, 2005). The track of this phenomenon has been well documented by Wheeler and Hendon (2004) which divide the track by 8 phases (Fig. 4.13). The relation between MJO and SST in the western Pacific ocean has been reported by Shinoda et al. (1998). The amplitude of the SST variation produced by MJO is about 0.25°C. This fact raises a question regarding the influence of MJO to the HE occurrence.

The relation between the occurrence of HE030528 and MJO is presented in Fig. 4.14 and 4.15. The Hövmoller diagram in 2003 clearly shows the signals of MJO. The eastward propagation of strong upward wind and high precipitation is detected on Jan/Feb, May, Jun/July, August and October (Fig. 4.14). The most prominent signal is on May with the eastward propagation of about 4.6 m/s which is associated with the occurrence of HE030528 in its end stage. Moreover, the effect of the suppressed phase of MJO for the development of HE030528 is presented in Fig.4.15. The track of eastward propagation of upward wind indicates MJO is clearly seen from phase 2 at Indian Ocean until phase 5 at the western equatorial Pacific followed by the eastward propagation of air subsidence indicates suppressed phase. During development stage of HE030528 (25-30 May 2003), the suppressed phase of MJO interacted with the branch of Intertropical Convergence Zone creating the subsidence bar along the equator, in the western equatorial Pacific. Thus, the high solar radiation during the development stage of HE030528 was affected by the MJO. Since the amplitude of HE030528 is 0.3°C, this value is close to the SST variation produced by MJO provided by Shinoda et al (1998).

Further analysis of 71 HE cases found in the western equatorial Pacific shows that only 11 HEs are associated with MJO and not every MJO results the HE occurrence. Those HEs are HE030528, HE030825, HE031021 HE040218, HE040520, HE040909, HE041015, HE041114, HE060527, HE061010, and HE090503. The prominent characteristic of HEs associated with MJO is their location, i.e., along the equator at the northern coast of New Guinea Island and Solomon Islands following the track of MJO propagation. Nevertheless, this analysis cannot find other typical characteristic of HEs associated with MJO. This problem is left for future study.

4.6. Discussion

The “remote convection” mechanism for HE generation in the western equatorial Pacific has been previously described by Qin and Kawamura (2010). However, there is a significant difference from the “remote convection” found in this study. By using the cloud motion wind and cloud cover data obtained from geostationary satellite measurements, Qin and Kawamura (2010) found that the deep convection over the area of HE0611-East act as “remote convection” to generate HE0611-West (Fig. 4.16). The occurrence of HE0611-East was supported by the subsurface SST anomaly associated with the El Niño. Thus, their result indicates the zonal circulations through HE0611-East and -West.

In contrast, the present study shows the meredional circulation of the "remote convection" mechanism during the development of HE030528. Convergence surface winds associated with the ascending branch of the Walker circulation air the typical characteristics of the western equatorial Pacific (Rasmusson and Wallace 1983). Thus, precipitation tends to be high in this convergence area (Lukas and Lindstorm 1991, Ando and McPhaden 1997). Along the equator, this convergence/convection areas turned into subsidence areas during the development of HE030528, creating the tropospheric "freewheel effect". The subsidence area along the equator was flanked by the convection areas along the higher latitudes. However, the zonal circulation associated with the MJO may also occur during the development stage of HE020528 with the larger scale but weaker circulation as shown in Fig. 4.15. This interaction should be investigated further in the next study.

The "remote convection" mechanism over the very high SST has been described schematically by Tompkins (2001) by using an idealized 3D experiment of cloud-resolving model (Fig. 4.17). In the summary, he emphasized the importance of surface latent heat flux that limits SSTs to 32°C and eventually propagates the convection toward the high SST areas, reducing SSTs. In the case of HE030528, I propose an hypothesis that those processes may be enhanced due to the westerly wind blow, increasing evaporation as well as latent heat flux. Next, convection was reactivated and this became the end stage of HE030528. The relation between convection and westerly wind in the western equatorial Pacific has been reported by Kiladis et al. (1994) who provided the evidence that 6- to 30- day convection often occurs in conjunction with deep westerly flows. In HE030528 case, westerly wind might caused by the westward propagation of low pressure system interacted with land surface topography. Nevertheless, further investigations are needed to examine the relation between the decay of HE and the westward propagation of the low pressure system.

4.7. Conclusions

The analysis of atmospheric parameters during the development and decay stage of HE are concluded as follows.

1) During development stage, the solar radiation (wind speed) in the HE area is much enhanced (reduced) than during decay stage.

2) The suppressed convection above the HE030528 area during the development stage is the feedback result of the deep convection from remote area outside the HE. Thus, the theory of ‘remote convection’ is proven for the HE formation mechanisms.
3) The large SLP gradient magnitude between the area at the south side of the gap and the area at the northern coast of Solomon Islands which flew the strong wind through the gap to the low SLP area indicates air-sea-land interaction process during the decay of HE030528.
4) The HE formation in the western equatorial Pacific is indicated by positive anomaly of solar radiation from its climatology while its decay is denoted by the anomaly of surface wind direction.
5) The positive anomaly of solar radiation during the development stage of HE is partly contributed by the suppressed phase of MJO in the western equatorial Pacific.
6) Surface wind has important role to influence the variability of solar radiation during HE occurrence by controlling the water vapor supply in the upper troposphere through surface evaporation and surface convergence variation. Thus, surface wind play as the key factor for HE occurrence in the western equatorial Pacific.

Table 4.1 Summary of atmospheric variability during the development and decay stage of HE030528.

	Development stage	Decay stage
Solar radiation	high	low
cloud cover	Clear sky	cloudy
vertical velocity	Downward (no convection)	Upward (convection)
Relative humidity	Low (dry air)	High (wet air)
divergence	divergence at lower layer convergence at upper layer	convergence at upper layer divergence at upper layer

Table 4.2 Summary of atmospheric variability at the lower level during the development and decay stage of HE030528.

	Development stage	**Decay stage**
Vertical velocity	Weak upward wind	Strong upward wind
Conv. Heating rate	Low convection in both layer	Strong convection in both layer
Low cloud cover	Thin cloud	Thick cloud

Table 4.3 Summary of surface wind variability during the development and decay stage of HE030528.

	Development stage	**Decay stage**
Wind speed	weak	strong
U component	Weak easterly	Strong westerly
V component	stable	stable
SLP difference	small	large

Table 4.4 Summary of relation between surface wind and convection variability during the development and decay stage of HE030528.

	Development stage	**Decay stage**
Surface wind speed	weak	strong
Surface evaporation	low	high
Relative humidity at upper troposphere	low	high
Surface convergence	weak	strong
vertical velocity at low troposphere	Weak upward wind	Strong upward wind
Convective heating rate at upper troposphere	weak	strong
Vertical velocity at upper troposphere	Downward motion	Upward motion
Solar radiation	high	low

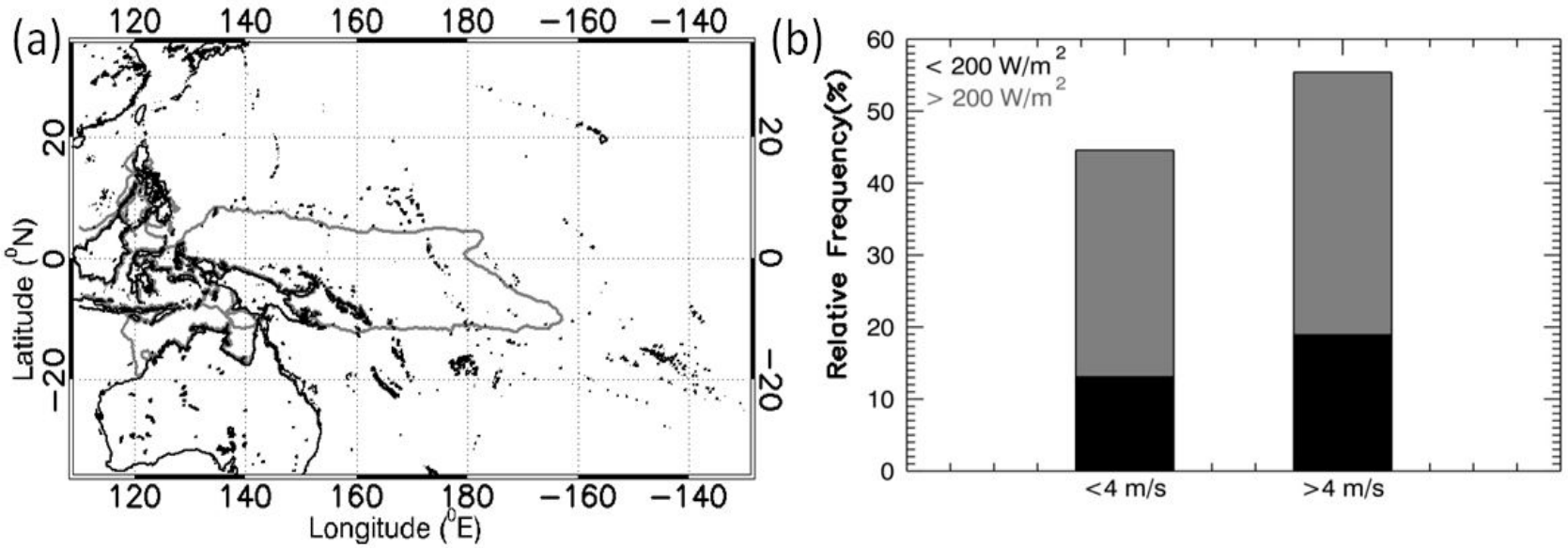

Fig.4.1 (a) The frequent HE occurrence area denoted by the HE occurrence rate of more than 5% (*gray contour*) (b) The histogram of the relative frequencies of wind speed of more than 4 m/s (*right bar*) and less than 4 m/s (*left bar*) and solar radiation of more than 200 W/m^2 (*upper bar*) and less than 200 W/m^2 (*lower bar*) inside the frequent HE area depicted in Fig. (a) from 2003 to 2011.

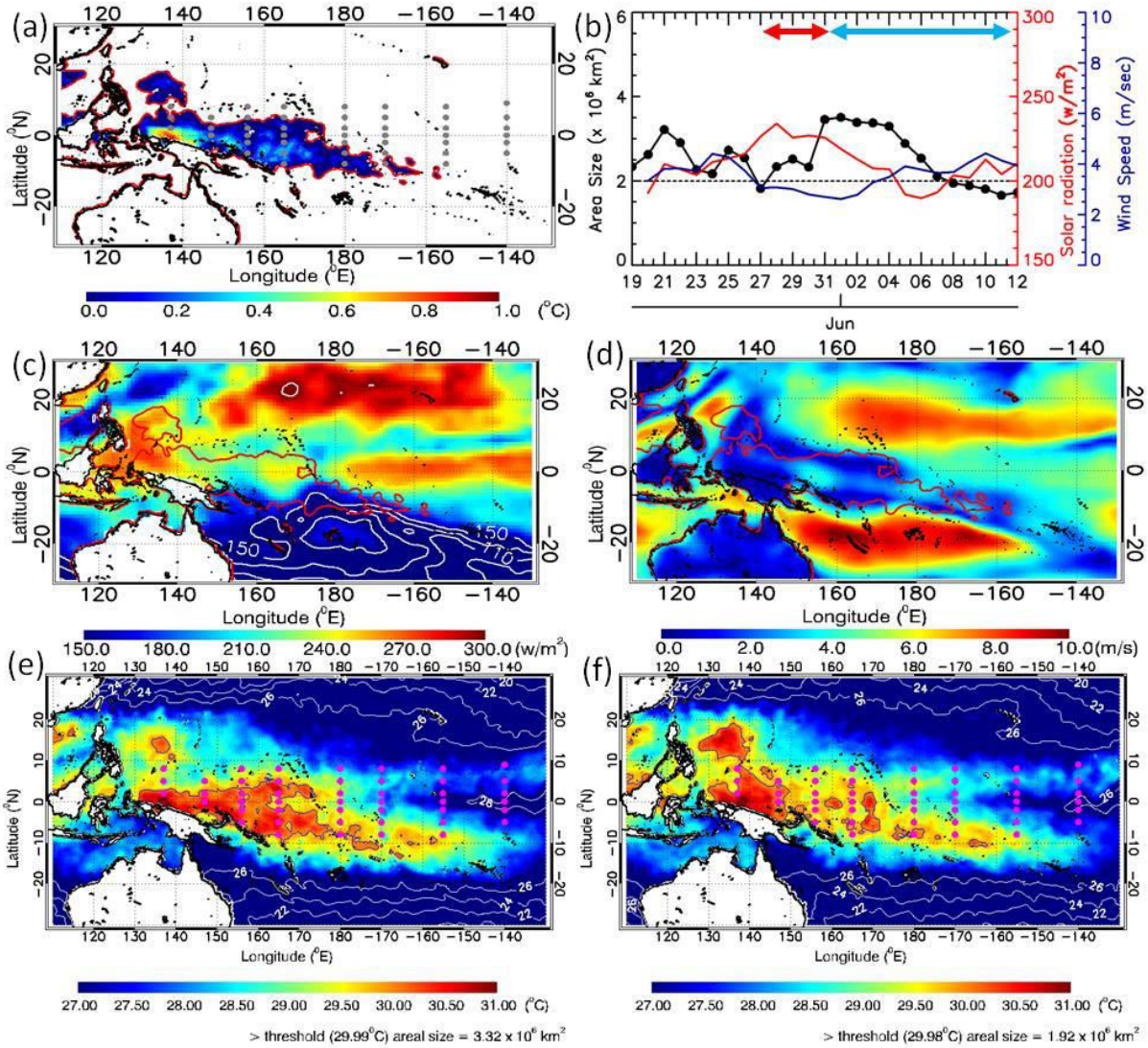

Fig. 4.2 General feature of HE030528 i.e., (a) amplitude map, (b) temporal evolution of areal size and time series of solar radiation and wind speed inside the HE area, (c) mean solar radiation map, (d) mean wind speed map, (e) SST map at the peak of HE period (31/5/2003), and (f) SST map at the decay stage of HE (6/6/2003). The *red contours* in Figs. (a), (c) and (d) denote the HE area. The *red* and *blue arrows* in Fig. (b) denote the development and decay stages, respectively. The *gray contours* in Figs. (e) and (f) denote the SST threshold.

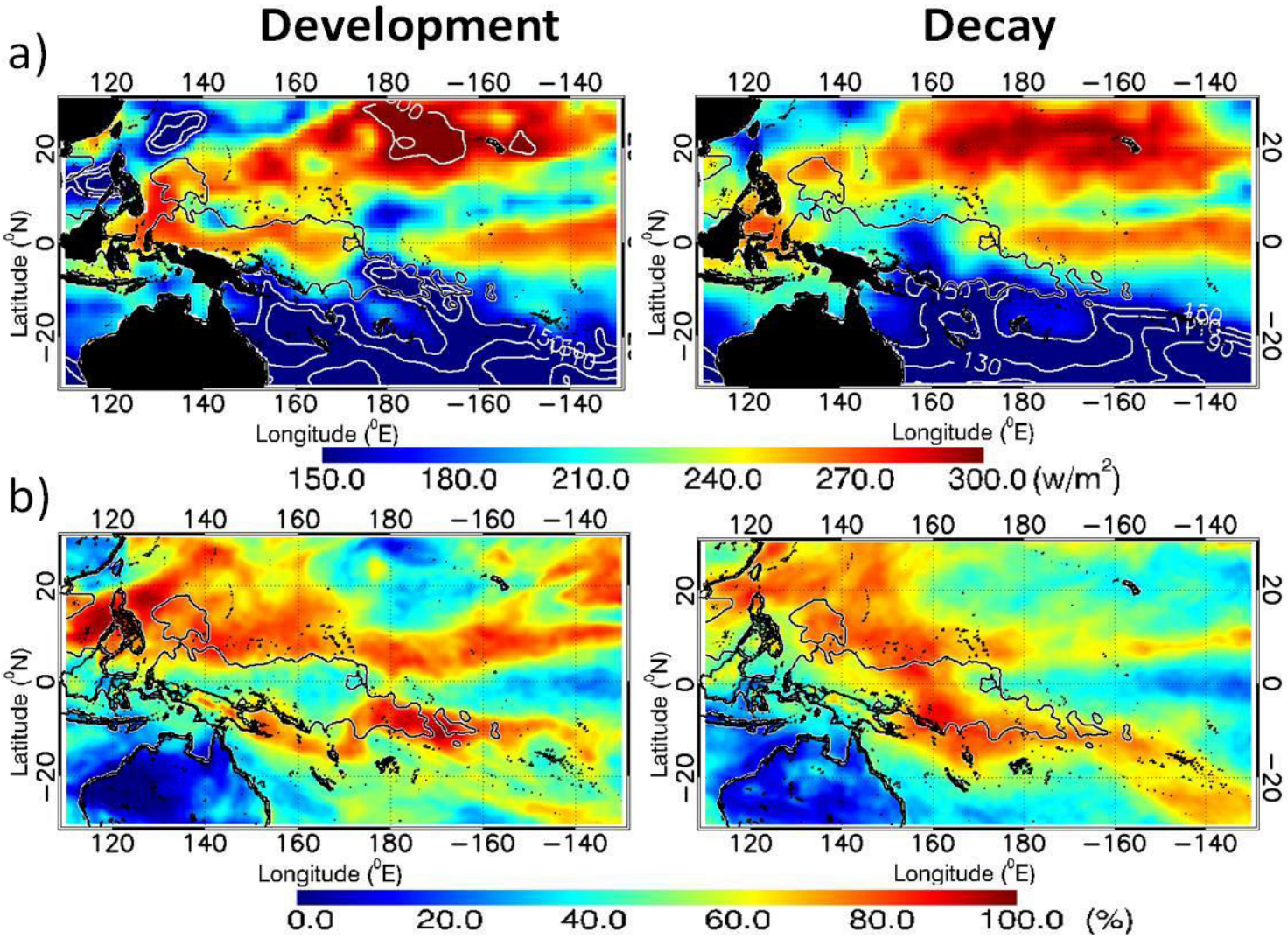

Fig. 4.3 (a) Solar radiation and (b) total cloud cover map during the development and decay stages of HE030528. The *black contour* denotes the HE area.

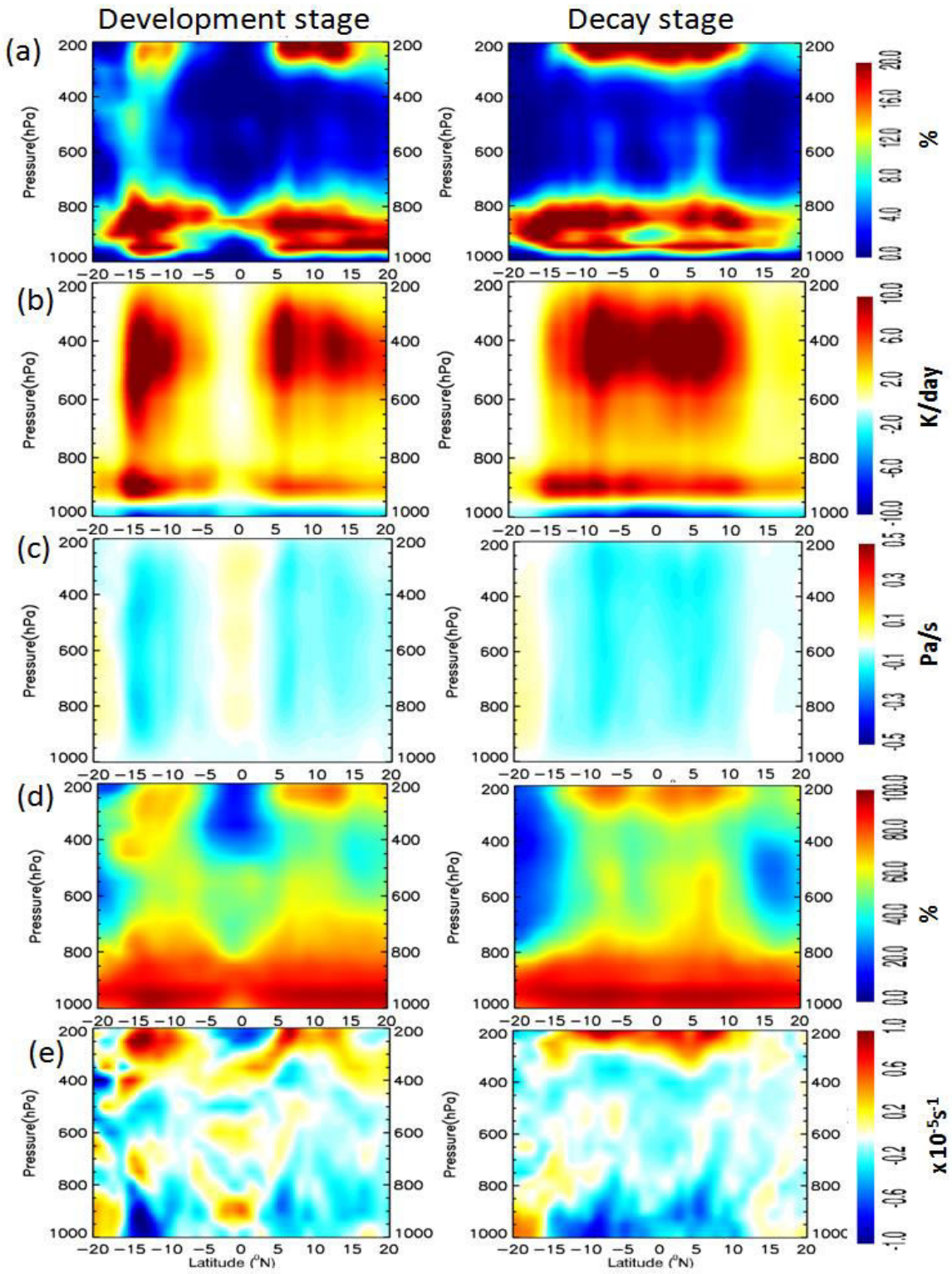

Fig. 4.4 Vertical section (155°E – 160°E, 20°S – 20°N) of (a) cloud cover, (b) convective heating rate (c) vertical velocity (d) relative humidity and (e) divergence during development and decay stage of HE030528. HE area is located around 5°S to 5°N.

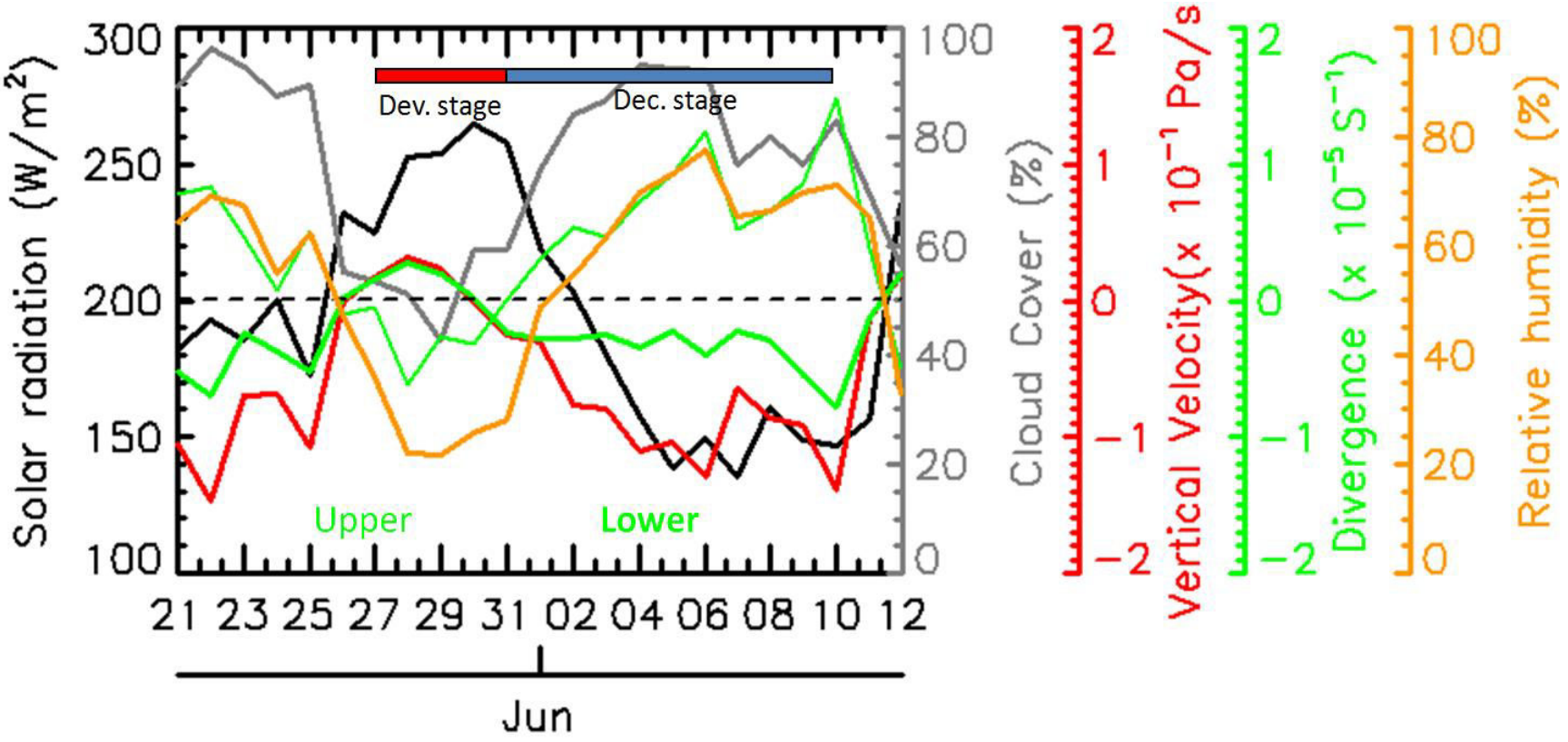

Fig 4.5 The time series of mean solar radiation, total cloud cover, relative humidity, divergence and vertical velocity at 155°E – 160°E, 5°S – 5°N. Mean divergence is taken at 950hPa – 850 hPa (lower) and 250 hPa – 150 hPa (upper), mean relative humidity is at 400 hPa – 200 hPa and mean vertical velocity is at 850 hPa – 200 hPa.

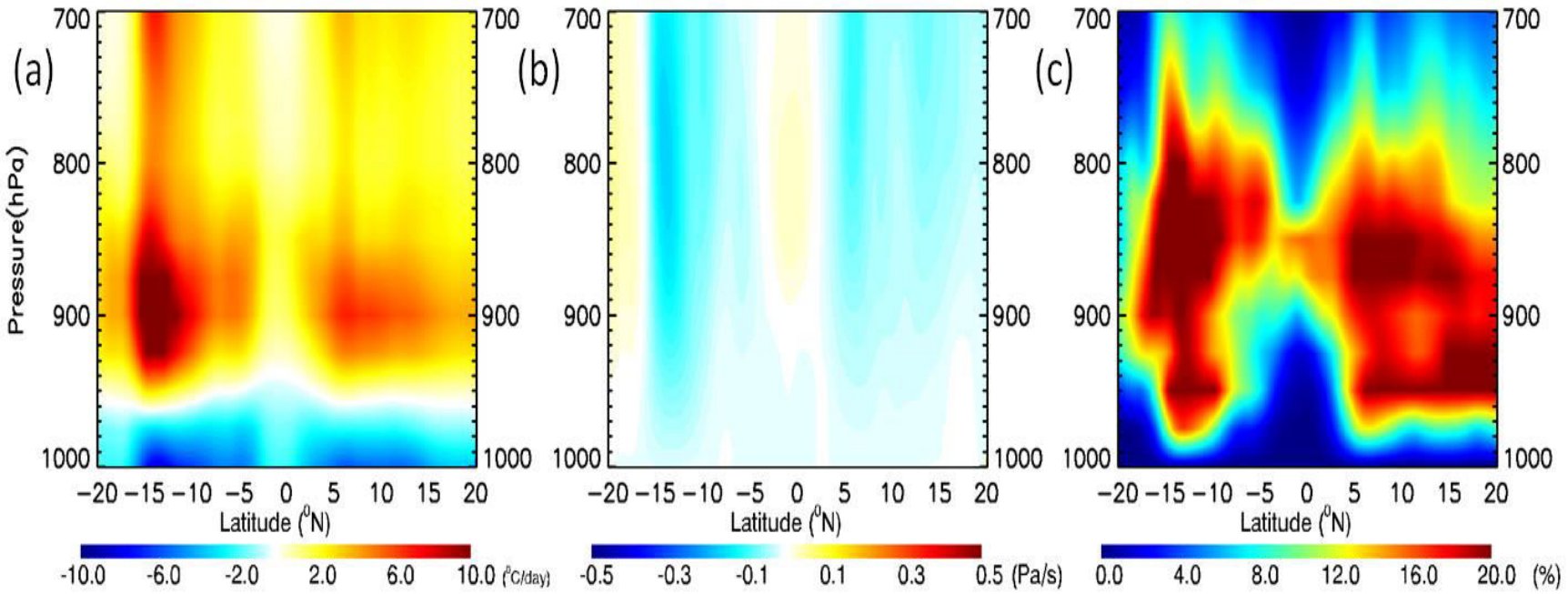

Fig. 4.6 Vertical section (155°E – 160°E, 20°S – 20°N) of (a) convective heating rate, (b) vertical velocity and (c) cloud cover during the development stage of HE030528 at the low atmosphere. The HE area is located around 5°S to 5°N.

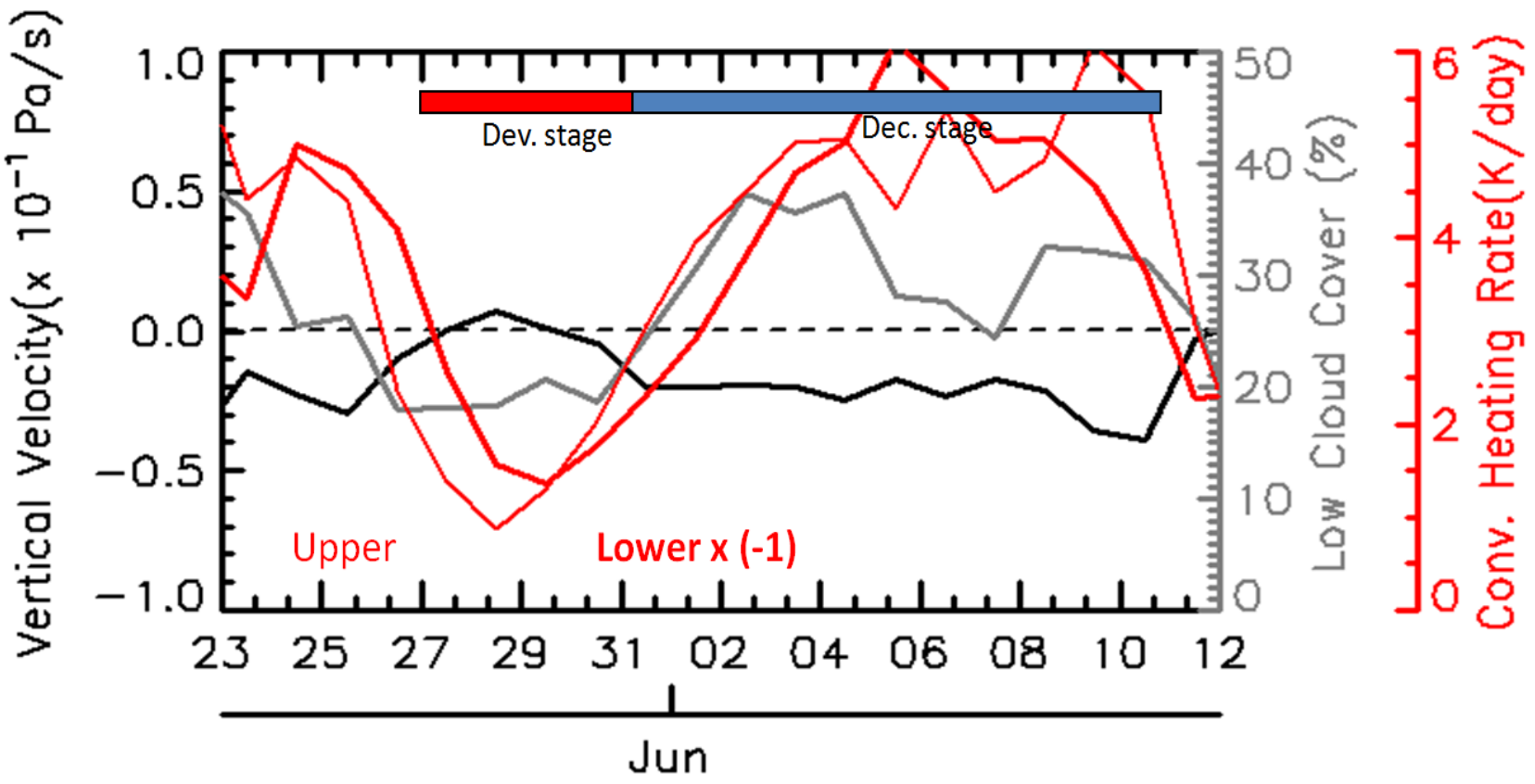

Fig 4.7 The time series of vertical velocity, convective heating rate and low cloud cover (850 to 1100 hPa) at 155°E – 160°E, 5°S – 5°N. Mean convective heating rate is taken at 1000 hPa – 950 hPa (lower) and 950 hPa – 900 hPa (upper) and mean vertical velocity is at 1000 hPa – 900 hPa.

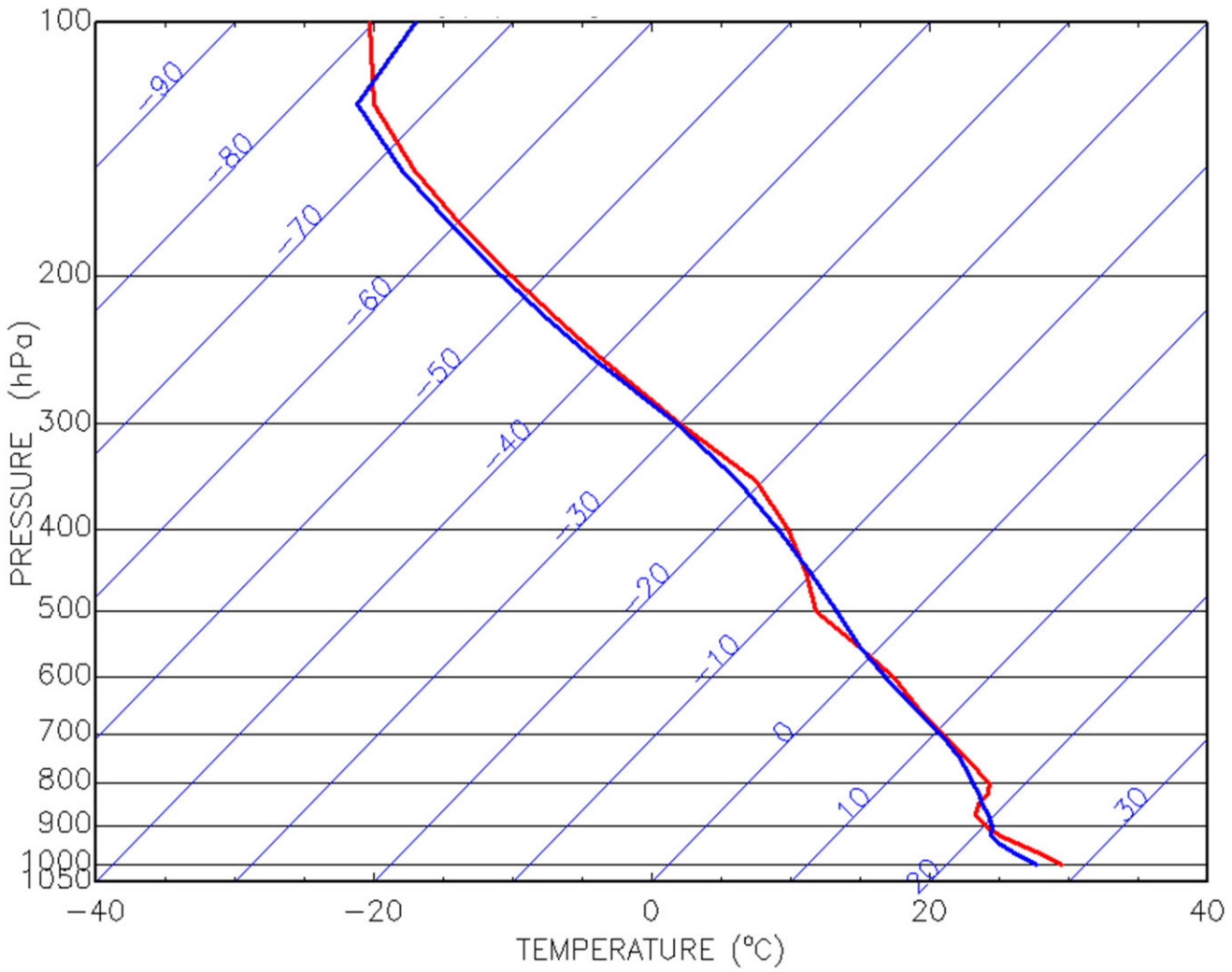

Fig. 4.8 Skew-T, Log-P diagram of air temperature at 0°N, 157°E in 29/05/2003 (*red line*) represents development stage and 07/06/2003 (*blue line*) represents decay stage.

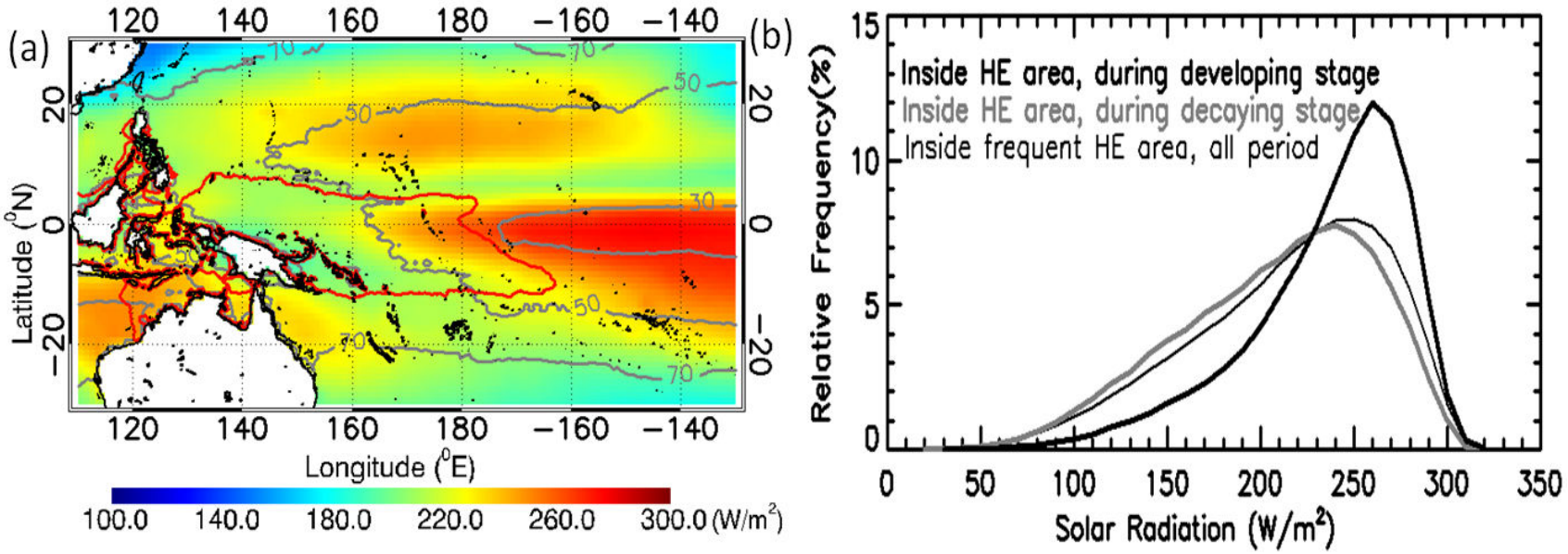

Fig. 4.9 (a) Climatology of solar radiation in the western equatorial Pacific (2003-2011). The *gray contour* denotes its standard deviation and the *red contour* represents the frequent HE area with the occurrence rate of more than 5%. (b) Relative frequency of solar radiation with discrete interval 10 W/m^2.

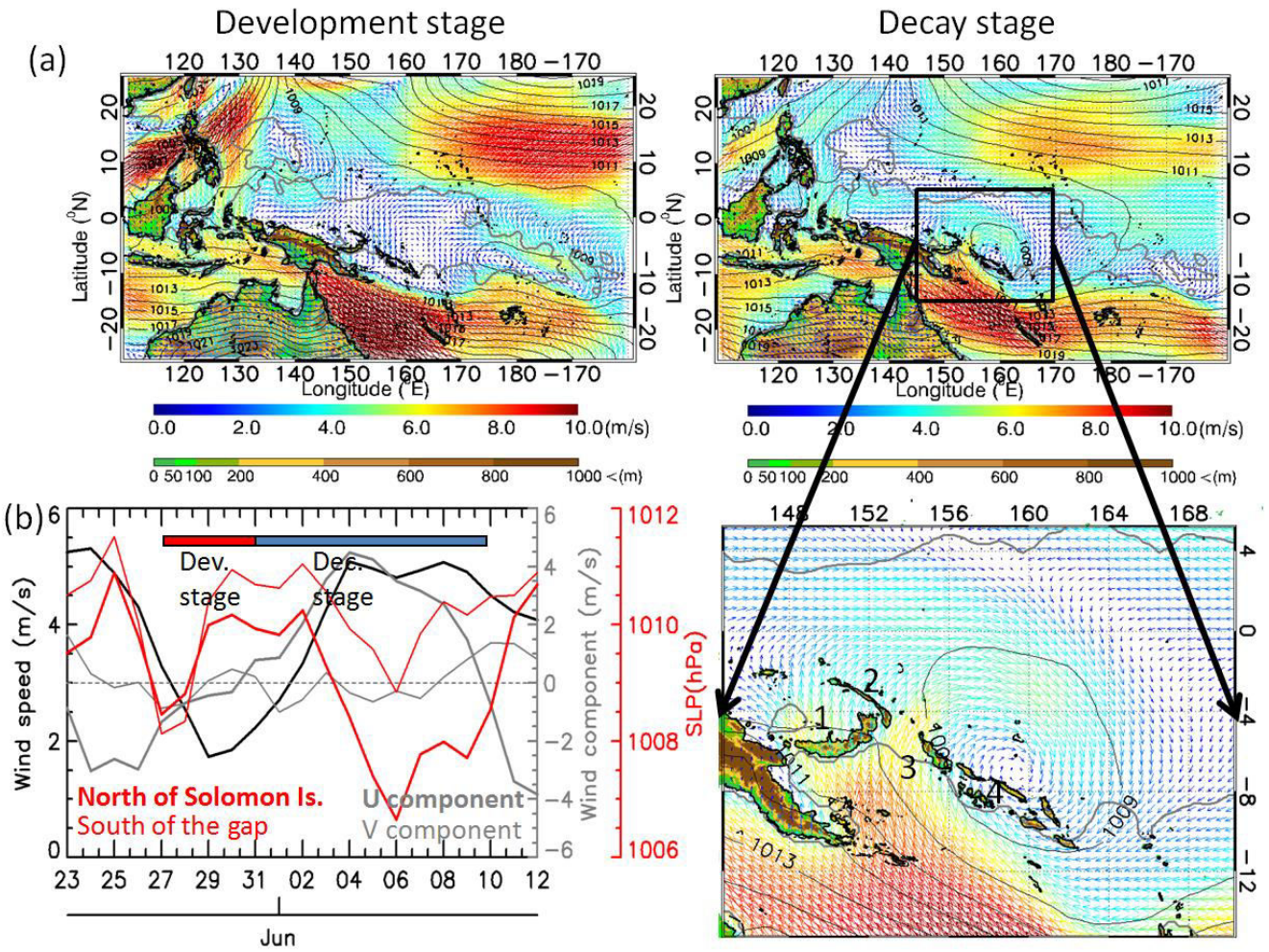

Fig. 4.10 (a) surface wind vector overlaid by SLP contour during development and decay stage of HE20030528. In the zoomed area, 1, 2, 3 and 4 denote New Britain Island, New Ireland Island, Bougainville Island and Solomon Islands respectively (b) The time series of wind speed, wind component at 145°E-165°E, 5°S-5°N and SLP at the south side of the gap (150°E-155°E, 10°S-5°S) and at the northern coast of Solomon Island (158°E-163°E,7°S-2°S).

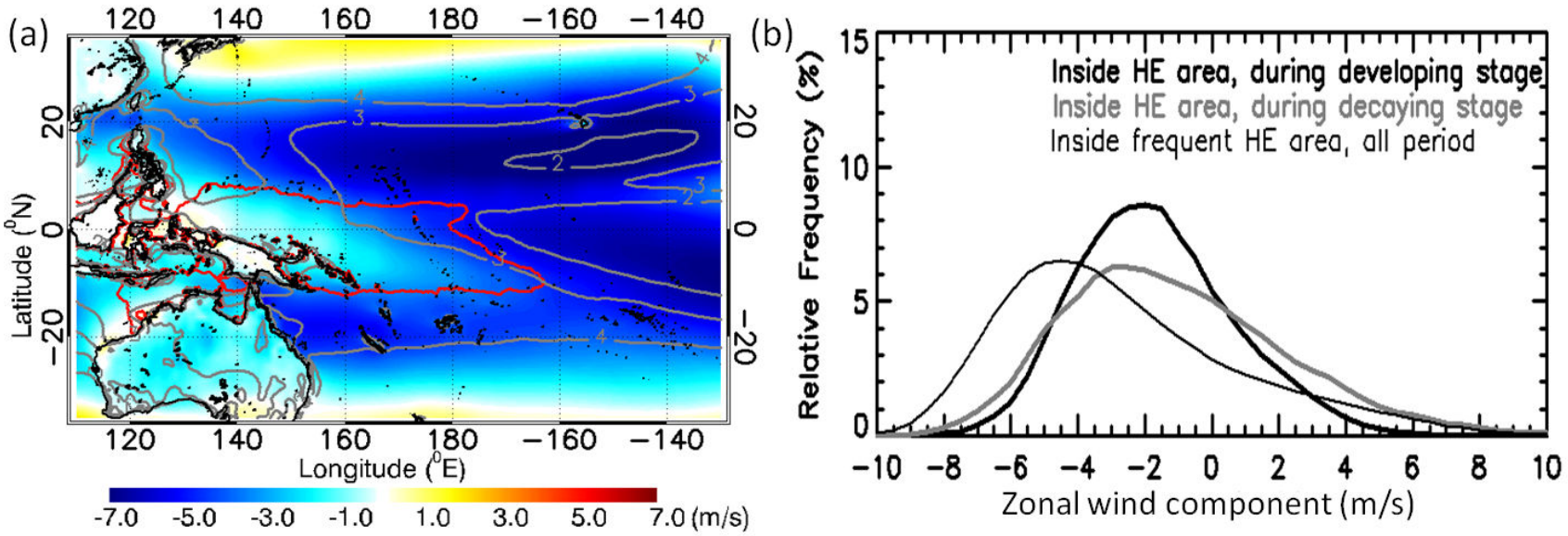

Fig. 4.11 (a) Climatology of zonal surface wind component in the western equatorial Pacific (2003-2011). The *gray contour* denotes its standard deviation and the *red contour* represents the frequent HE area with the occurrence rate of more than 5%. (b) Relative frequency of zonal surface wind component with discrete interval 0.5 m/s.

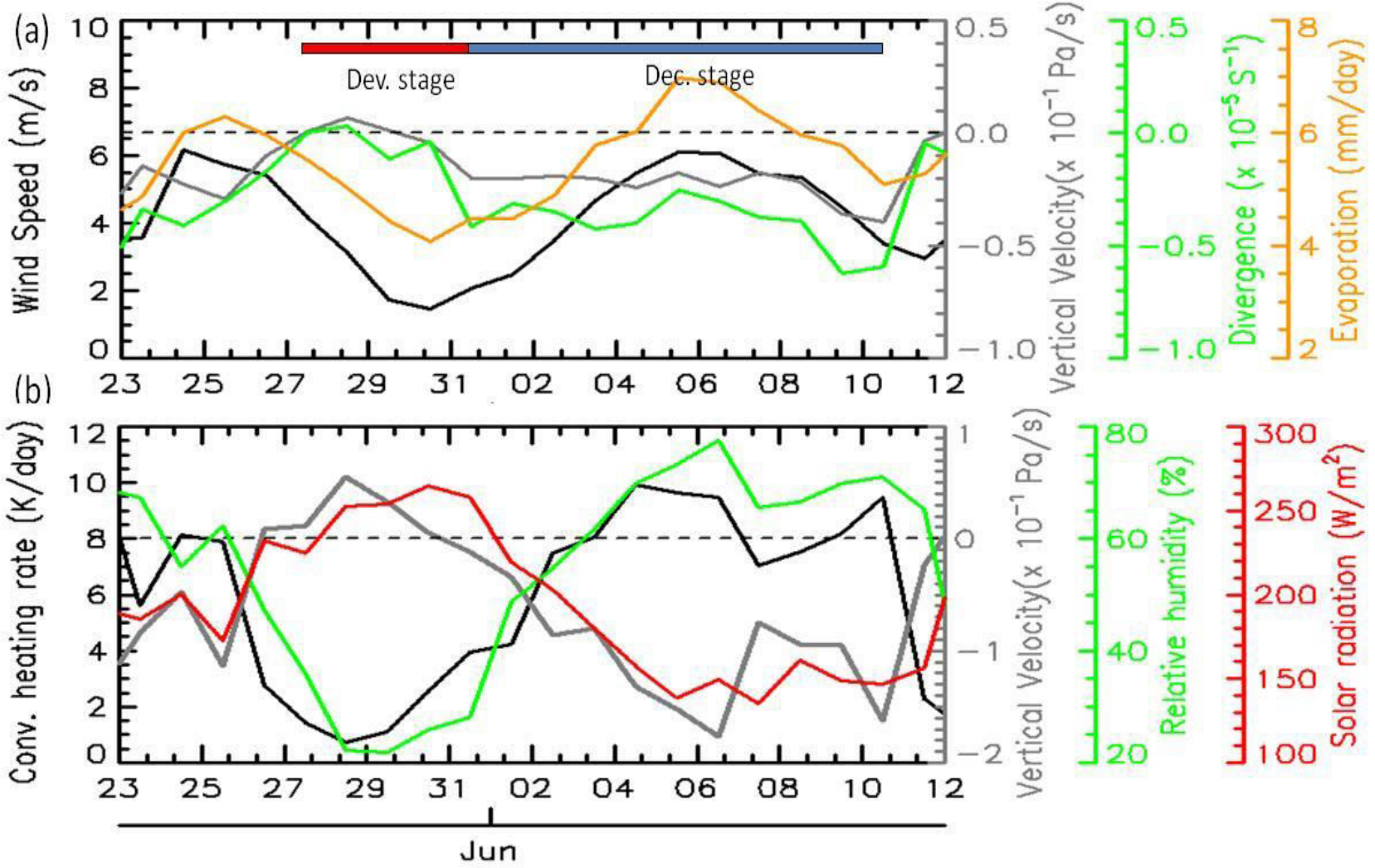

Fig. 4.12 The time series of atmospheric parameters at 155°E – 160°E, 5°S – 5°N. (a) wind speed, evaporation and divergence at the surface level, vertical velocity (1000 hPa-900 hPa) and (b) convective heating rate, vertical velocity and relative humidity (400 hPa-200 hPa) and solar radiation. Surface divergence is calculated from surface wind.

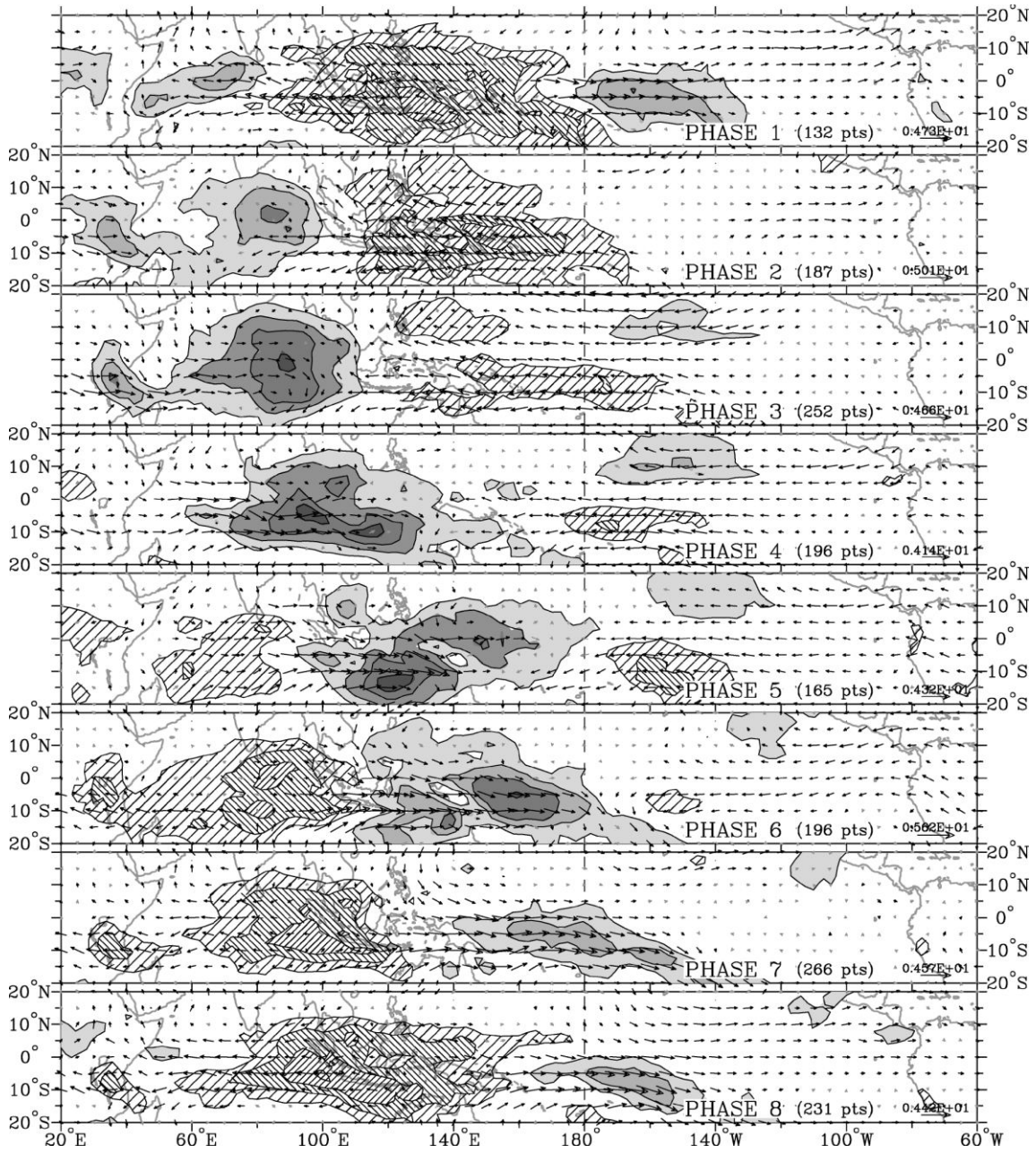

Fig. 4.13 December, January and February composite outgoing longwave radiation (OLR) anomaly and 850-hPa wind vector anomalies. *Shading levels* denote OLR anomalies less than -7.5, -15, -22.5, and -30 W/m^2, respectively which represent the active phase of the MJO, and *hatching levels* denote OLR anomalies greater than 7.5, 15, and 22.5 W/m^2, respectively which represent the suppressed phase of the MJO. *Black arrows* indicate wind anomalies that are statistically significant at the 99% level, based on their local standard deviation and the Student's *t* test. The magnitude of the largest vector is shown on the bottom right, and the number of days (points) falling within each phase category is given. Cited from Wheeler and Hendon (2004).

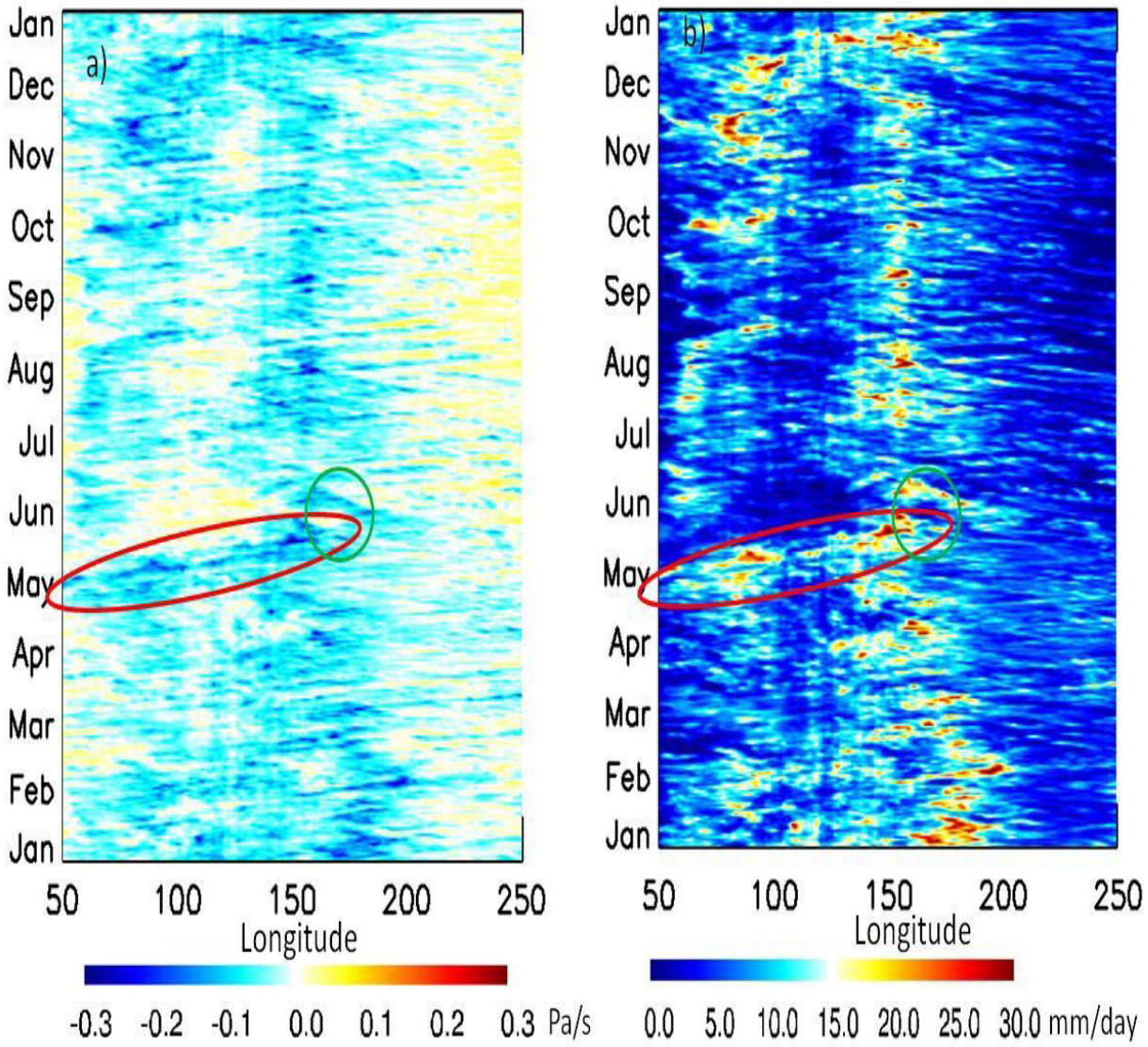

Fig. 4.14 Hovmöller diagram (10°S-10°N) of (a) vertical velocity at 600 hPa and (b) precipitation in 2003. *Green circle* denote the occurrence of HE030528 and *red curve* denote the MJO event associated with HE030528.

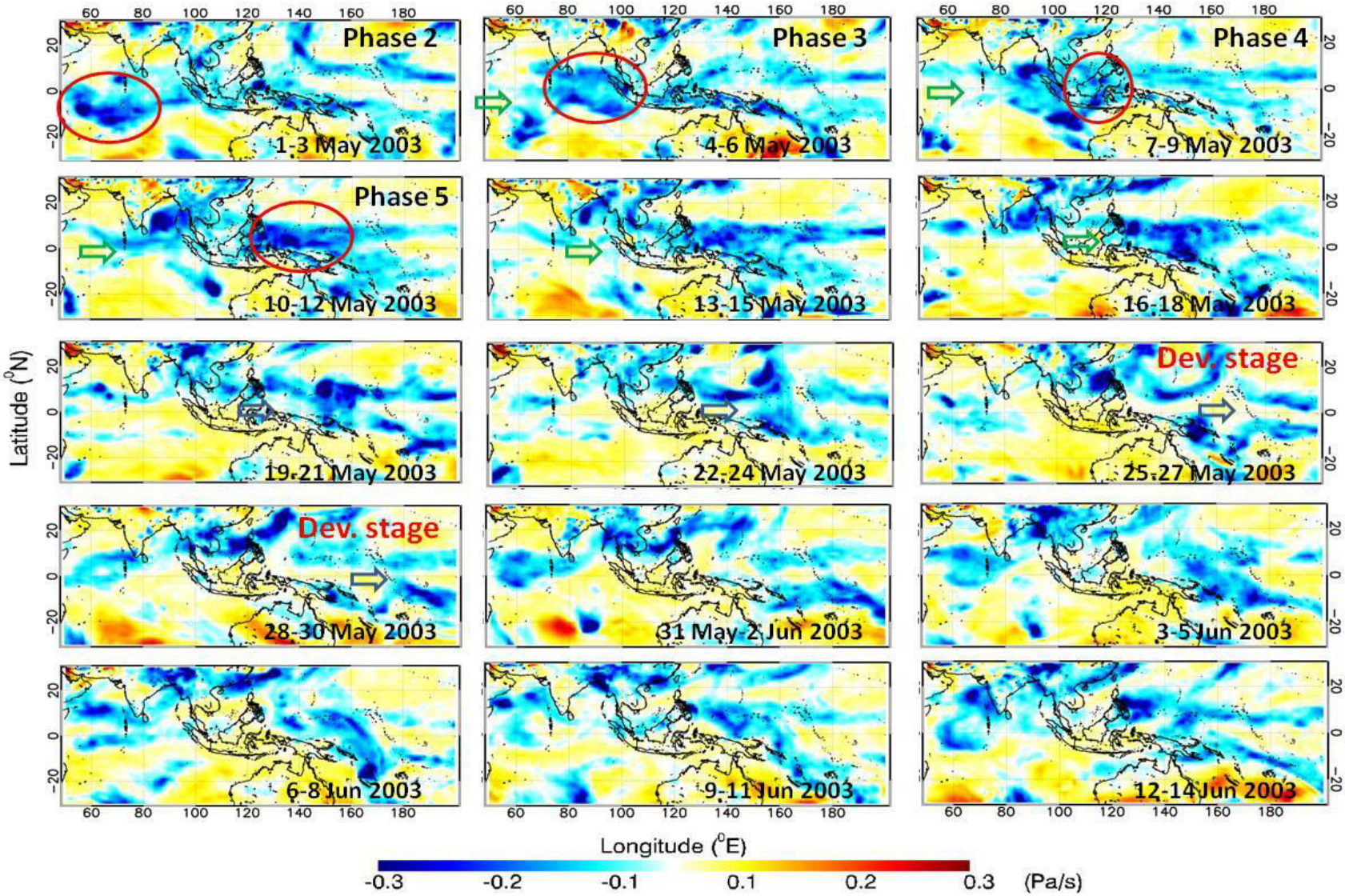

Fig. 4.15 The time series of vertical velocity map at 600 hPa. *Red circle* denote the strong upward motion (active phase) of the MJO and *green arrow* is the suppressed phase of the MJO.

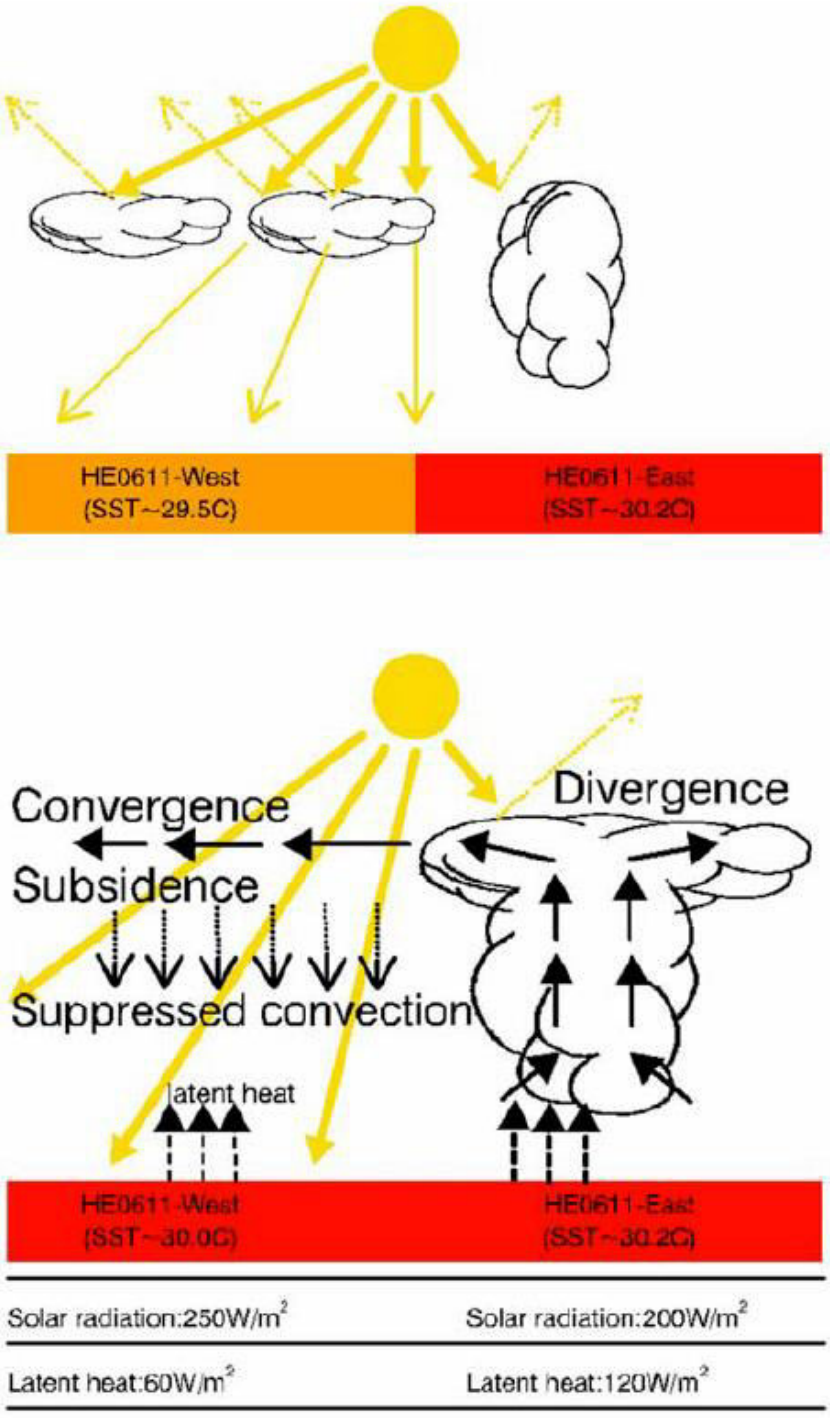

Fig. 4.16 Schematic diagrams of interaction between HE0611-West and -East. (top) The conditions before HE0611 formation. (bottom) The interaction between HE0611-West and -East when the deep convective system developed over HE0611-East. Cited from Qin and Kawamura (2010).

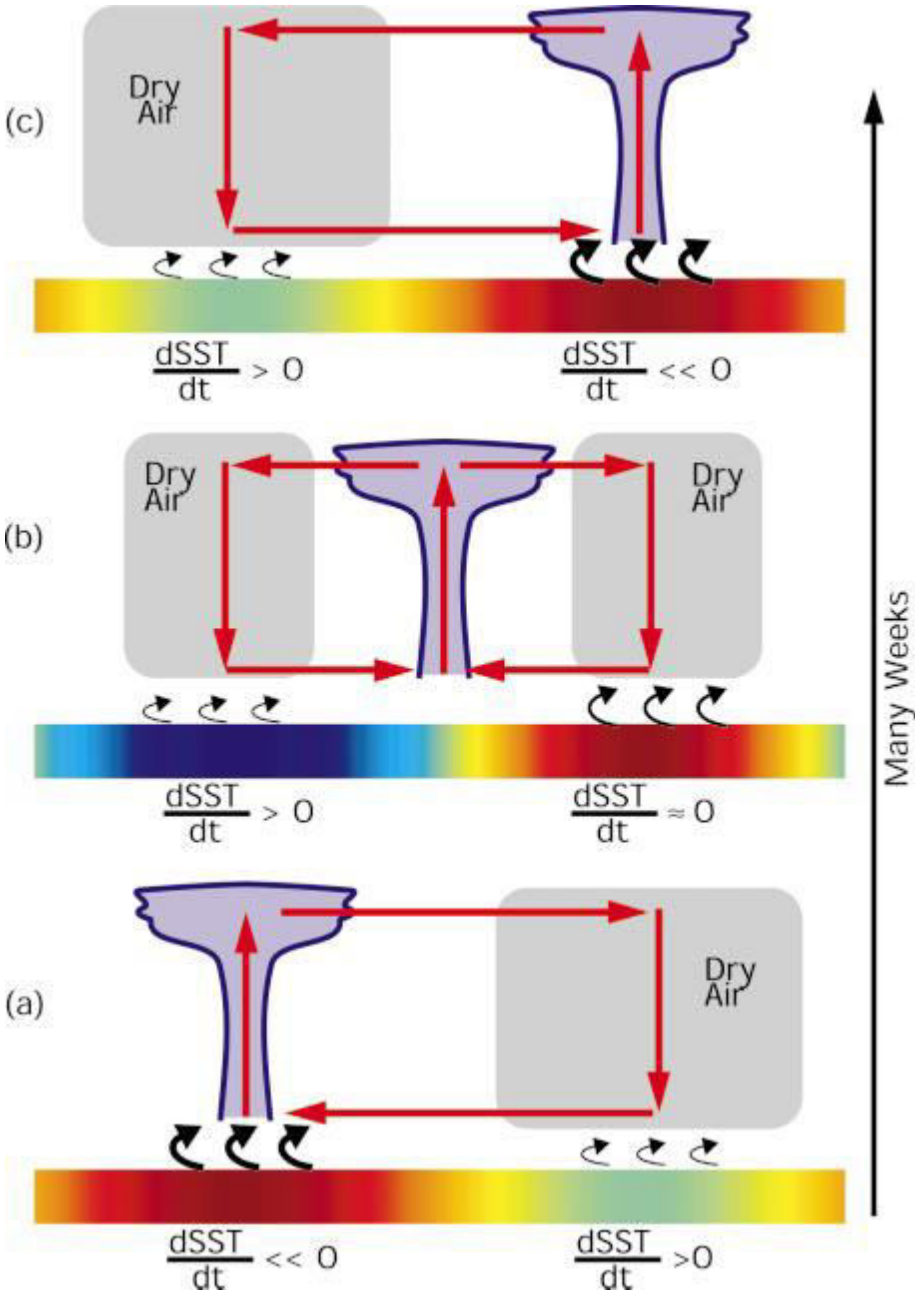

Fig. 4.17 Schematic of interaction between deep convection and SST in the Tropics. The cloud shows the location of convection, the large red arrows show the mean large-scale circulation, and the stripped bar shows schematically the SST evolution with red colors representing the warmest SSTs and blue the coolest SSTs. The small arrows near the surface represent surface latent heat fluxes, with the thickness indicating the relative magnitude of the mean fluxes. The total time-scale of SST progression is several weeks.

Chapter 5

Oceanic variability during the development and decay stage of HE

5.1. Introduction

The relation between the Pacific warm pool and HE has already been explained in Chapter 3 in term of statistical long term mean SST versus the HE occurrence rate. The higher frequencies of occurrence rate, the higher long term mean SST is resulted in the western equatorial Pacific. To understand the physical process underlying their relation, the variability of oceanic structure in the Pacific warm pool should be investigated.

Qin and Kawamura (2008) found the strong thermal stratification of water column during the HE occurrence derived by the radiative surface heating. The same tendency is also found in this study by using only the single buoy analysis showing in Fig. 3.4a. In this chapter, the more numbers of TAO/TRITON buoy and HE case are used to analyze the oceanic variability during the development and decay stage of HE and to investigate the physical process underlying the relation between HE and the Pacific warm pool. Section 5.2 emphasizes the thermal structure variability and Section 5.3 focus on the relation between HE and the Pacific warm pool.

5.2. Thermal structure variability

5.2.1. Thermal structure of the western equatorial Pacific

The western equatorial Pacific is characterized by warmer and more stable mixed layer at the west side (140°E-170°E) than at the central side (170°E-200°E). The thermal structure is relatively stratified at the west side and uniform at the central side. The stratification at the west

side is shown by the lag of the contour interval among SST, temperature at 40m (T40m) and temperature at 80m (T80m). In contrast, the contours of SST, T40m and T80m coincide at the central side. Thus, the mixed layer depth at the west side is shallower than the central (Fig. 5.1). This thermal structure pattern is consistent with the previous studies (e.g., Lukas and Lindstrom (1991); Ando and McPhaden (1997)).

Lukas (1988) stated that the importance of wind and buoyancy forcing makes the mixed layer in these two regions quite different. Figure 5.1d shows that the winds at the central until eastern Pacific are strong and stable. In contrast, the winds at the west side are weak on average, and highly intermittent. The strong (weak) winds at the central (west) side correspond to the low (high) stratification area (Fig. 5.1a). Despite not being investigated in this study, the relation between buoyancy forcing and thermal stratification in the western equatorial Pacific has been investigated by Lukas and Lindstrom (1991). The strong and stable stratification at the west side is caused by the strong buoyancy forcing associated with an excess of precipitation over evaporation (Fig. 5.2). At the east side, the influence of stable and strong wind speed is dominant over the evaporation excess inducing the equatorial upwelling.

The relation between thermal structure and HE occurrence rate is also shown in Fig. 5.1. The frequent HE occurrence is located at the west side. Thus, the west side which is characterized by the warm, stable, stratified and having shallow mixed layer depth may become the anvil for the occurrence of HE leading to the higher HE occurrence rate in this area.

5.2.2. Thermal structure variability during the development and decay stage of HE

The thermal structure during the development stage of HE is significantly different from that during the decay stage. Figure 5.3a shows that the temperature was more stratified during the development stage. The areal size rimmed by the contour of SST threshold was much wider than T40m and T80m. Moreover, the threshold contour of T40m almost coincided with T80m. The time series in Fig. 5.4 also shows that although there were the increase of T1-T40 and T1-T80 which was parallel with increasing SST, almost there was no thermal difference between 1 m and 10 m depth during the HE occurrence. This means that the increasing temperature only occurred at surface layer. Moreover, it is also shown that below/at the thermocline layer, the temperature was not influenced by the HE occurrence. This result shows that there was a

stratification during the development stage of HE which is caused by the increasing temperature at the surface layer. Calling back the result in Chapter 3, the hourly buoy data as depicted in Fig.3.4b shows that the surface layer stratification during the development stage of HE correspond to the high amplitude of diurnal SST. During the decay stage, the thermal structure became more uniform shown by the shrinkage of the SST threshold contour approaching T40m and T80m.

The thermal stratification during the development and decay stages of HE corresponds to the solar radiation and surface wind speed condition. Figure 5.3bc shows the zonal section of sub-surface temperature, wind speed and solar radiation averaged from 3°S to 3°N. Surface wind speed (solar radiation) during the development stage was lower (higher) than during the decay stage at the HE area (140°E-170°E). Furthermore, the influence of surface wind speed and solar radiation to the thermal stratification was observed in detail at around 155°E. The contour of temperature threshold was pulled to the surface due to the higher (lower) surface wind speed (solar radiation) than its surroundings. The time series shown in Fig. 5.4 also demonstrates the same tendencies. During the development stage, the solar radiation increased drastically from ~140 W/m^2 to ~270W/m^2 only in 3 days and wind speed decreased more slowly from ~4 m/s to ~1.5 m/s in 4 days. As a result, the temperature at the surface layer increased. After the increase (decrease) of surface wind speed (solar radiation) during the decay stage, the temperature becomes more uniform, lower at the surface and higher at the deeper layer.

The development stage of HE030528 was characterized by the stratification at the surface layer due to the surface heating. During the decay stage, surface (deeper) layer temperature became lower (higher). This characteristic becomes more pronounced for the longer period HE cases with higher solar radiation intensity and slower wind speed (Fig. 5.5). In case of HE041216 and HE071003, the contour of temperature threshold can penetrate very deeply approaching the thermocline since the solar radiation (surface wind speed) was higher (lower) than HE030528 i.e., about 300 W/m^2 (< 2 m/s). Then, the thermal structure during the HE occurrence formed trapezoidal shape. Thus, considering the whole process of HE, the occurrence of HE in the western equatorial Pacific can be identified by the trapezoidal shape of the thermal structure change in the mixed layer. The schematic picture of the HE occurrence is shown in Fig.5.6 and this can becomes the typical characteristic of HE occurrence in the western equatorial Pacific.

5.3. The physical process underlying the relation between Hot Event and the Pacific warm pool

The mechanisms of the trapezoidal shape of the HE occurrence can be explained by the parameter of surface current and latent heat flux (Fig.5.7). During the development stage, the water column in the mixed layer was relatively calm denoted by the zero current divergence and low current speed at the sea surface. Latent heat flux was also low. Thus, the heat received from the solar radiation was accumulated at the sea surface causing the increase of SST and thermal stratification. This condition created the half shape of the trapezoid. During the decay stage, the downwelling and horizontal mixing occurred, denoted by the increase of current convergence and current speed at the sea surface. It is also reported by Lukas and Lindstorm (1991) that westerly winds straddling the equator cause an Ekman convergence at the equator, resulting in a downwelling response in that area. Latent heat flux also became high. Hence, the accumulated heat gained during the development stage was transported to the deeper layer through the downwelling process as the sensible heat flux and released to the atmosphere through the increase of latent heat flux during the decay stage resulting the lower (higher) temperature at the surface (deeper layer). This condition created another half of the trapezoidal shape. Therefore, the trapezoidal shape of HE occurrence represents the heat mixing mechanism in the mixed layer.

The longer period of observation shows the role of HE for the formation of Pacific warm pool. I compared three months period in 2003 which had frequent HE occurrence and in 2007/2008 which had no HE occurrence in the area of 152°E - 157°E and 3°S - 3°N (Fig.5.8). In the interannual terms, 2003 is categorized as normal while 2007/2008 is moderate La Niña (http://www.cpc.ncep.noaa.gov/products/analysis_monitoring/ensostuff/ensoyears.shtml; Fig. 5.9). Thus, the thermocline layer is very deep in 2007/2008 i.e., more than 100 m. The trapezoidal shape of subsurface temperature variation was detected in the mid April 2003 which correspond to the occurrence of HE030413, late April 2003 and mid May 2003 which correspond to HE030430, late May 2003 which correspond to HE030528 and late Jun 2003 which correspond to HE030627. It is also noticed that except for HE030413, their development and decay correspond to the zonal wind variation as explained in the previous chapter; weak wind during the development stage and westerly wind during the decay stage. We also can see the accumulated heat at the surface during the development stages and sensible heat transfer from the surface to the deeper layer during the decay stages as known as the mechanisms of the

trapezoidal shape of HEs. In 2007/2008, the trapezoidal shape was not detected resulting no sensible heat transfer to the deeper layer. The easterly wind was consistently strong during all period. The weak wind only occurred in January 2008 which was coincident with low solar radiation. Therefore, HE was not generated.

As a result, the period of 2003 is warmer than 2007/2008 since more sensible heat was transported to the deeper layer in 2003. The warm subsurface temperature was maintained during 2003. In contrast, in the end period of 2007/2008, the subsurface temperature was cooler than its beginning period. Thus, HE plays important role to maintain the warm mixed layer in the western Pacific warm pool by the transporting the sensible heat accumulated at the surface during the development stage of HE to the deeper layer during the decay stage. This becomes the positive feedback of HE to the Pacific warm pool formation. This result becomes the physical evidence of the relation between HEs and the Pacific warm pool as statistically proven in Chapter 3. Moreover, this result also emphasize the role of surface wind as a key for the HE generation since the surface wind controls current speed, current divergence and latent heat flux during the HE occurrence. However, this analysis ignored the difference of the interannual background between those 2 periods which may also influence the variation of subsurface temperature. This problem is left for future study.

5.4. Discussion

The thermal structure of HE has been discussed by Qin et al. (2008). Although the thermal stratification was detected during the occurrence of HE0611-west, the trapezoidal shape was not shown apparently in their analysis (Fig.5.10a). This is because their analysis only focused on the development stage. Figure 5.10b shows that the integrated heat input of HE0611-West still increased in the ending period of their analysis. As stated in the previous section, the decay stage is important to show the accumulated heat distributions; released to the atmosphere and transported to the depth. The whole HE processes create the trapezoidal shape of the thermal structure.

In much longer timescales, the role of surface wind in driving the ocean circulation for the Pacific warm pool formation has been explained by Clement et al. (2005). They focused on how the higher heat gain at the equator is transported to the higher latitude to form the warm pool. Under easterly wind stress, the thermocline is deep in the west and shallow in the east.

Because of this, poleward Ekman transport of water at the surface, compensated by equatorward geostrophic flow below and linked by equatorial upwelling, creates a cold tongue in the east but homogenizes SST in the west, creating warm pool. In the present study the mechanisms of how the surface wind forcings control the heat transport in the mixed layer of the Pacific warm pool is described in the shorter time scale. Although the mechanisms of the mixed layer formation have been widely known as shown systematically by Marshall and Plumb (2008) (Fig.5.11), I emphasized that through the concept of trapezoidal shape, the process of radiative heating at the surface does not occur simultaneously with the heat transport controlled by the wind forcings and this may characterize the heat transport mechanisms in the mixed layer of the Pacific warm pool. This step-by-step process may be more effective to distribute the heat received at the sea surface to the deeper layer. As shown in Fig. 5.8, although both radiative forcing and wind forcing were strong in December 2007 and March 2008, there were less heat transported to the deeper layer. Therefore, the trapezoidal shape of subsurface temperature can become a new perspective of heat input mechanisms into the mixed layer in the western equatorial Pacific.

5.5. Conclusions

The oceanic variability during the development and decay stages of HE is concluded as follows.

1. The warm and relatively stable thermal structure at the west side of the Pacific warm pool may become the anvil for the HE occurrence so that the highest occurrence rate of HE is found in this area.
2. The occurrence of HE in the western equatorial Pacific can be identified by the trapezoidal shape of the thermal structure change in the mixed layer. This trapezoidal shape can be described as follows: during the development stage, higher temperature is accumulated in the surface layer while during the decay stage, the temperature at the surface (deeper layer) decrease (increase).
3. HEs play an important role to maintain the warm mixed layer in the western Pacific warm pool by transporting the heat accumulated at the surface during their development stage to the deeper layer during their decay stage.
4. Since surface winds control the heat accumulation and heat transport in the mixed layer by influencing current speed, current divergence and latent heat flux, the surface winds

become the key factor for the HE occurrence and the formation of the thermal structure in the Pacific warm pool.

Table 5.1 Summary of the subsurface variability during the development and decay stage of HE030528.

	Development stage	**Decay stage**
SST	high	low
Surface wind speed	low	high
Solar radiation	high	low
Stratification	strong	weak

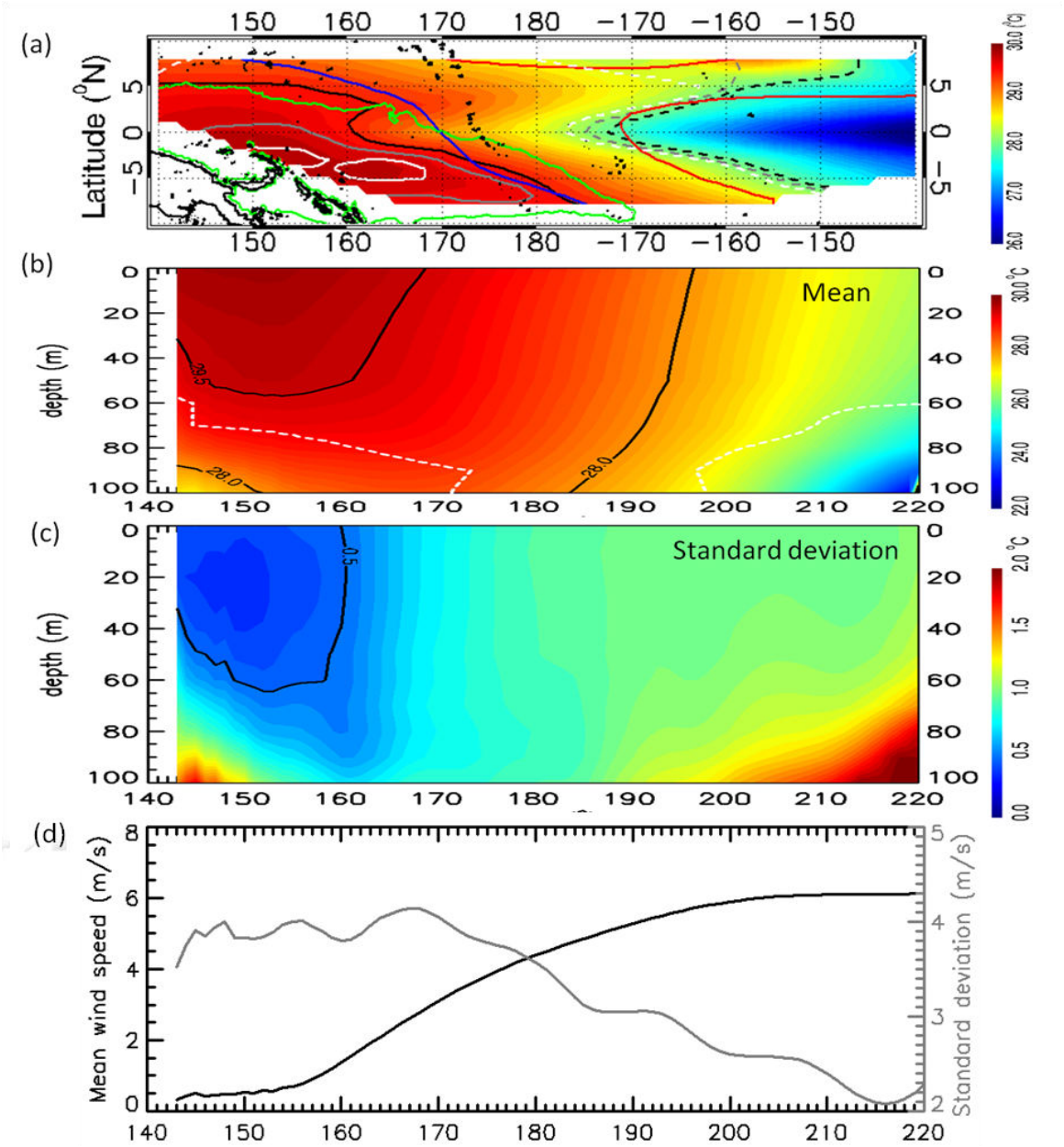

Fig. 5.1 (a) The SST (T1m) climatology map of western equatorial Pacific. *Black, gray* and *white contours* denote SST, T40m and T80m respectively. *Solid* and *broken contours* denote the isotherm of 29.5°C and 28°C. *Blue* and *red contour* denote 3.5 m/s and 5.5 m/s wind speed respectively. *Green contour* represents the frequent HE area with the occurrence rate of more than 10%. (b,c) Zonal section (5°S-0°N) of climatological mean and standard deviation of sub surface temperature. *Broken white contour* is the mixed layer depth ≈ vertical gradient of 0.02°C/m. (d) Zonal section (5°S-0°N) of climatological mean and standard deviation of wind speed.

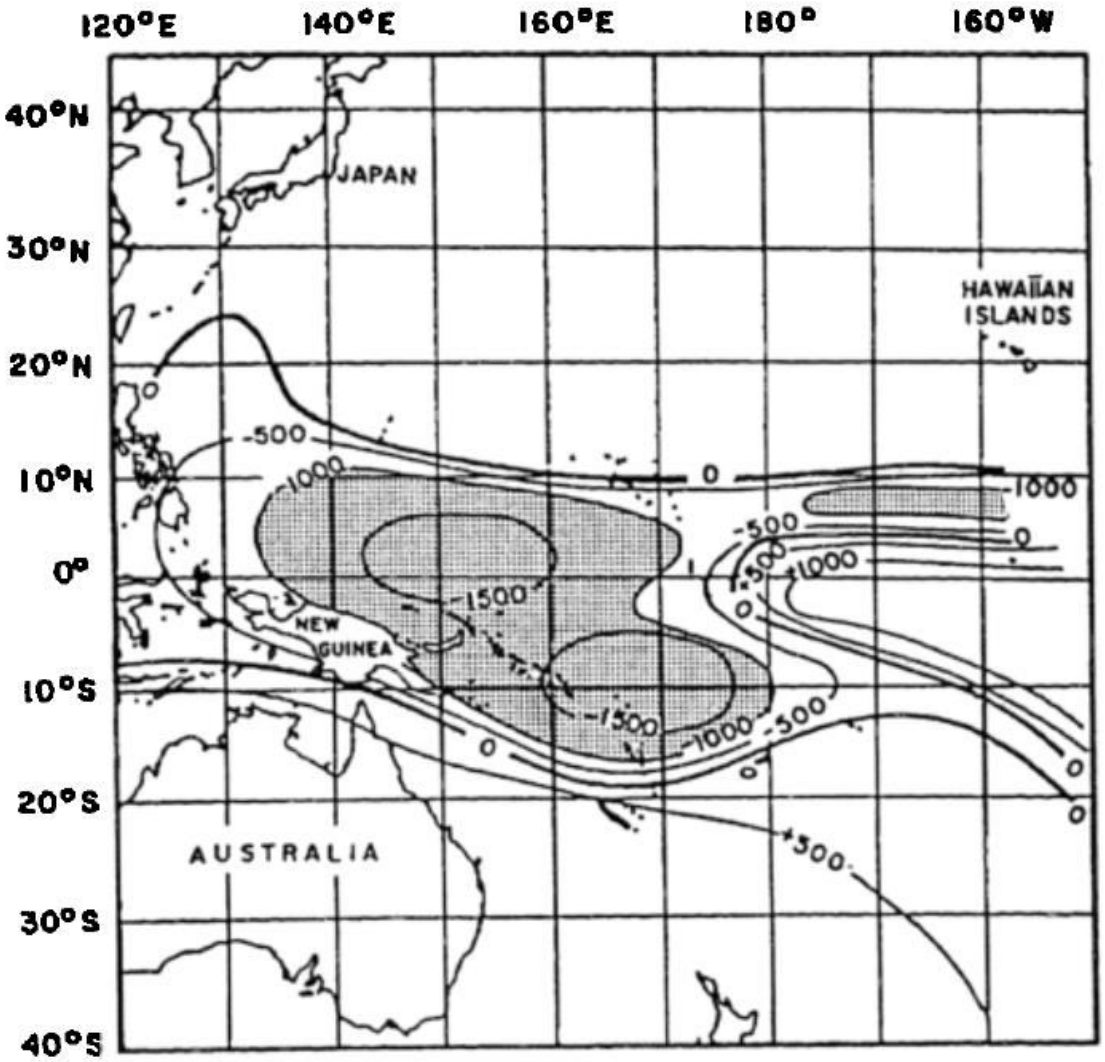

Fig. 5.2 Annual average net evaporation minus precipitation (mm) in the western tropical Pacific. Regions of greater than 1 m/year of freshwater input are stippled. Cited from Lukas and Lindstorm (1991).

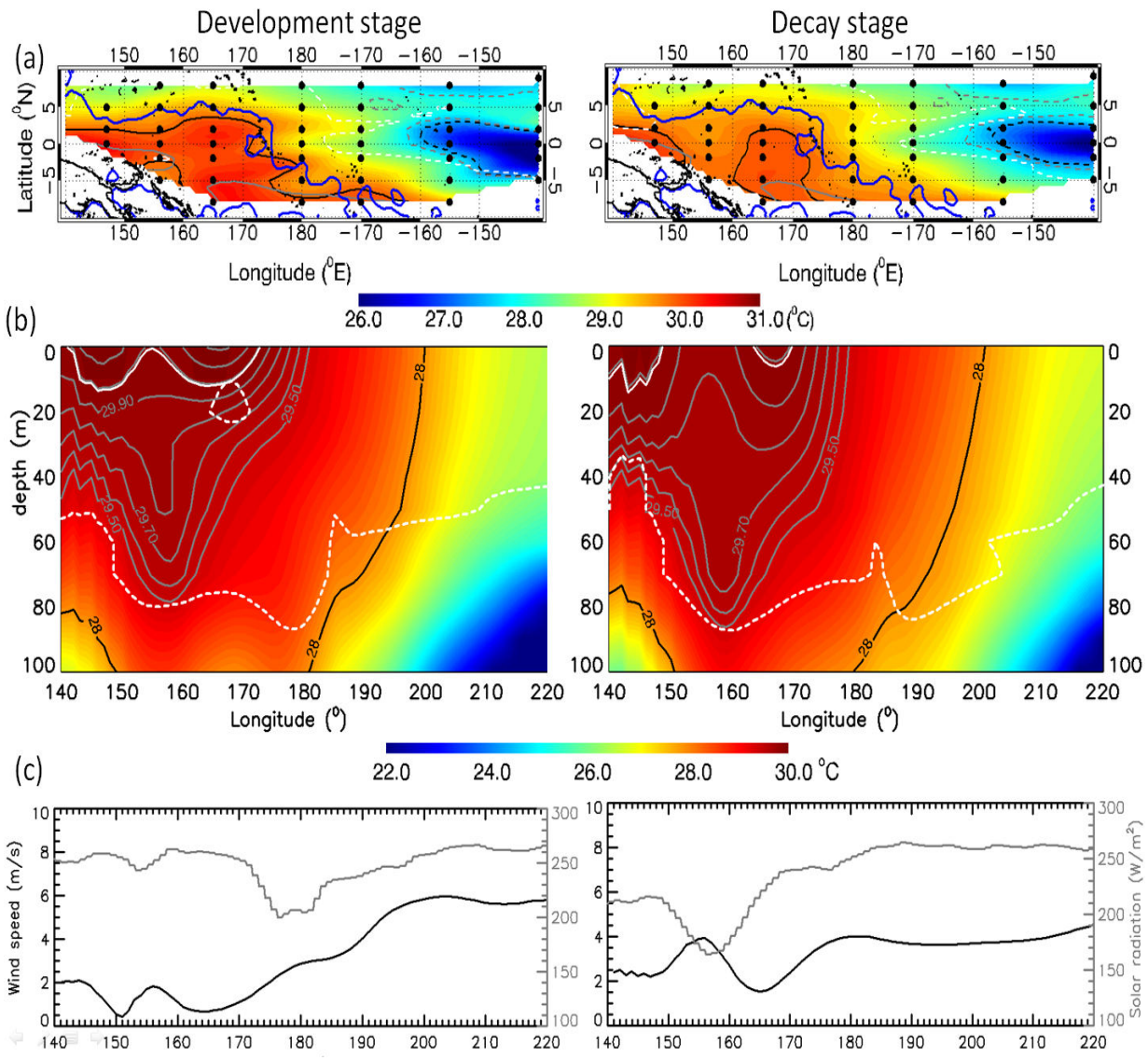

Fig. 5.3 (a) Sub-surface temperature composites of the development and decay stage of HE030528. *Blue line* is the HE area obtained by NGSST. *Black, grey* and *white lines* denote T1m, T40m and T80m respectively, obtained by the buoy observations. *Solid* and *broken lines* denote SST threshold and 27.5°C respectively. (b,c) Zonal section of subsurface temperature, wind speed and solar radiation OAFLUX (3°S - 3°N) of the development and decay stages of HE030528. The *solid (broken) white contour* denotes the SST threshold (mixed layer depth ≈ vertical gradient of 0.02°C/m).

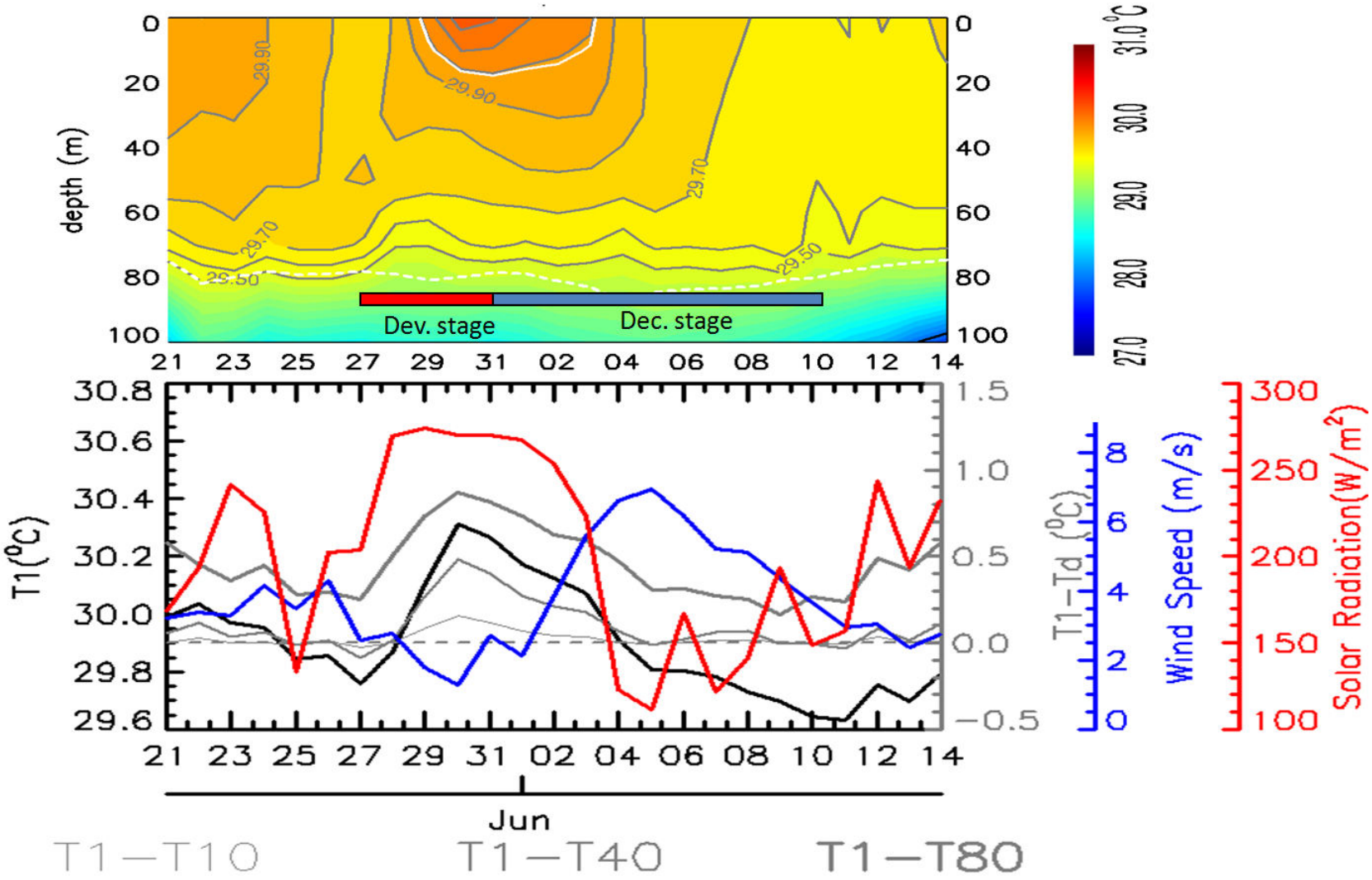

Fig. 5.4 The time series of surface temperature, the difference between surface and subsurface temperature, wind speed and solar radiation for HE030528 at 152°E - 157°E and 3°S - 3°N. *Solid (broken) white contour* is the SST threshold (mixed layer depth).

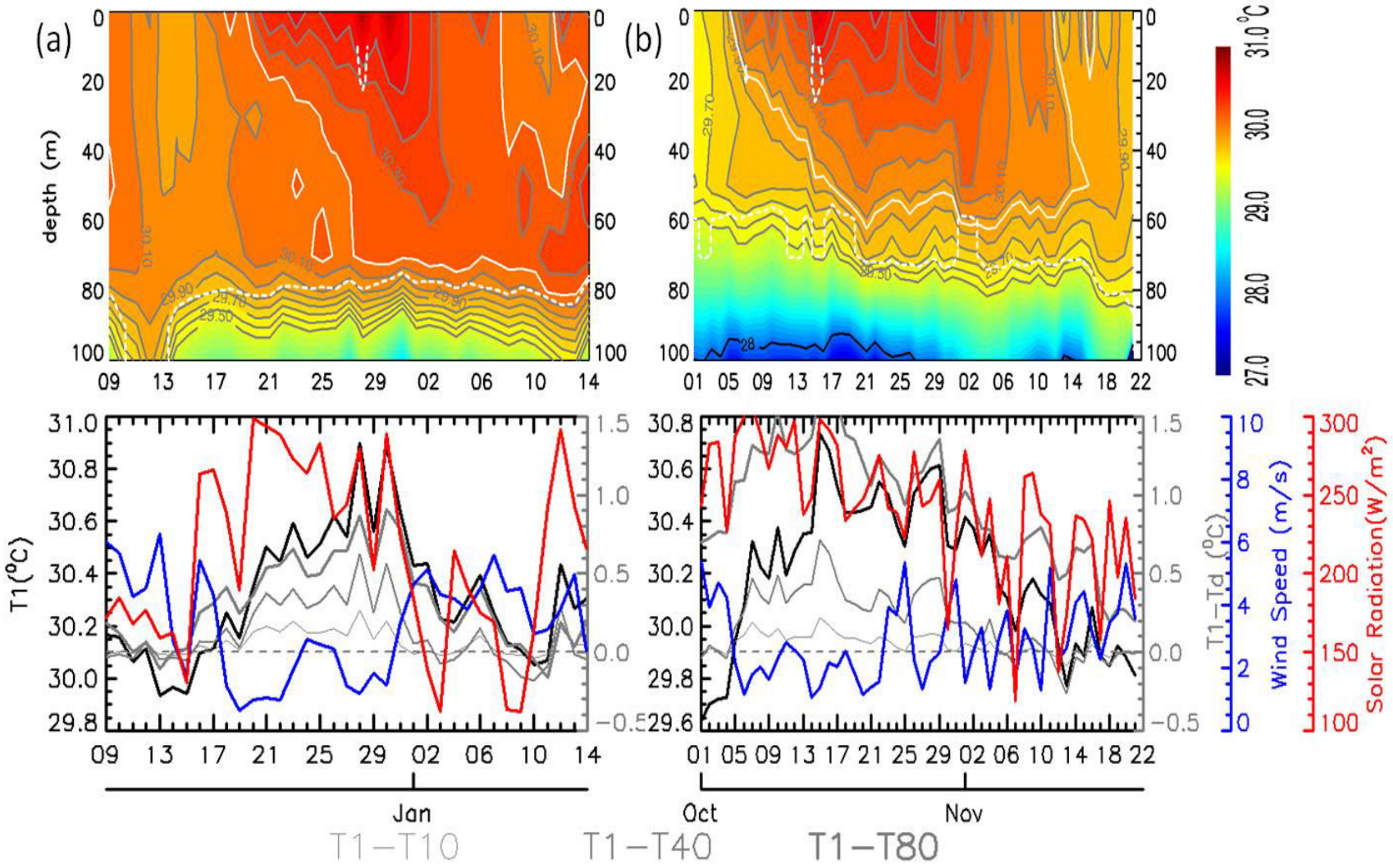

Fig. 5.5 Same as figure 5.3 for (a) HE041216 at 165°E - 170°E,5°S to 0°N and (b) HE071003 at 145°E-150°E and 0°N-5°N.

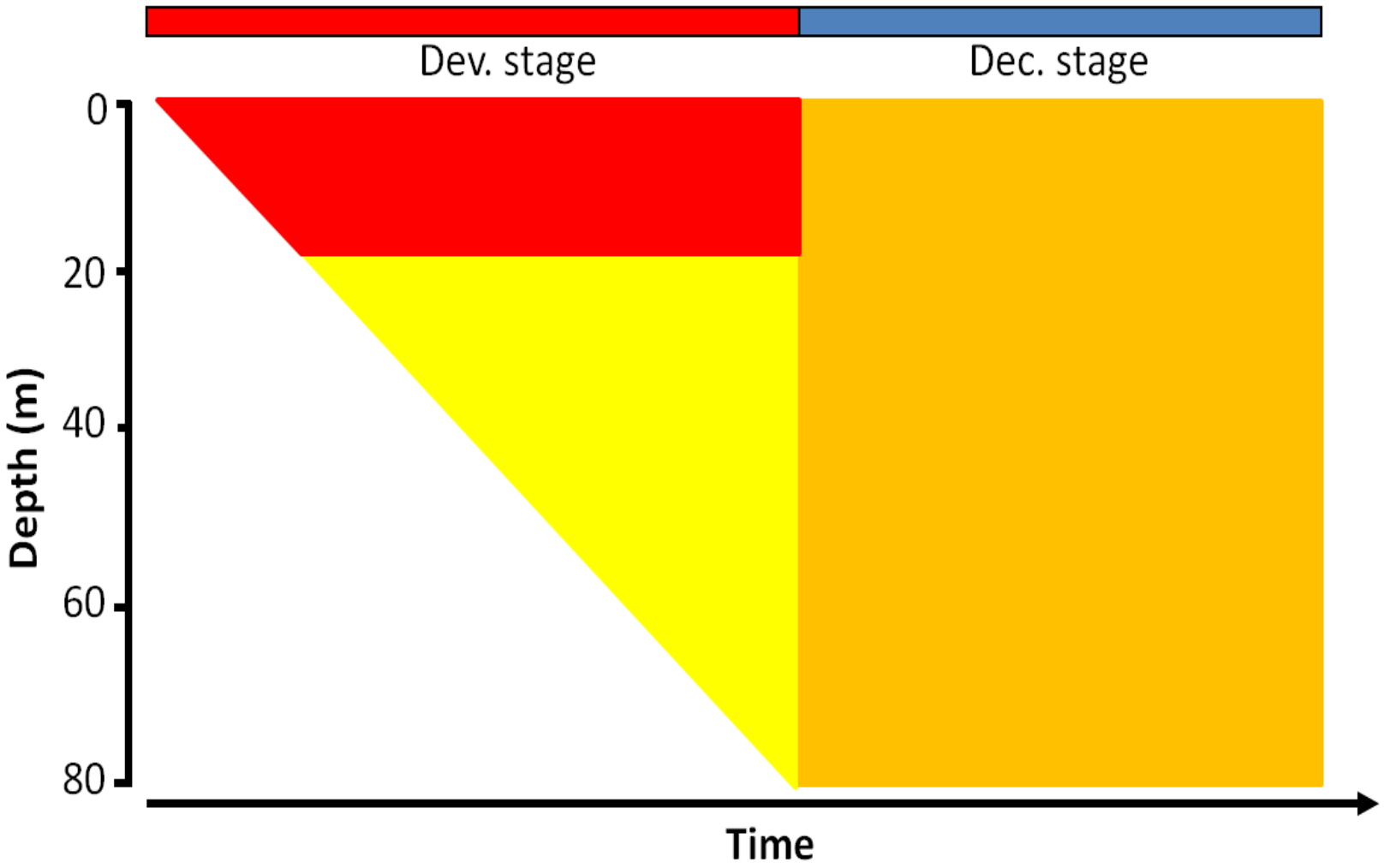

Fig.5.6 Schematic picture of the trapezoidal shape of subsurface temperature during the HE occurrence. *Yellow, orange* and *red colors* denote the increasing temperature.

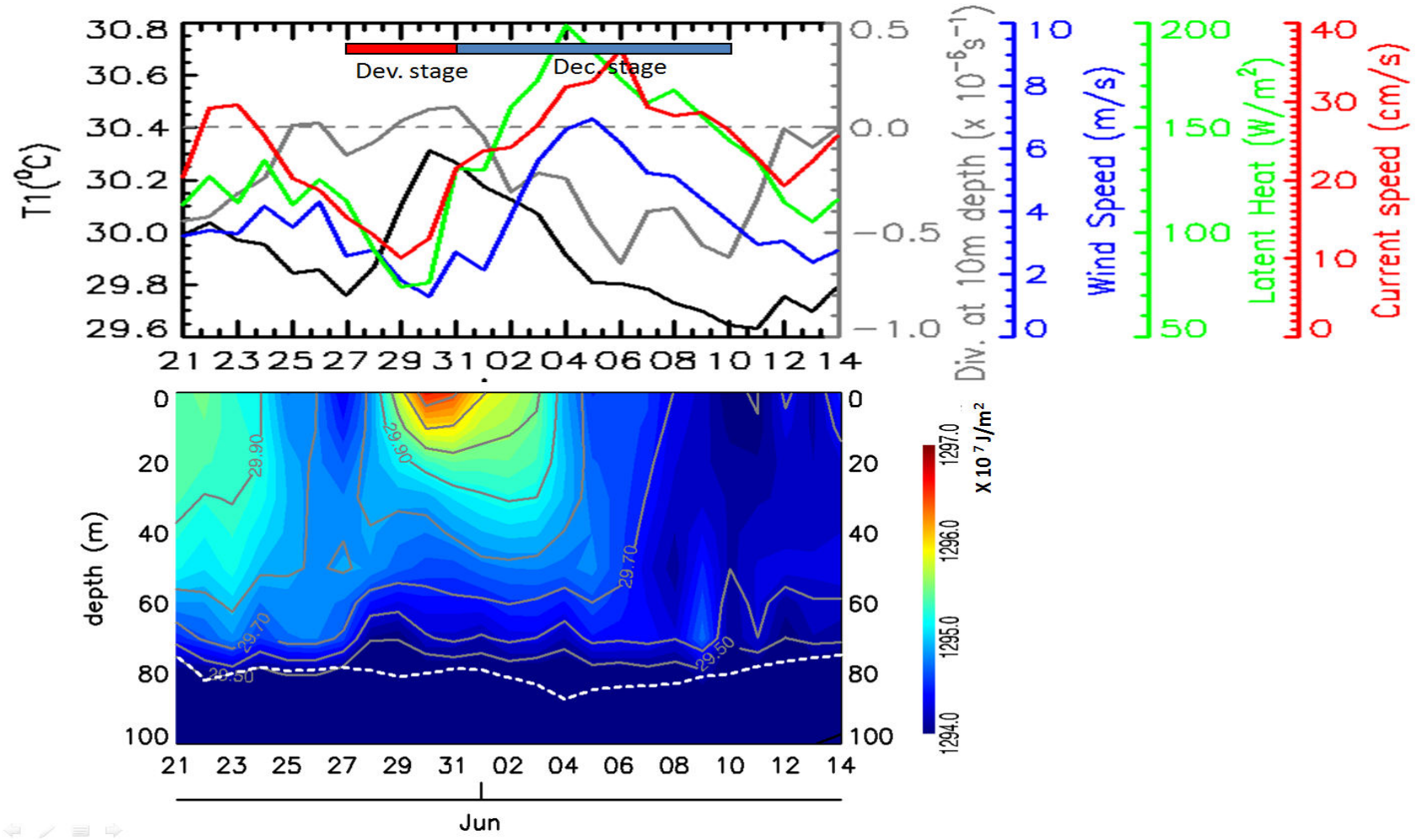

Fig. 5.7 The time series of SST, wind speed, current divergence at 10 m depth, current speed at 10 m depth latent heat (upper panel) and heat content (lower panel) for HE030508 at 152°E - 157°E and 3°S - 3°N. *Broken white contour* denotes mixed layer depth (vertical gradient temperature = 0.02°C/m) and *solid gray contour* denotes subsurface temperature.

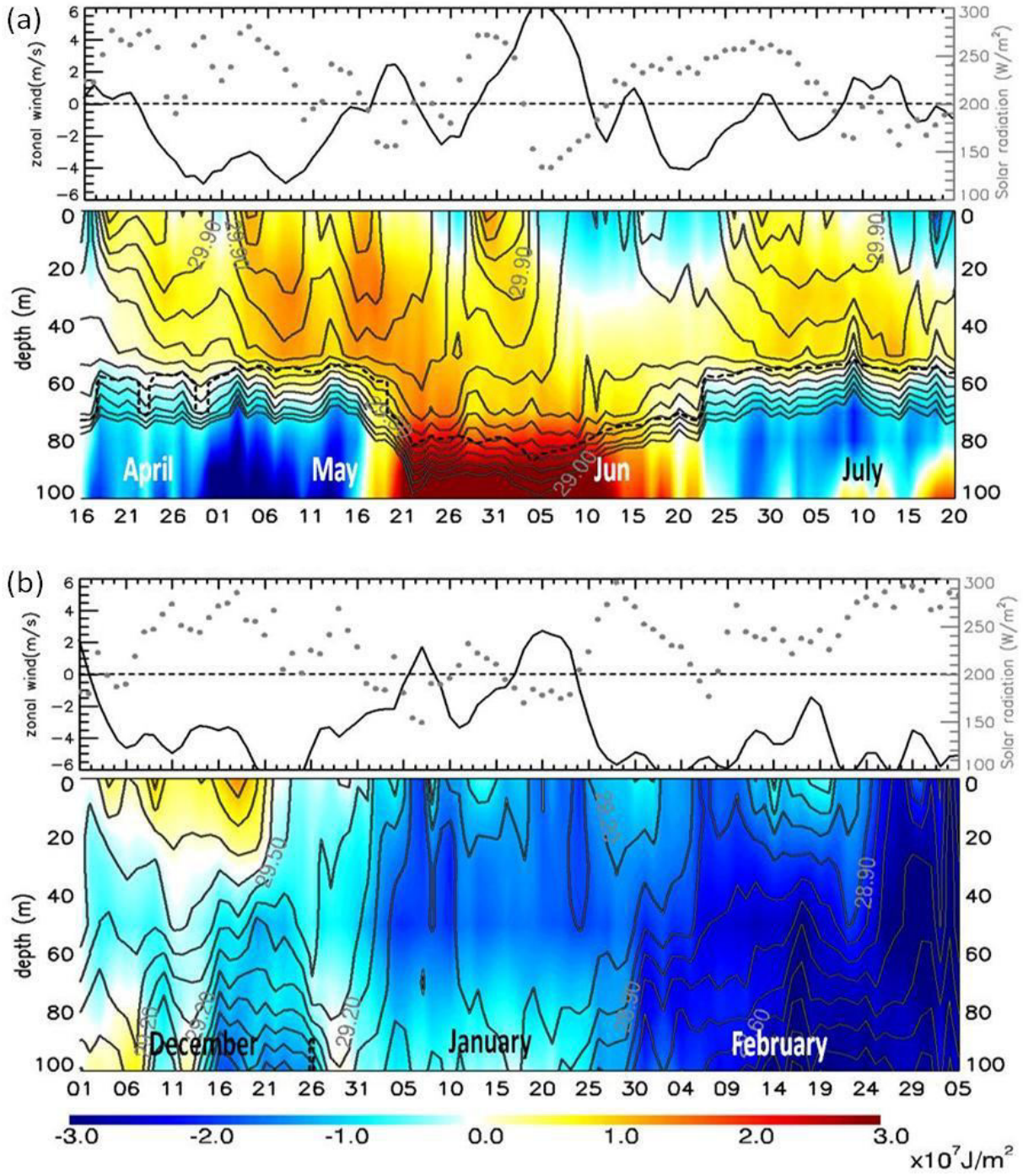

Fig. 5.8 The time series of zonal wind component, solar radiation and heat content in (a) 2003 and (b) 2007/2008 at 152°E - 157°E and 3°S - 3°N. The heat content was normalized by subtracting to the first date's value. *Broken contour* denotes mixed layer depth (vertical gradient temperature = 0.02°C/m), *solid contour* denotes subsurface temperature. Zonal wind and solar radiation were smoothed by 3 days average.

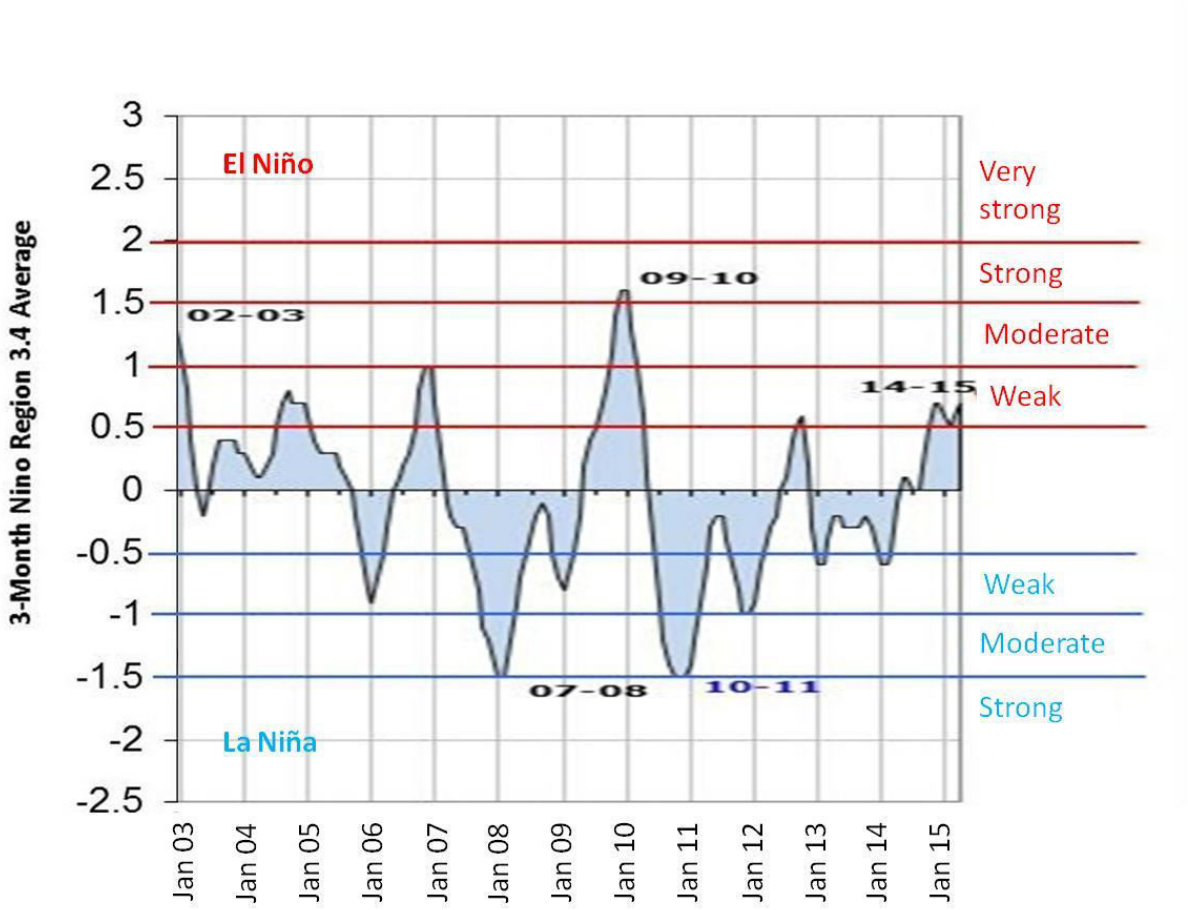

Fig. 5.9 Oceanic Niño Index (ONI) modified from http://ggweather.com/enso/oni.htm. ONI data is from http://www.cpc.ncep.noaa.gov/products/analysis_monitoring/ensostuff/ensoyears.shtml

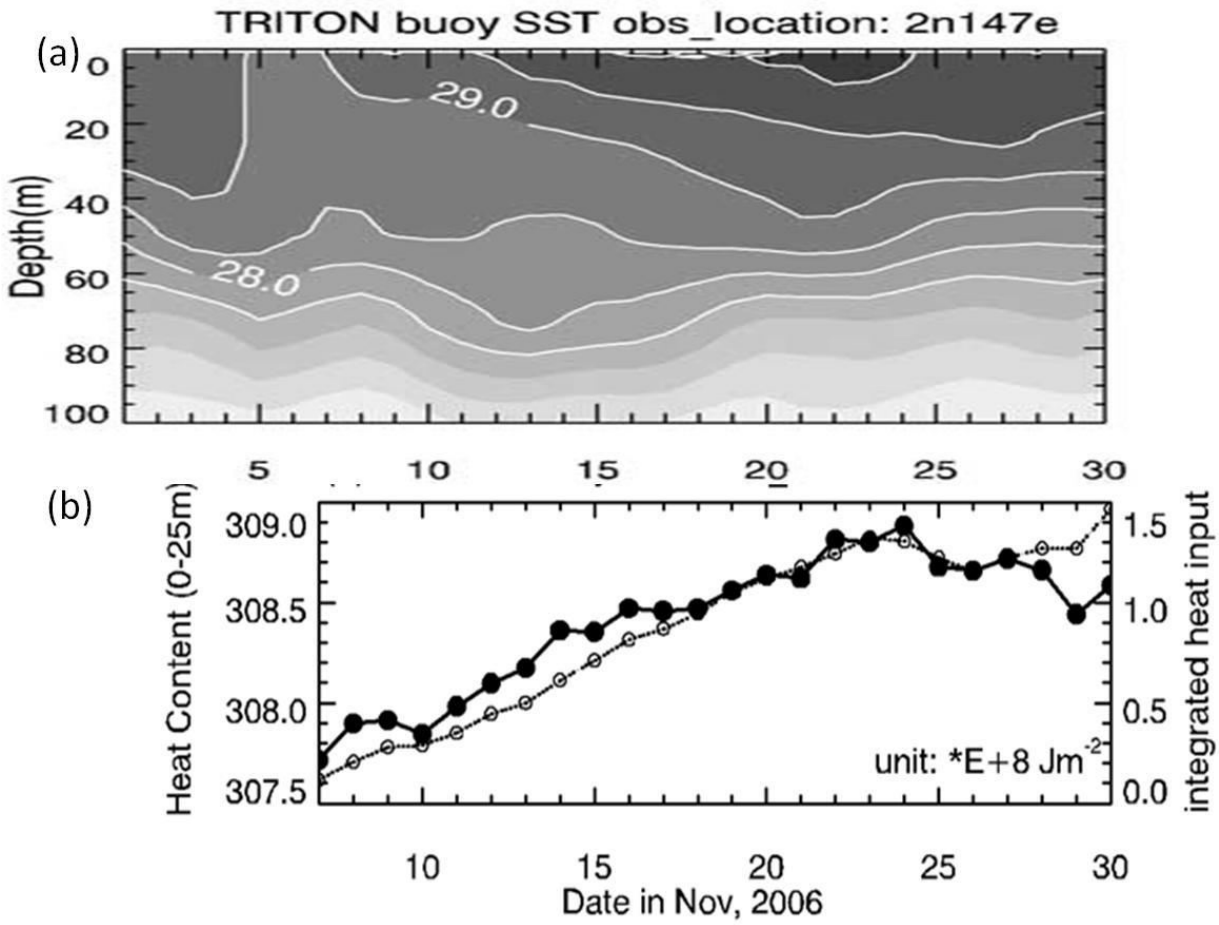

Fig. 5.10 (a) Time-longitude plot of the vertical temperature and (b) the mix-layer heat content (*solid line*) and the accumulated heat gain (*dashed line*) calculated from observations of the buoy (2°N, 147°E) in HE0611-West

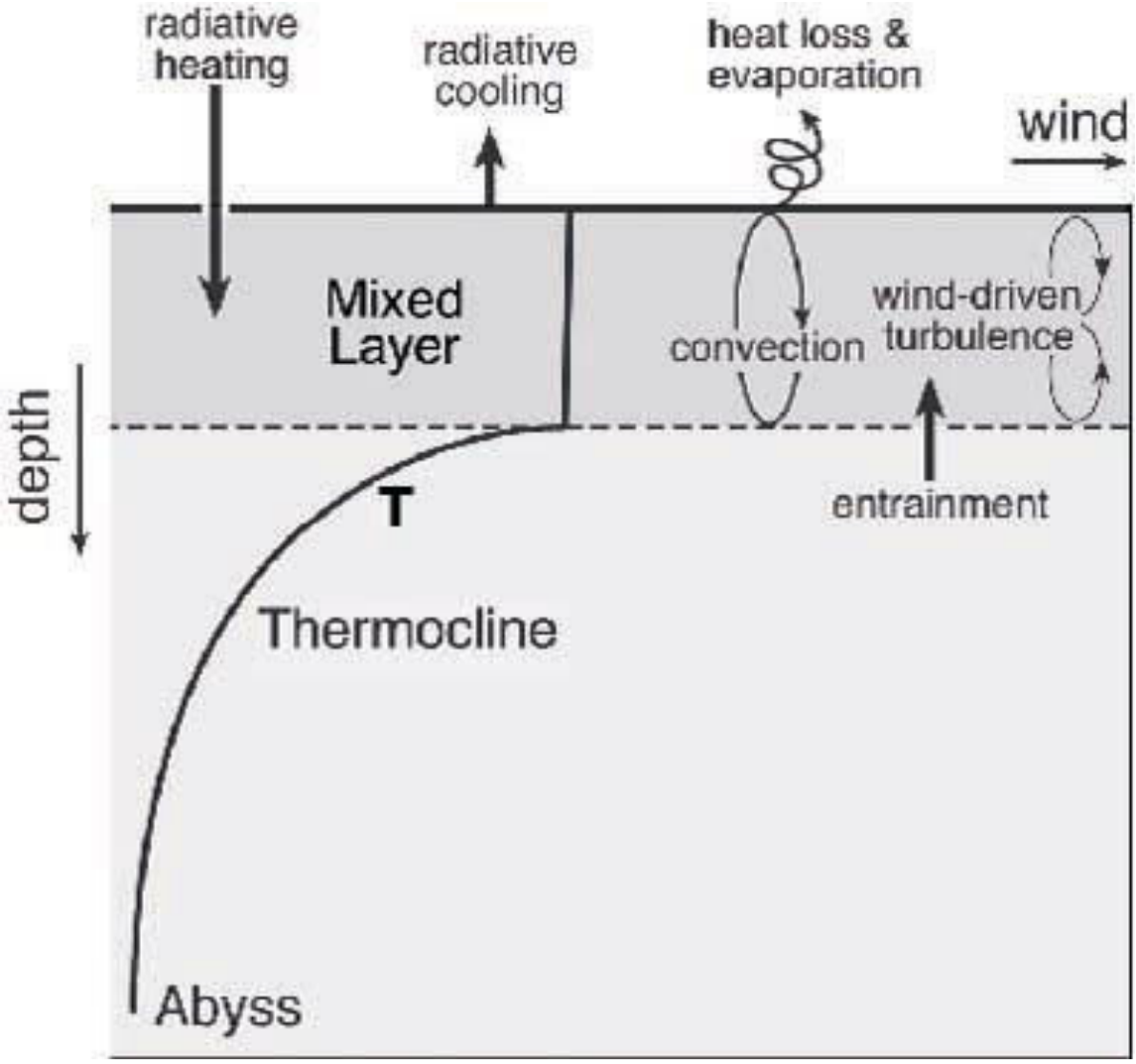

Fig. 5.11 A schematic diagram showing processes governing the mixed layer temperature variations. Cited from Marshall and Plumb (2008).

Chapter 6
General conclusions and remarks

Study on Hot Events in the western equatorial Pacific has been conducted through both case study and climatology analysis. For detecting HE in the western Equatorial Pacific NGSST-O-Global-V2.0a was chosen. The diurnal correction applied for two microwave sensors composing NGSST-O-V2.a, significantly improve the observation coverage and reduce the errors arising from merging observations at different times. I also proposed new threshold which is free from seasonal effect for detecting HE. Then, I defined an HE as a connected region with an SST higher than the space-time dependent threshold of about 30°C, with a minimum areal size of 2×10^6 km, and a duration period longer than 6 days. Thus, through the special treatment of examined SST dataset and the improved detection method, the characteristics, mechanisms and interactions of HEs with the Pacific warm pool can be explained as follows.

1) **Characteristics**
   a. 71 HEs during 2003–2011 were detected in the western equatorial Pacific. These HEs have a mean areal size of 6.30×10^6 km^2, a mean duration period of 18.14 days, a mean amplitude of 0.33°C, and a mean speed of development (decay) of 0.28 (0.31) × 10^6 km^2/day.
   b. The HEs are distributed within the equatorial band to subtropical Pacific (20°S – 30°N) and extended eastward to 150°W. HEs frequently occur along the northern coasts of the New Guinea Island and the Solomon Islands, with an eastward extension to 180°E.

c. The HE formation in the western equatorial Pacific is indicated by positive anomaly of solar radiation from its climatology while its decay is denoted by the anomaly of surface wind direction.
d. The occurrence of HE in the western equatorial Pacific is characterized by the trapezoidal shape of the thermal structure change in the mixed layer. This trapezoidal shape can be described as follows: during the development stage, higher temperature is accumulated in the surface layer while during the decay stage, the temperature at the surface (deeper layer) decrease (increase).

2) Mechanisms

a. The condition of high solar radiation and low surface wind speed is required for the HE occurrence. Moreover, during the development stage, the solar radiation (wind speed) in the HE area is much more enhanced (reduced) than during the decay stage.
b. The mechanisms of HE occurrence is related with how the heat is received by the sea surface during the development stage and how it is released to the atmosphere and transported into the depth during the decay stage.
c. During the development stage, surface wind speed and convergence are low. In the atmosphere, the weak surface wind influences the convection process by reducing the latent heat flux as well as the evaporation rate. Because of the decreasing convection, dry air from the top of troposphere sank and gave positive feedback to suppress the convection. The subsidence area corresponds to the clear sky area which leads to the high solar radiation during the development stage of HE. In the ocean, the weak surface winds prevent oceanic mixing. Thus, during the development stage, the increase of SSTs of more than ~30°C is caused by the accumulated heat received by the sea surface from the solar radiation (Fig. 6.1 left).
d. During the decay stage, surface wind speed and convergence are high. The strong convergences activate the convection process and accelerate the cloud formation. Eventually, the solar radiation decreases. The strong wind speed increases the latent heat released to the atmosphere and induces the downwelling that transports the heat to the deeper layer of the mixed layer. These processes reduce SSTs in the decay stage (Fig. 6.1 right).

3) **Interactions with the Pacific warm pool**
   a. Statistically, the distribution of HE occurrences indicates the relation of HEs with the Pacific warm pool in terms of long-term mean SST. Higher occurrence rates of HE correspond to higher climatological SST in the Pacific warm pool.
   b. The warm and relatively stable thermal structure at the west side of the western Pacific warm pool may become the anvil for the HE occurrence so that the highest occurrence rate of HE is found in this area. Nevertheless, the HE occurrences give feedback to maintain the warm mixed layer in the western Pacific warm pool by spreading the heat accumulated at the surface during the development stage of HE to the deeper layer during the decay stage.

Although new features of HEs have been investigated in the present study, many are left for future works.

1) In Chapter 3, the characteristics (duration, amplitude, areal size, and speed of development and decay) of HE detected in the western equatorial Pacific are variable. There should be some mechanisms governing this variation.
2) In Chapter 4, the HE mechanisms were investigated by focusing on the local scope of the atmospheric variability over the HE area. Therefore, the possible larger and longer scale phenomena which may affect that local atmospheric variability were less considered. Through the case study of HE030528, the development stage of HE was contributed by the suppressed phase of the MJO while its decay stage was associated with the westward propagation of the low pressure systems. On the other hand the relationship between the MJO and the tropical cyclone as well as the low pressure system has been documented by Liebmann et al. (1994). Thus, further investigation of the relationships among HE, MJO and the tropical cyclone will be the potential subject for future works.
3) In Chapter 5, the role of HE in governing the mixed layer temperature variations in the western Pacific warm pool has been investigated. However, some possible factors such as subduction, entrainment, lateral mixing and also the interannual background were neglected in the present study. The further investigation involving all possible factors

may give better understanding of the HE contribution to the formation of warm mixed layer in the Pacific warm pool.

4) HEs were generated under the condition of high solar radiation and low wind speed which correspond to the high amplitude of DSST. Despite not the primary factor, the precipitation rate also influences the DSST variation (Webster et al. 1996). As a convection area, the heavy rainfall often occurs in the western equatorial Pacific with the preferential rainfall during predawn hours (Cronin and McPhaden 1999). This early morning rainfall may stabilize the water column so that HE is more easily generated during daytime. This possible mechanism is left for the next study.
5) The western Pacific warm pool has an important role to influence the global climate variation by transporting heat and water vapor from the warm pool to the higher latitude. During the HE period, latent heat release is suppressed and thus, the surface evaporation process is regulated. Hence, the frequent HE occurrence might influence the vapor transport through the large-scale circulation. This possible effect is left for future study.

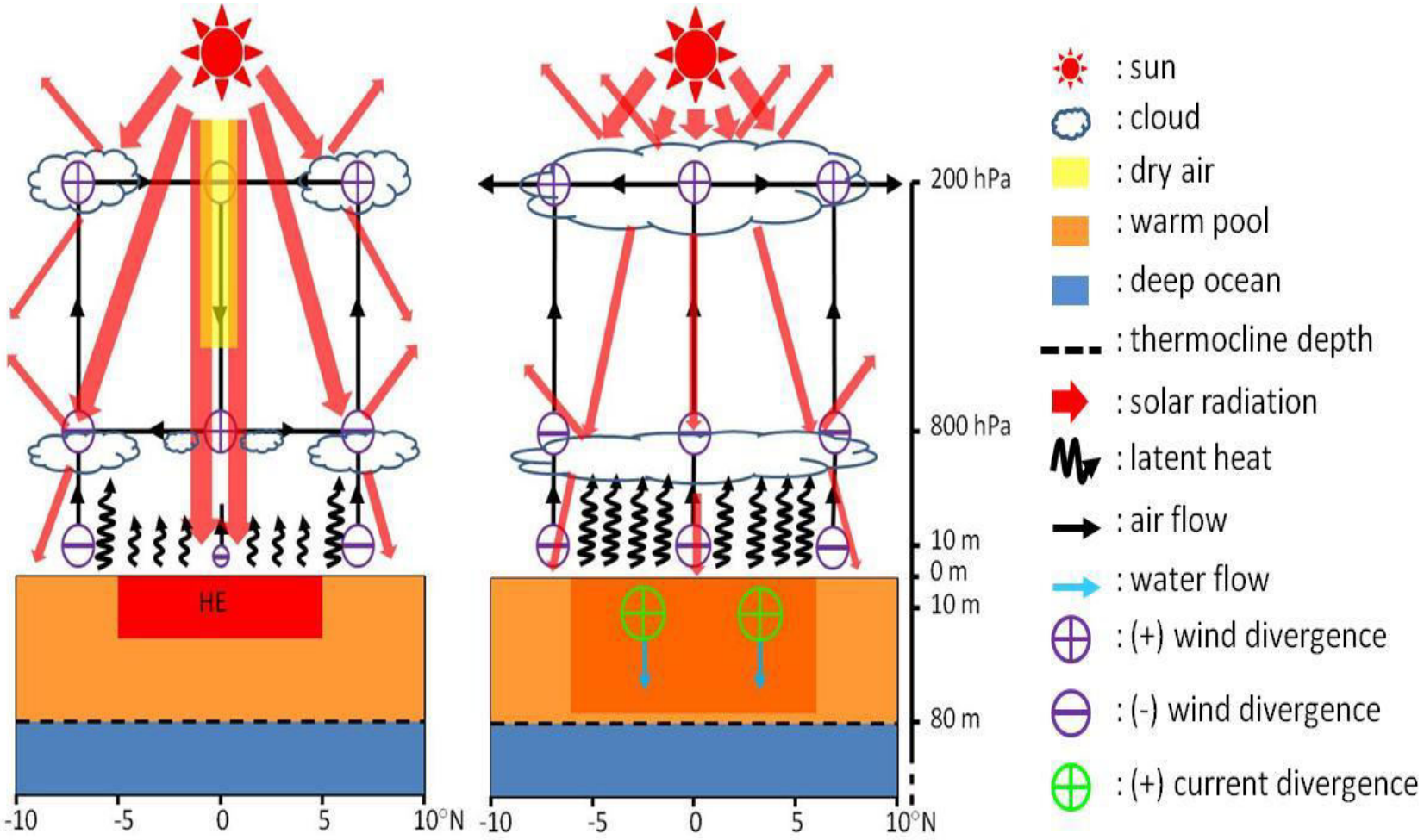

Fig. 6.1 Scenario of the HE mechanisms in the western equatorial Pacific.

Appendix I. The amplitude map of HE in the western equatorial Pacific calculated from eq. (1). Each HE is named by its start day as HEyymmdd and its properties are listed in Table 3.1.

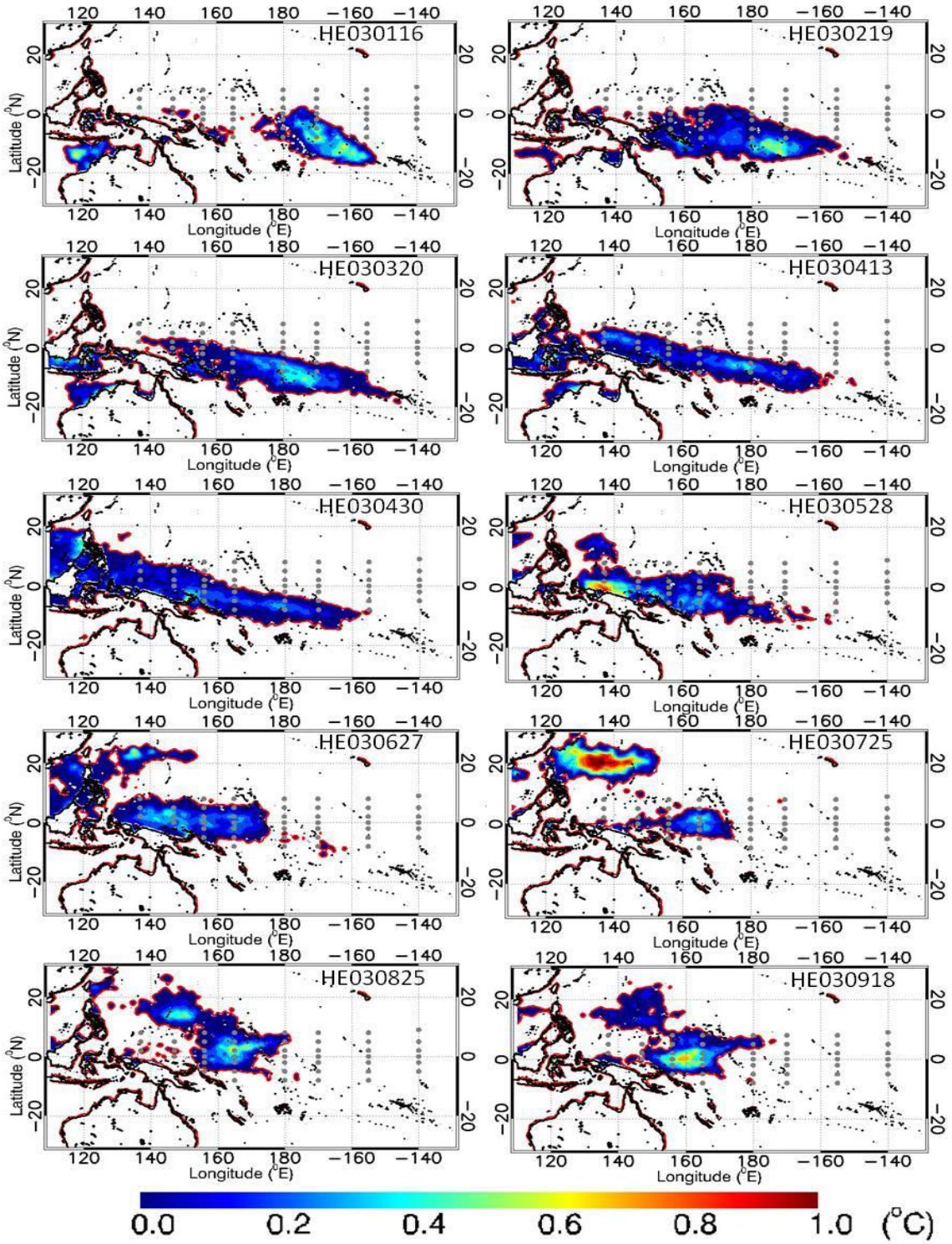

Appendix I. continue 1

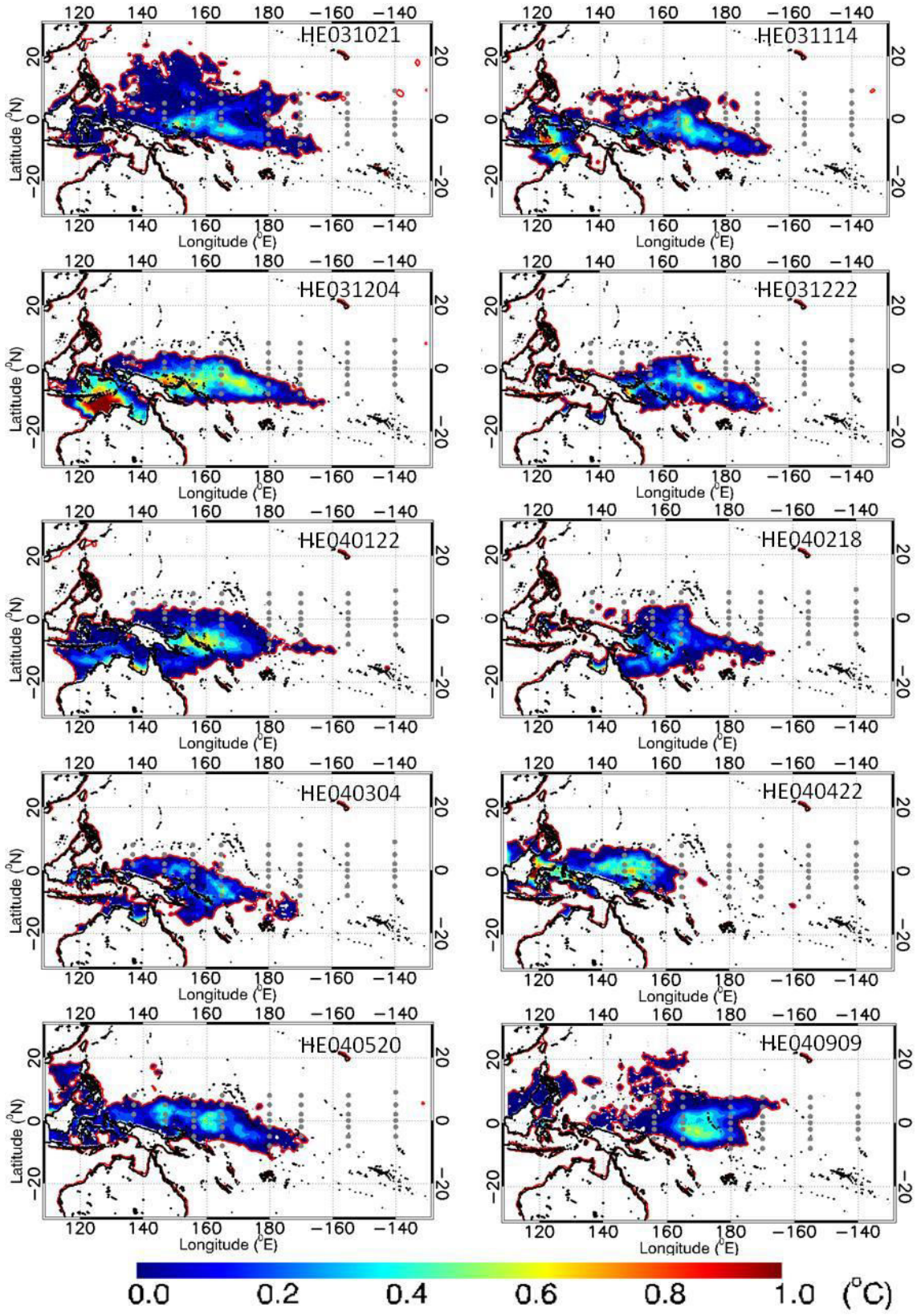

Appendix I. continue 2

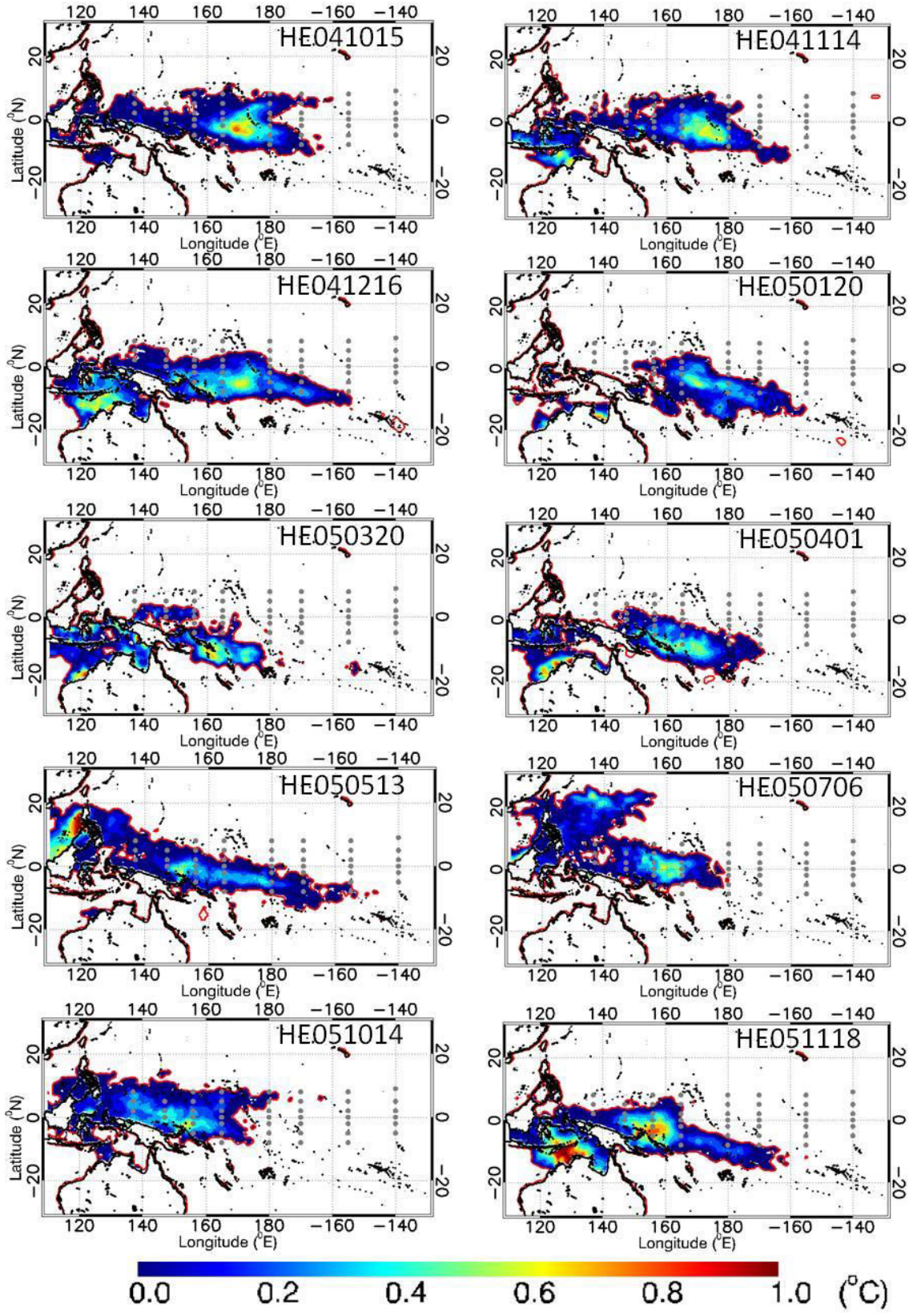

Appendix I. continue 3

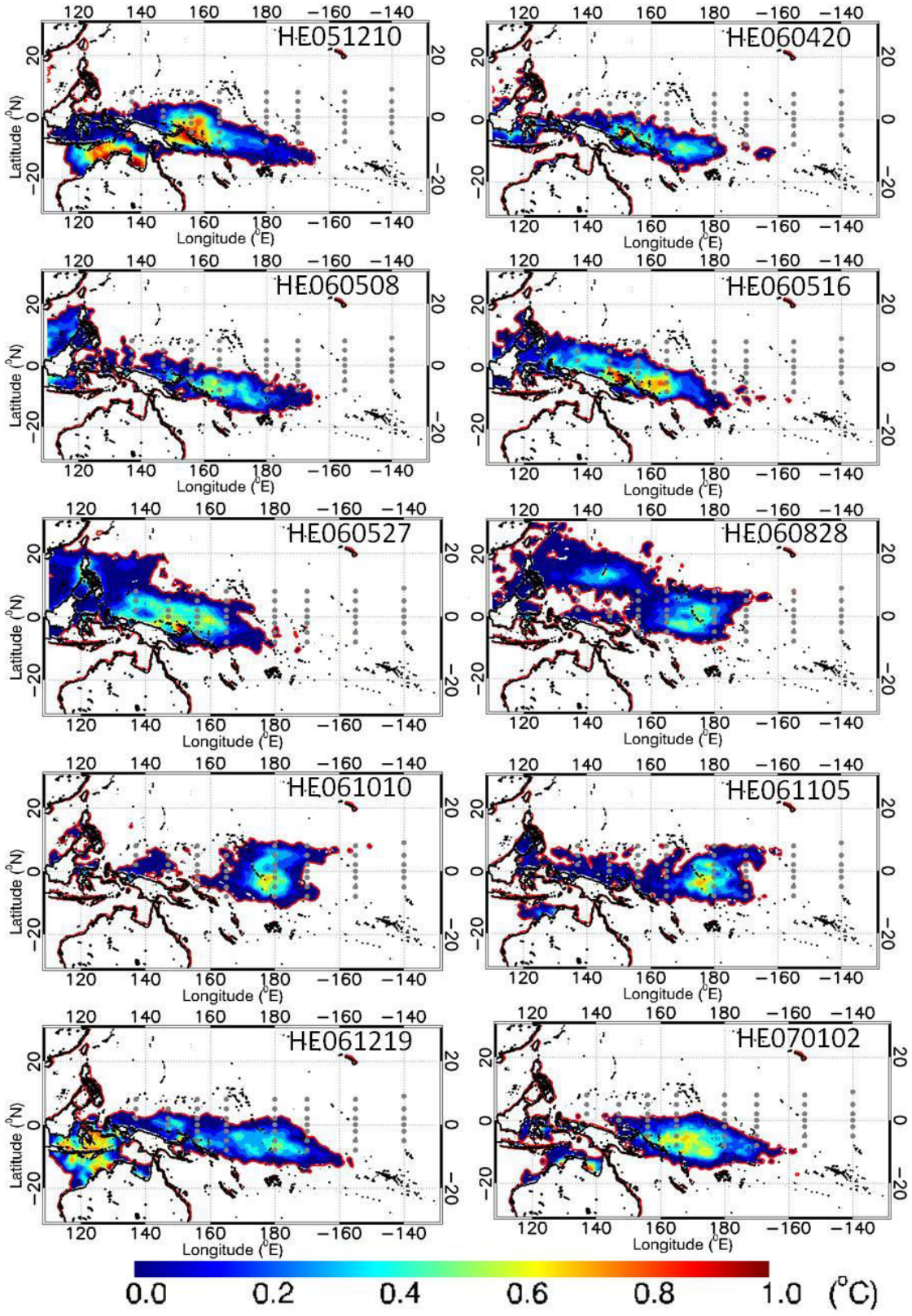

Appendix I. continue 4

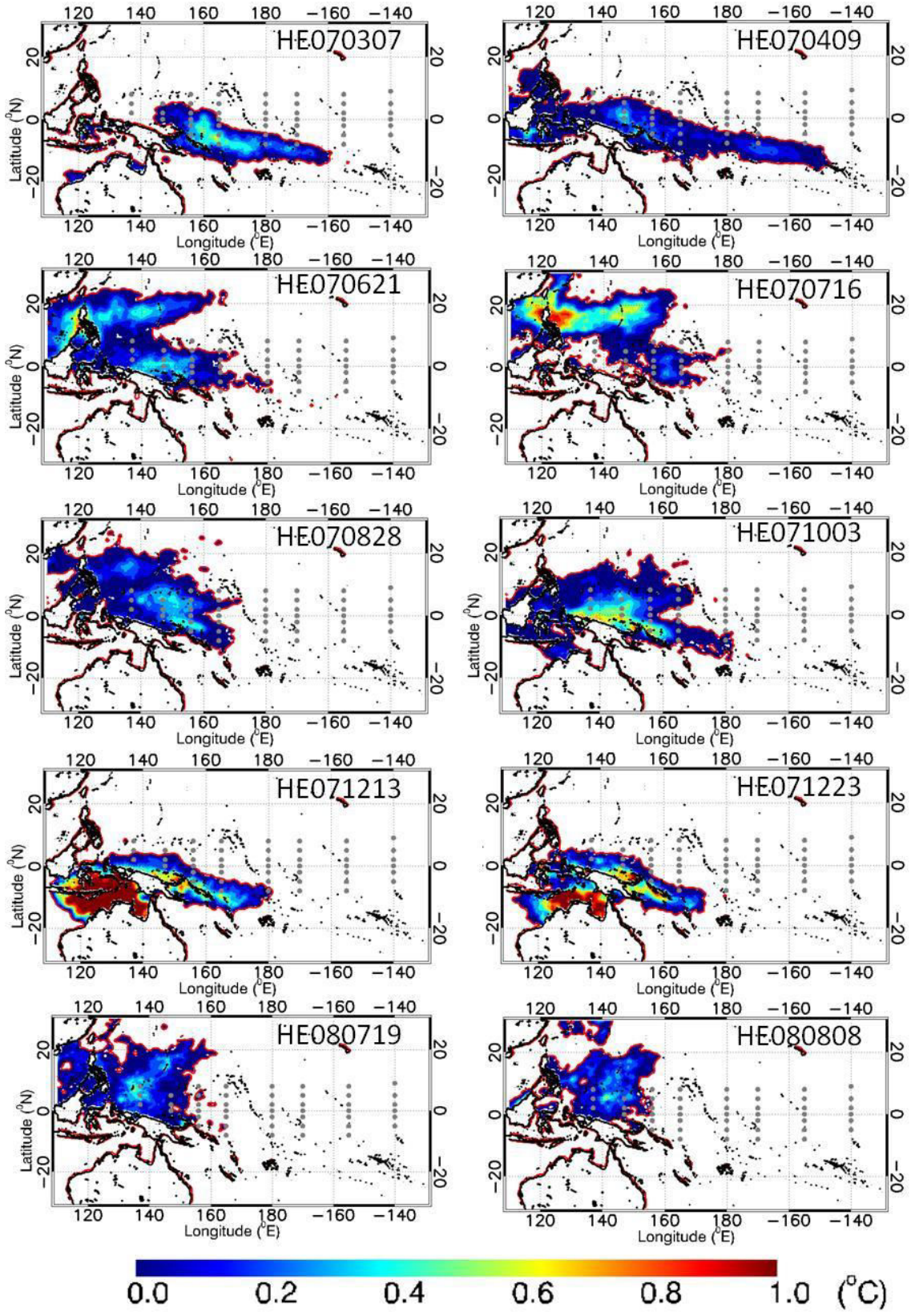

Appendix I. continue 5

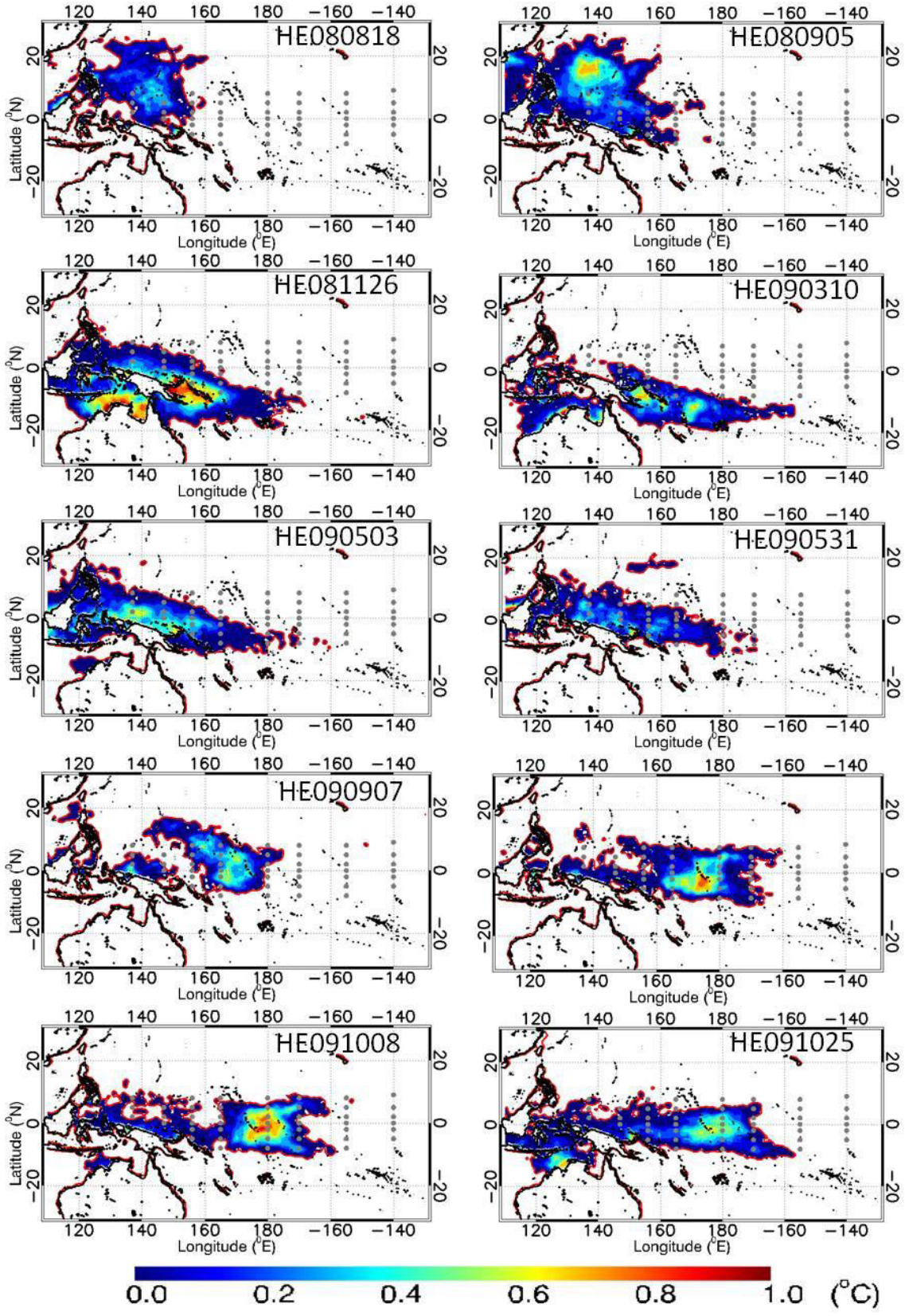

Appendix I. continue 6

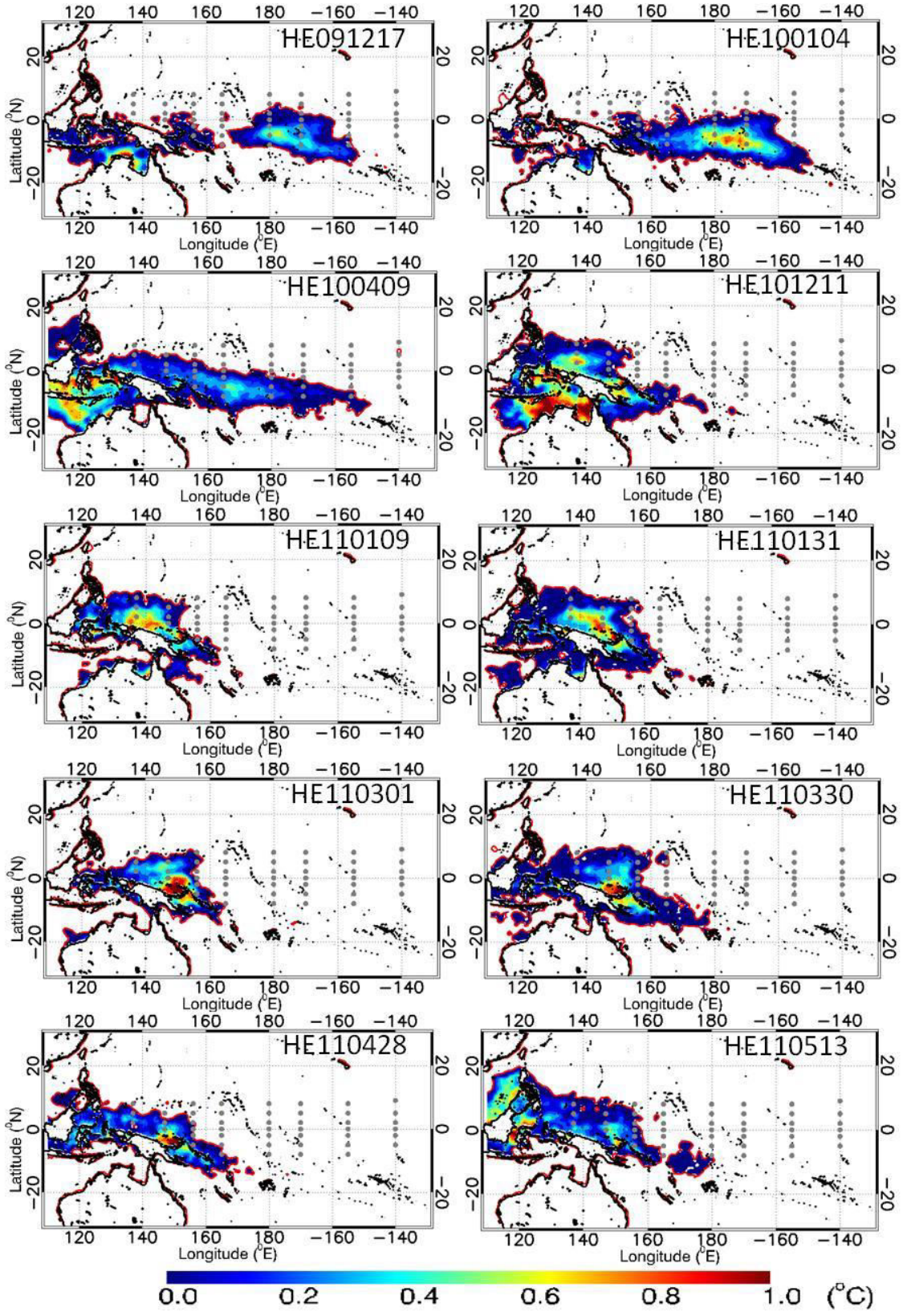

Appendix I. continue 7

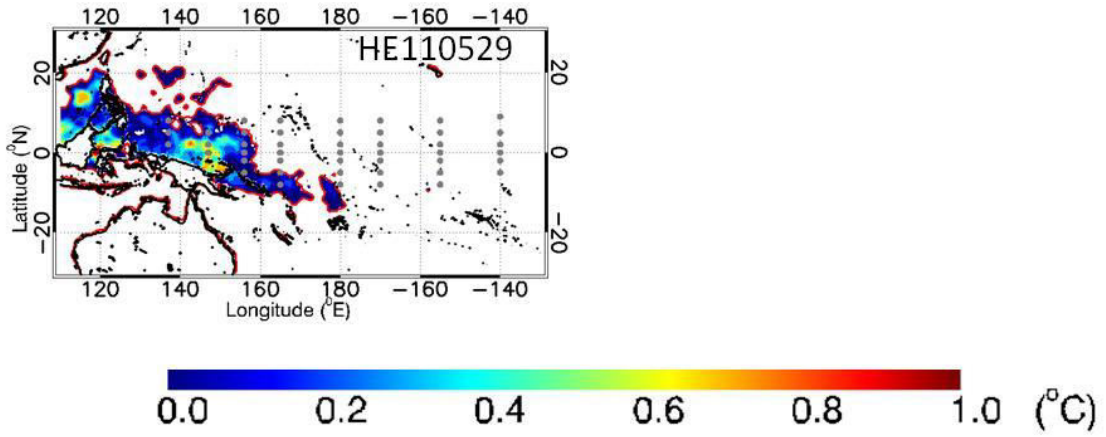

Acknowledgements

Firstly I would like to express my deepest gratitude and respect to Prof. Hiroshi Kawamura for his continuously support, encouragement, direction and supervision during my study period. He is the one who introduced me to the phenomena of air-sea interaction that later become my field of interest. I am also deeply grateful to Dr. Teruhisa Shimada and Dr. Kohtaro Hosoda for always providing time for discussion and helping me to solve the research problems.

My warm gratitude is also given for other member of Ocean Environmental Group of Center for Atmospheric and Oceanic Studies and Physical Oceanography Group of Tohoku University (i.e., Prof. Futoki Sakaida, Prof. Toshio Suga, Prof. Shoichi Kizu, Dr. Syusaku Sigimoto and all students). Their suggestions, comments, and questions during the semi-annual seminar helped me to improve the result of my research.

I also would like to thank to Directorate General of Higher Education of Indonesian Republic for the scholarship support and all member of the Faculty of Fisheries and Marine Sciences, Diponegoro University, Semarang, Indonesia for the strong support.

Finally, for my family and friends especially for my beloved wife, daughter, son, parents, brothers and sisters, from the deepest of my heart, there is no other words except “Thank You..”.

List of Acronyms

3D : 3 Dimensional

AMSR-E : Advanced Microwave Scanning Radiometer on the Earth Observing System

AVHRR : Advanced Very High Resolution Radiometer

DSST : Diurnal sea surface temperature

FAR : False alarm ratio

GTOPO30 : Global 30 Arc-second elevation

HE : Hot Event

HRC : Highly Reflective Cloud

ISCCP : International Satellite Cloud Climatology Project

JCDAS : JMA Climate Data Assimilation System

JMA : Japan Meteorological Agency

JRA-25 : Japanese 25-year Reanalysis

JRA-55 : Japanese 55-year Reanalysis

MGDSST : Merged satellite and in-situ data Global Daily Sea Surface Temperature

MAR : Misses alarm ratio

MJO : Madden-Julian Oscillation

NGSST-O-Global-V2.0a : New Generation Sea Surface Temperature version 2.0a

OISST V2 : Optimum Interpolation Sea Surface Temperature ver. 2.0

POD : Probability of detection

PSD : Power Spectral Density

RMSE : Root mean square error

SLP : Sea level pressure

SST : Sea surface temperature

TAO/TRITON : Tropical Atmosphere Ocean/Triangle Trans-Ocean Buoy Network

References

Akima H (1996) Algorithm 761 - Scattered-data Surface Fitting that has the Accuracy of a Cubic Polynomial. ACM Trans Math Softw 22(3): 362 - 371

Ando K, McPhaden MJ (1997) Variability of surface layer hydrography in the tropical Pacific Ocean. J Geophys Res 102(C10): 23063-23078

Arking A Ziskin D (1994) Relationship between clouds and sea surface temperatures in the western tropical Pacific. J Climate 7: 988-1000

Bathen KH (1972) On the seasonal changes in the depth of the mixed layer in the north Pacific Ocean. J Geophys Res 77:7138-7150

Chongyin L, Mingquan M, Guangqing Z (1999) The variation of warm pool in the equatorial western Pacific and its impacts on climate, Advances in Atmos Sci 16(3): 378-394

Clement A, Seager R (1999) Climate and the tropical oceans. Am Meteorol Soc 12: 3383-3401

Clement AC, Seager R, Murtugudde R (2005) Why are there tropical warm pools? J Climate 18: 5294-5310

Cronin MF, McPhaden MJ (1999) Diurnal cycle of rainfall and surface salinity in the western Pacific warm pool. Geophys Res Lett 26(23): 3465-3468

Harweijer C, Seager R, Winton M, Clement A (2005) Why ocean heat transport warms the global mean climate. Tellus 57A: 662-675

Horel JD (1982) On the annual cycle of the tropical Pacific atmosphere and ocean. Mon Weather Rev 110: 1863-1878

Hosoda K (2013) Empirical method of diurnal correction for estimating sea surface temperature at dawn and noon. J Oceanogr 69: 631-646 doi: 10.1007/s10872-013-0194-4

Hosoda K, Kawamura H, Sakaida F (2015) Improvement of New generation Sea Surface temperature for Open ocean (NGSST-O): a new sub-sampling method of blending microwave observations. J Oceanogr 71:205-220 doi: 10.1007/s10872-015-0272

Kawai Y, Kawamura H, Takahashi S, Hosoda K, Murakami H, Kachi M, Guan L (2006) Satellite-based high-resolution global optimum interpolation sea surface temperature data. J Geophys Res 111: C06016. doi:10.1029/2005JC003313

Kawamura H, Qin H, Ando K (2008) In-situ diurnal sea surface temperature variations and near-surface thermal structure in the tropical Hot Event of the Indo-Pacific warm pool. J

Oceanogr 64: 847-857

Keen R A (1982) The role of cross-equatorial tropical cyclone pairs in the Southern Oscillation, Mon. Weather Rev. 110:1405-1416.

Kiladis GN, Meehl GA, Weickmann KM (1994) large-scale circulation associated with westerly wind bursts and deep convection over the western equatorial Pacific. J Geophys Res 99(D9): 18527-18544

Kim ST, Yu JY, Lu MM (2012) The distinct behaviors of Pacific and Indian Ocean warm pool properties on seasonal and interannual time scales. J Geophys Res 117: D05128. doi: 10.1029/2011JD016557

Kobayashi S, Ota Y, Harada Y, Ebita A, Moriya M, Onoda H, Onogi K, Kamahori H, Kobayashi C, Endo H, Miyaoka K, and Takahashi K (2015) The JRA-55 Reanalysis: General Specifications and Basic Characteristics. J Meteor Soc Japan 93(1): 5-48, doi:10.2151/jmsj.2015-001

Kurihara Y, Sakurai T, Kuragano T (2006) Global daily sea surface temperature analysis using data from satellite microwave radiometer, satellite infrared radiometer and in situ observations. Weather Serv Bull (Sokkou-Jihou) 73: S1-18 (in Japanese).

Lau KM, Sui CH (1997) Mechanisms of short-term sea surface temperature regulation : Observations during TOGA COARE. J Climate 10: 465-472

Lander MA (1990) Evolution of the cloud pattern during the formation of tropical cyclone twins symmetrical with respect to the equator. Mon Weather Rev 118: 1194-1202

Liebmann B, Hendon HH, Glick JD (1994) The relationship between tropical cyclone of the western Pacific and Indian oceans and the Madden –Julian Oscillation. J Meteor Soc Japan 72(3): 401-412

Lin CY, Ho CR, Zheng Q, Kuo NJ, Chang P (2011) Warm pool variability and heat flux change in the global oceans. Glob Planet Change 77: 26-33

Lukas R, Lindstorm E (1991) The mixed layer of the western equatorial Pacific Ocean. J Geophys Res Suppl 96:3343-3357

Marshall J, Plumb RA (2008) Atmosphere, Ocean and Climate Dynamics: An Introductory Text. Elsevier Academic Press, Cambridge, Massachusetts p.175

McPhaden MJ, Ando K, Bourles B, Freitag HP, Lumpkin R, Masumoto Y, Murty VSN, Nobre P, Ravichandran M, Vialard J, Vousden D, Yu W (2010) The global tropical moored buoy

array. In hall J, Harrison DE, Stammer D (eds) Proceedings of the "OceanObs '09: Sustained Ocean Observations and Information for Society" conference, vol 2, Venice, Italy, 21-25 Sep 2009, ESA publication WPP-306

Nitta T (1989) Development of a twin cyclone and westerly bursts during the initial phase of the 1986-87 El Niňo. J Meteor Soc Japan. 67: 677-681

Ogura Y, Chin HN (1987) A case study of cross-equatorial twin vortices over the Pacific in the northern winter using FGGE data. J Meteor Soc Japan 65:669-674.

Onogi K, Tsutsui J, Koide H, Sakamoto M, Kobayashi S, Hatsushika H et al (2007) The JRA-25 Reanalysis. J Meteor Soc Japan 85: 369-432

Pierrehumbert RT (2000) Climate change and the tropical Pacific: The sleeping dragon wakes. PNAS 97(4): 1355-1358

Qin H, Kawamura H, Kawai Y (2007) Detection of hot event in the equatorial Indo-Pacific warm pool using advanced satellite sea surface temperature, solar radiation, and wind speed. J Geophys Res 112: C07015, doi:10.1029/2006JC003969

Qin H, Kawamura H, Sakaida F, Ando K (2008) A case study of the tropical hot event in November 2006 (HE0611) using a geostationary meteorological satellite and the TAO/TRITON mooring array. J Geophys Res 113: C08045. doi:10.1029/2007JC004640

Qin H, Kawamura H (2009) Atmosphere response to a hot SST event in November 2006 as observed by AIRS instrument. Adv Space Res 44: 395-400. doi:10.1016/j.asr.2009.03.003

Qin H, Kawamura H (2010) Air-sea interaction throughout the troposphere over a very high sea surface temperature. Geophys Res Let, 37: 1-4. doi:10.1029/2009GL041685

Ramanathan V, Collins W (1991) Thermodynamic regulation of ocean warming by cirrus clouds deduced from observations of the 1987 El Niño. Nature 351: 27–32

Rasmusson EM, Wallace JM (1983) Meteorological aspects of the E1 Niño/Southern Oscillation. Science. 222: 1195-1202

Reynolds RW, Rayner NA, Smith TM, Stokes DC, and Wang W (2002) An improved in situ and satellite SST analysis for climate. J Climate 15: 1609-1625

Sakaida F, Kawamura H, Takahashi S, Sfimada T, Kawai Y, Hosoda K, Guan L (2009) Research, development, and demonstration operation of the New Generation Sea Surface Temperature for Open ocean (NGSST-O) product. J Oceanogr 65:859-870

Sherwood SC (1999) Convective precursors and predictability in the tropical western Pacific. Mon Weather Rev 127: 2977–2991

Shinoda T, Hendon H, Glick J (1998) Intraseasonal variability of surface fluxes and sea surface temperature in the tropical western Pacific and Indian Oceans. J Climate 11: 1685-1702

Thoron TG, Rosenthal Y, Bassinot F, Beaufort L (2005) Stable sea surface temperatures in the western Pacific warm pool over the past 1.75 million years. Nature 433: 294-298

Tompkins AM (2001) On the relationship between tropical convection and sea surface temperature. J Climate 14: 633-637

Waliser DE, Graham NE (1993) Convective cloud systems and warm-pool sea-surface temperatures: Coupled interactions and self-regulation. J Geophys Res 98 (D7): 12881–12893

Waliser DE (1996) Formation and limiting mechanisms for very high sea surface temperature : Linking the dynamics and the thermodynamics. J Climate 9: 161-188

Wallace JM (1992) Effect of deep convection on the regulation of tropical sea surface temperature. Nature 357: 230–231

Webster PJ, Clayson CA, Curry JA (1996) Clouds, radiation, and the diurnal cycle of sea surface temperature in the tropical western Pacific. J Climate 9: 1712–1730

Wheeler M, Hendon HH (2004) An all-season real-time multivariate MJO index: Development of an index for monitoring and prediction. Mon Weather Rev 132: 1917–1932

Wilks DS (2006) Forecast verification, in Statistical methods in the atmospheric sciences. Academic, San Diego, Calif, pp. 260-277

Wyrtki K (1964) The thermal structure of the eastern Pacific Ocean. Dstch Hydrogr Zeit Suppl Ser A 8:6-84

Wyrtki K (1989) Some thoughts about the west Pacific warm pool. paper presented at Western Pacific International Meeting and Workshop on TOGA COARE, Nouméa, New Caledonia: 99-109

Yan, X-H, Ho CR, Zheng Q Klemas V (1992) Temperature and size variabilities of the western Pacific warm pool. Science 258: 1643-1645

Yu L, Weller RA (2007) Objectively Analyzed air-sea heat Fluxes for the global ice-free oceans (1981–2005). Bull Am Meteor Soc 88: 527–539

Zhang C (2005) Madden-Julian Oscillation. Rev of Geophys 43:1-36

Zhang GJ, Ramanathan V, McPhaden MJ (1995) Convection evaporation feedback in the equatorial Pacific. J Climate 8: 3040–3051

Zhang Y-C, Rossow WB, Lacis AA, Oinas V, Mishchenko MI (2004), Calculation of radiative fluxes from the surface to top of atmosphere based on ISCCP and other global data sets: Refinements of the radiative transfer model and the input data. J Geophys Res 109: 1-27. doi: 10.1029/2003JD004457